GEORGIA INSTITUTE OF TECHNOLOGY
SCHOOL OF MECHANICAL ENGINEERING
ATLANTA, GEORGIA

MEASUREMENT OF SOLID PROPELLANT BURNING RATES DURING RAPID DEPRESSURIZATION

ANNUAL REPORT NO. 1

By

A. Clary
S. Shelton

For

AIR FORCE OFFICE OF SCIENTIFIC RESEARCH
1400 WILSON BOULEVARD
ARLINGTON, VIRGINIA 22209

Grant No. AFOSR -70-1934

September 1, 1971

14. KEY WORDS	LINK A		LINK B		LINK C	
	ROLE	WT	ROLE	WT	ROLE	WT
COMBUSTION						
SOLID PROPELLANT						
COMBUSTION INSTABILITY						
DEPRESSURIZATION EXTINGUISHMENT						
BURNING RATE MEASUREMENT						
MICROWAVE DOPPLER SHIFT						
BURNING RATE RESPONSE						

ib

ic

MEASUREMENT OF SOLID PROPELLANT BURNING RATES DURING RAPID DEPRESSURIZATION
ANNUAL REPORT NO. 1

By

A. Clary
S. Shelton

School of Mechanical Engineering
Georgia Institute of Technology
Atlanta, Georgia

September 1, 1971

Sponsored by

AIR FORCE OFFICE OF SCIENTIFIC RESEARCH
1400 Wilson Boulevard
Arlington, Virginia
Grant No. AFOSR-70-1934

S. Shelton, Principle Investigator

Stothe P. Kezios, Director
School of Mechanical Engineering

GEORGIA INSTITUTE OF TECHNOLOGY

School of Mechanical Engineering

FOREWORD

This project is being carried out in the research laboratories of the Georgia Institute of Technology under the Grant No. AFOSR - 70 - 1934 and directed by the principle investigator Dr. Sam Shelton. For the program period covered by this report, Graduate Research Assistant Mr. Albert Clary participated directly in carrying out the work which he submitted in partial fulfillment of the requirements for the degree Master of Science in Mechanical Engineering. The work was partially supported by the School of Mechanical Engineering under the matching-fund provision of the grant.

Sam Shelton
Principle Investigator

September 1, 1971

TABLE OF CONTENTS

Table of Contents (Continued)

ABSTRACT

Combustion instability in solid propellant rocket engines continues to be a plaguing problem to the propulsion engineer. Acoustic instability, which has its origin in the response of the burning rate to rapid pressure transients, is perhaps the most common of those instability phenomena. For this reason knowledge of propellant burning rates under unsteady pressure conditions would be an invaluable aid to the prediction and prevention of acoustic instability. To the present day, however, very few techniques have demonstrated the ability to measure burning rates under fully unsteady conditions.

A microwave continuous measurement technique has been utilized to measure burning rates of a CTPB and AP composite solid propellant during rapid decompression. A microwave signal oscillating at a known source frequency is passed through the end of a burning propellant strand opposite the burning surface and allowed to reflect off the burning surface, which is receding at some unknown velocity. By continuously comparing the phase angle of this reflected signal with the phase angle of another signal oscillating at the original source frequency, a relative phase angle between the two signals is obtained. The rate of change of this relative phase angle with time is proportional to the propellant's burning rate.

Several important conclusions were reached in the course of the investigation. Roughness of the propellant surface can definitely be a source of error, but the types of roughness generally encountered should

induce errors no larger than ten percent. Reflection from the flame zone, originally thought to be a major source of error, were proven to be quite negligible, if they exist at all. The main limitation on the technique was found to lie in the resolution and inherent noise of the output of the phase sensing equipment.

This limitation will be eliminated in future work and measurements made for various propellants during rapid depressurization and oscillating pressure.

LIST OF ILLUSTRATIONS

List of Illustrations (Continued)

List of Illustrations (Concluded)

LIST OF SYMBOLS

a	wide dimension of a rectangular waveguide
A	fixed reflection vector in phasor diagram
AP	ammonium perchlorate
B	burning surface reflection vector in phasor diagram
c	speed of light
C	test signal vector in phasor diagram
CTPB	carboxyl terminated polybutadiene
E_i	voltage amplitude of the incident wave
E_r	voltage amplitude of the reflected wave
f_i	frequency of the incident signal
f_r	frequency of the reflected signal
p	reflection coefficient
P_{dB}	relative power of two microwave signals referenced to each other
P_{dBm}	power of a microwave referenced to one milliwatt
P_{mW}	power of microwave in milliwatts
P_o	pressure just prior to decompression
r	velocity of burning surface
r_o	burning rate just prior to decompression
tan $\emptyset$	loss tangent
TE	transverse-electric microwave propagation mode
VSWR	ratio between the maximum voltage and the minimum voltage
W_r	klystron radian frequency
ϵ/ϵ_o	dielectric constant

$\varepsilon'/\varepsilon_o$	real part of dielectric constant
$\varepsilon''/\varepsilon_o$	imaginary part of dielectric constant
λ_c	cutoff wavelength of waveguide
λ_g	group wavelength of wave of frequency w in waveguide
λ_o	wavelength of wave of frequency w in free space
λ_{pg}	group wavelength in propellant filled waveguide
ϕ_a	actual phase angle
ϕ_m	measured phase angle

CHAPTER I

INTRODUCTION

Background

In the design of solid-propellant combustion systems, oscillatory phenomena are common obstacles to the engineer. The combustion process is responsive to pressure and flow disturbances, and the resulting disturbances of the combustion reaction can, under certain conditions, amplify the original fluctuations. Due to the nature of the combustion process, which relies on diffusion, heat and transfer, and chemical kinetics to prepare the reactants for reaction, a particular combustion field has a limited supply of "ready" reactants at a given time. A sudden increase, or positive disturbance, in the combustion rate, depletes the supply of "ready" reactants and, consequently may result in a negative disturbance in the burning rate. The alterations of the "ready" reactant concentration may agitate the diffusion processes, while the changes in the rate of energy release can affect the heat transfer processes to the pre-heating zone of the propellant or to the yet unburned "ready" reactants. With all this interaction among the transport and chemical processes, it is no wonder that combustion tends to support periodic flow and pressure disturbances.

Since such oscillatory behavior is in most cases quite undesirable, extensive analytical and experimental research has been directed towards its understanding and elimination. Ideally, one would like to be able to predict and eliminate instabilities long before the testing stage

of a new full scale solid propellant system. However, this involves the ability to construct a theoretical model of the system at hand. Many approaches to this problem have been proposed, but, up to the present, solid propellant, unsteady state combustion modeling has been difficult to evaluate because of a lack of comprehensive experimental data with which to compare theoretical results (1).

Since, in many cases, oscillatory combustion is produced and amplified by pressure disturbances in the flow field (accustic instability), accurate experimental data relating to the response of the burning rate to rapid pressure transients would be a great aid in predicting the onset of instability. However, to obtain burning rates for use as unsteady state data, a technique must be used which has excellent propellant length resolution and a rapid response time.

A microwave technique has recently been developed which yields practically instantaneous burning rate values, contrary to previously demonstrated microwave methods, and also produces the desired resolution (2). The purpose of the subject thesis was to demonstrate a refinement of the system described in reference (2) and to present data to support its ability and reliability in the measurement of solid propellant burning rates. In addition, data relating to the burning rate response of a carboxyl-terminated poly-butadiene (CTPB) propellant with ammonium perchlorate (AP) oxidizer to rapid depressurization is presented.

Review of the Literature

Many different schemes for the measurement of solid propellant burning rates have been proposed and most offer sufficient accuracy as long as the system operates at near steady state conditions. However,

in order to study burning rates during rapid periodic pressure oscillations, as occur during acoustic instability, or during rapid depressurization, as in the case of propellant extinction studies, one must have more capability and flexibility than previous methods have demonstrated. Specifically, the technique must have excellent propellant length resolution and a rapid response time.

An estimate of the resolution necessary can be extracted by considering the following. At dP/dt values of 2000 psi per second, the solid-phase temperature profile departs from its steady state contour (3). Assuming 50 psi to be the upper limit on the pressure range, ΔP, over which an average burning rate is to be obtained, at 2000 psi per second the pressure drops 50 psi in 25 milliseconds as shown in Figure 1. Assuming a high burning rate of one inch per second, the burning surface travels 0.025 inch or 635 microns; as shown in Figure 1. For ten percent accuracy, the technique must measure this length change with a resolution of 0.0025 inches or 64 microns. If the burning surface movement could not be measured during a maximum time span of 25 milliseconds, the result would be average burning rates over pressure ranges greater than 50 psi. Relaxing the restrictions on the length resolution of 64 microns would yield less than ten percent accuracy.

In the subsequent discussion, the most promising techniques for measuring burning rates under conditions that begin to depart from steady state are reviewed and their individual advantages and inadequacies are pointed out.

Probably the simplest technique proposed is one which utilizes probes embedded in the propellant to detect the arrival of the burning

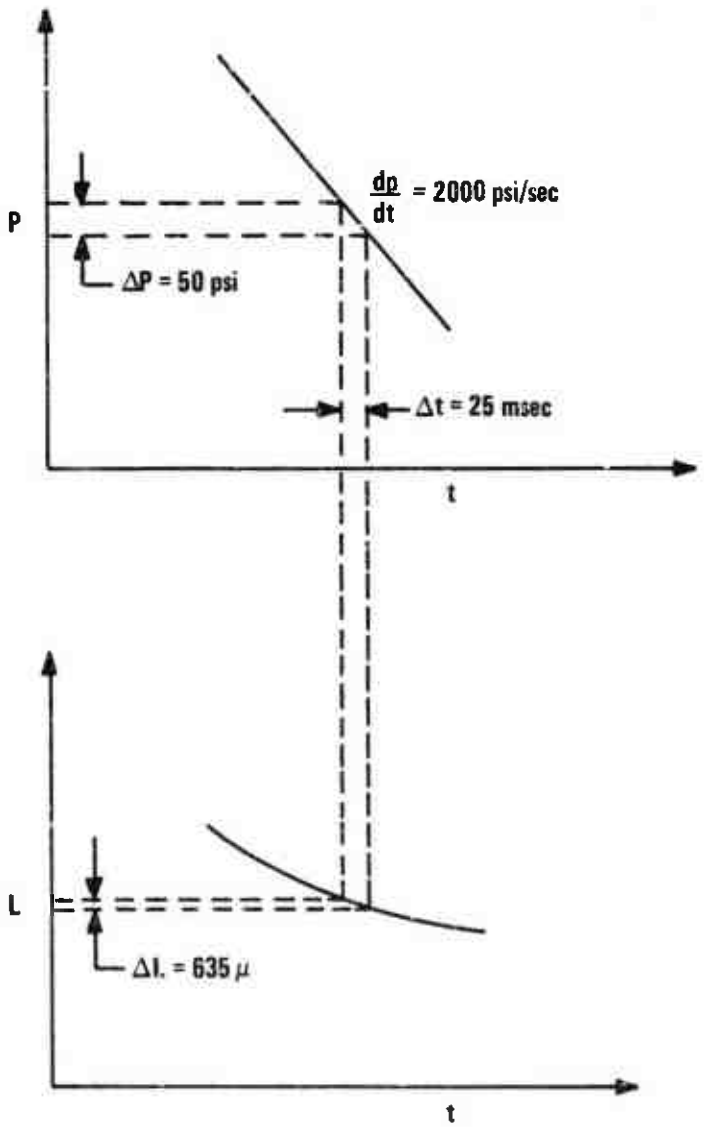

Figure 1. Relation Between Change of Length Measured ΔL and Pressure Range ΔP over which Burning Rate is Averaged.

surface. The probe may incorporate any type of sensing element that will detect the temperature rise as the burning plane passes; i.e., thermocouples, fuse wires, and conducting bridges. An example of a probe used in an erosive burning study is illustrated in Figure 2 (4). As the combustion gases arrived at the probe tip, there was a change in electrical conductivity between the ends of the wires, which in turn was used to actuate a display lamp. The system allowed the use of up to 50 probes, while the display lamps were photographed on moving 35-millimeter film by a camera operated by a ten millisecond timing pulse. The probes were mounted in the chamber prior to the casting of the propellant. This method allowed average burning rate measurementa over a period of approximately 0.5 seconds.

The main disadvantage of this system for measuring transient burning rates lies in the mechanical difficulty of mounting a sufficient number of probes to reduce the time over which burning rates must be averaged. In addition, the presence of the probes themselves may significantly alter the burning rate in the vicinity of the probes by disrupting the flow of gases and altering the heat transfer processes.

A similar technique, which eliminates some of the difficulties associated with probes, involves imbedding a fine resistance wire network in the propellant as in Figure 3. In one study (5), 0.0045 inch diameter lead-antimony wire was used to form a network which was embedded in a small specimen of the propellant. An x-ray picture of the small specimen was taken to determine the distance between the sharp bends of the cross-wires of the network. Since these bends were the first points hit by the burning surface, it was essential to know their relative

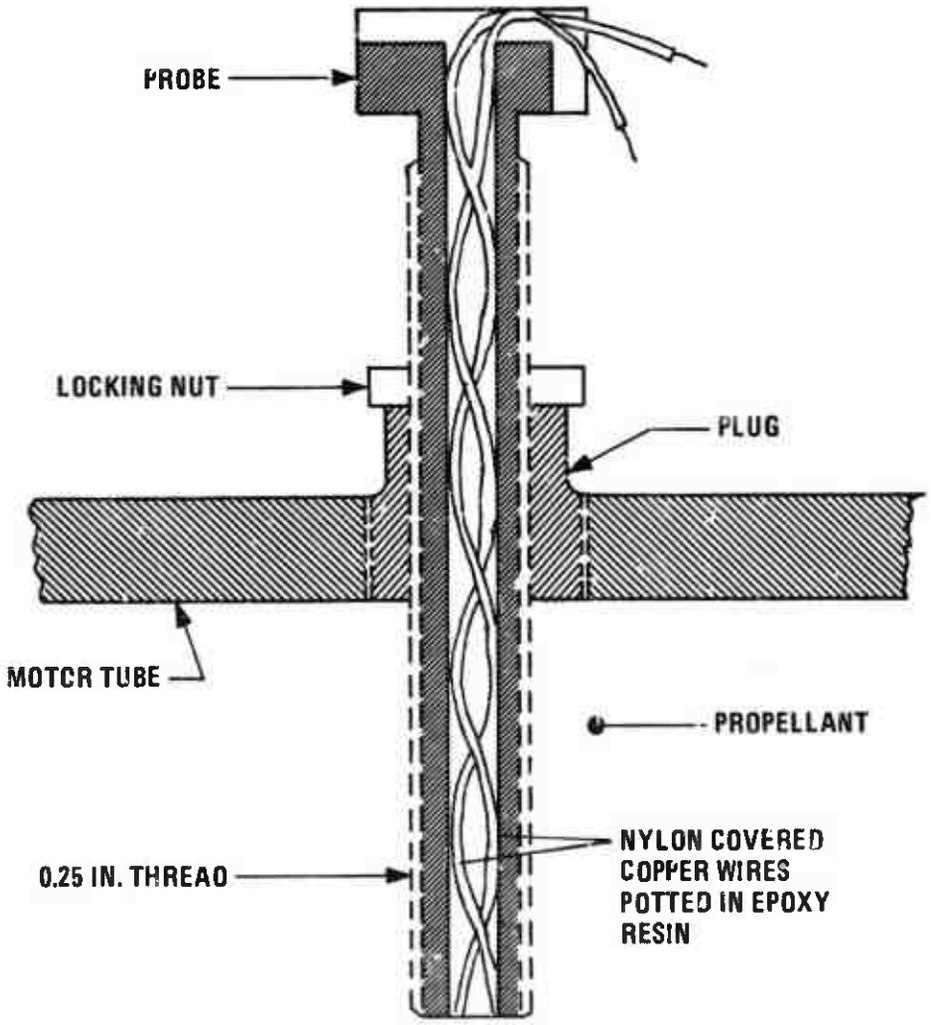

Figure 2. Dual Conductance Probe.

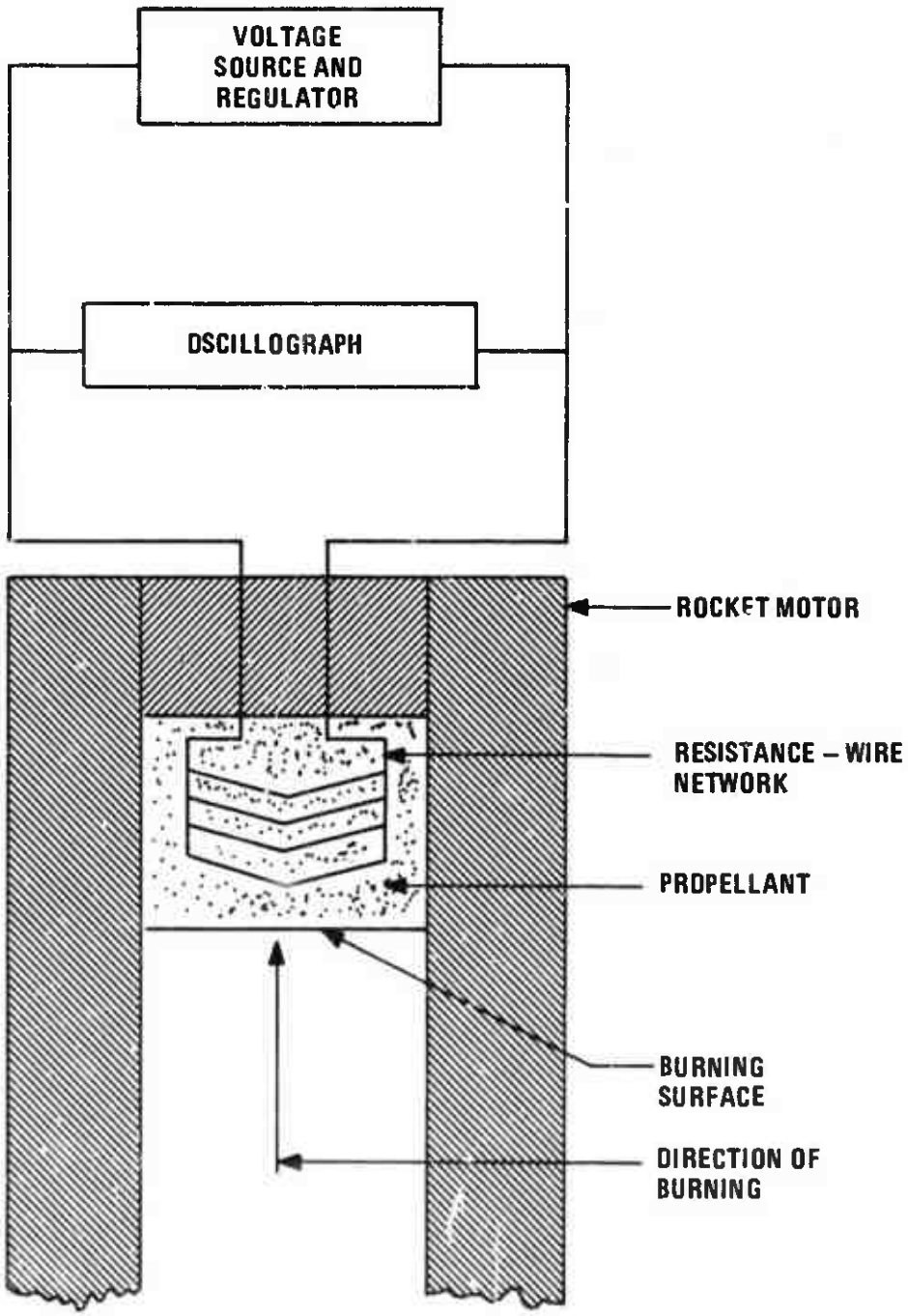

Figure 3. Schematic Diagram of the Resistance Wire Technique.

location in order to calculate burning rates. The small specimen was then bonded to the main block of propellant in a manner which allowed the plane of the wire network to be normal to the direction of burning. The test meter was then statically fired and the results were recorded on an oscillograph. As the burning surface clipped each cross-wire in succession, the resistance of the wire network changed, causing a corresponding current change through the oscillograph. Well defined steps appeared on the oscillograph which allowed the time to burn between each point on the wire network to be calculated. From this data the burning rate was easily deduced.

The choice of lead-antimony wire with its characteristic low melting point and low thermal diffusivity gave this method a distinct advantage over the previous probe method. The selection of lead-antimony wire was based on burning tests in which three different types of wire were utilized; 0.014 inch diameter copper, 0.0045 inch diameter copper, and 0.0045 inch diameter lead-antimony. The qualitative observation of partially burned samples indicated that the larger diameter copper wire caused considerable coning (formation of conical cavities around the embedded wire), the smaller copper wire caused less coning, and the lead-antimony wire caused no noticeable coning. This lack of coning indicated that the heat transfer from the burned gases to the unburned solid was not appreciably affected by the presence of the wire.

As with the probe method, the basic pitfall of using the embedded wire technique for measuring transient burning rates lies in its inability to measure average burning rates over periods less than the order of one-tenth of a second. The smallest time interval obtained

in the study (5) under consideration was 0.32 seconds. In order to obtain smaller time intervals, the wires would have to be so close that appreciable alteration of the burning rates in the vicinity of the wires would be likely to occur.

In the past several years, the Jet Propulsion Center at Purdue University has been the source of a great deal of research work done in the area of techniques for the measurement of solid propellant burning rates. A study completed in 1966 by personnel at Purdue demonstrated a technique for the "continuous" measurement of solid propellant burning rates (6). The method was continuous in that it utilized a positioning type servomechanism to properly feed a propellant strand into a combustion chamber, as shown schematically in Figure 4. As the burning surface receded during firing, its location was detected by a sensing element. The output from this sensor was used to control the speed of a servomotor which thus fed the propellant into the chamber at the same rate at which it was consumed, thereby causing the burning surface to remain at the same position relative to the chamber. By monitoring the rate at which the propellant was fed into the motor, a direct indication of the burning rate was obtained. The major difficulty encountered with this technique was the choice of an adequate sensing system to locate the burning surface and supply an accurate feedback signal for the servomotor.

In this study (6), investigators tested three types of sensing systems for potential use with the servomechanism apparatus. The first concept considered was a microwave beam directed through microwave windows in the chamber wall. A sensor would detect the attenuation of

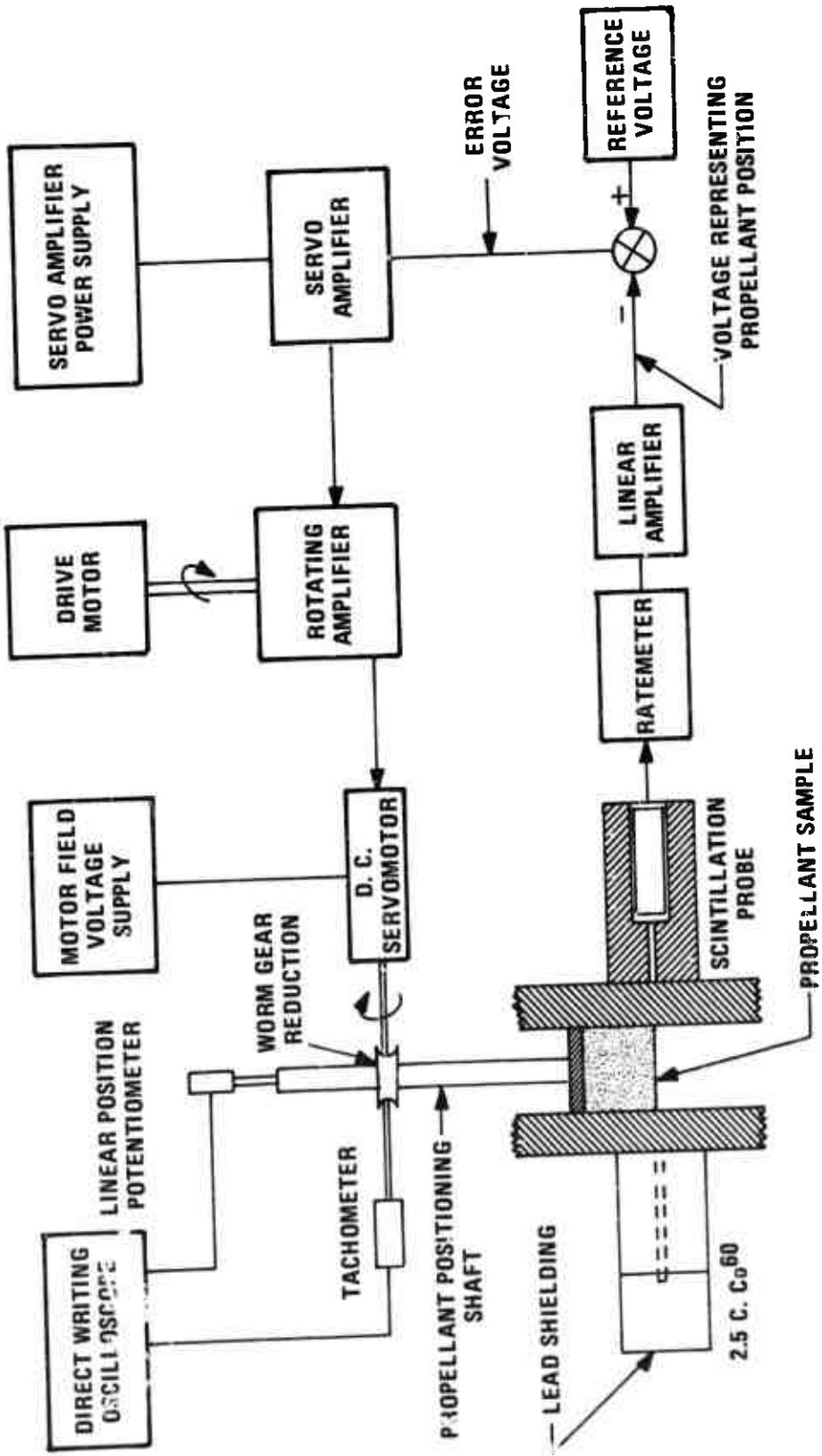

Figure 4. Servomechanism System.

the microwave beam as a function of the location of the burning surface. However, following a theoretical study, it was concluded that the microwave detection system was unsuitable for use as a feedback transducer due to extreme attenuation of microwaves by the combustion zone (7). The second concept that was analyzed involved the use of ultrasonic methods for detecting the burning surface. These included attenuation measurements, resonance measurements, and pulse-reflection measurements. In the analysis it was assumed that an electromechanical transducer would transmit ultrasonic waves through the propellant parallel to the burning surface. As a result of the unfavorable physical properties of the propellant itself, the attenuation and resonance approaches were labeled impractical. Pulse-reflection measurement was found to be the most suitable of the ultrasonic methods. However, it was found that in order to obtain a sufficiently large reflection, it was necessary to maintain the propellant at approximately -20 degrees Fahrenheit to -40 degrees Fahrenheit and operate at ultrasonic frequency ranges of 400 KHz or lower. The third concept investigated for detection of the combustion zone incorporated a gamma ray transducer and a radiation source. This proved to be the most suitable apparatus for use with the servomechanism technique and was subsequently developed into the system shown in Figure 4.

The nuclear radiation detection system consisted of a 2.5 curie source of Cobalt-60 and a scintillation detector. From the Cobalt-60 source, a collimated beam of gamma rays was directed through the chamber wall parallel to the burning plane. The scintillation probe was located opposite the radiation source and, as the burning surface passed, detected the change of density from the solid-propellant to combustion gases. The

output from the scintillation detector was used as a feedback signal to control the rate at which the propellant was fed into the chamber.

Another method for detection of the burning surface was demonstrated in a later investigation (8). This technique utilized a visible light beam system in which a series of lenses directed light from a tungsten strip lamp over the burning surface. The fraction of light passing the strand was detected by a photomultiplier tube and was used to generate the error signal for the servo-system.

In all of the above servo mechanism configurations the burning rate could always be found in either of two ways: 1) by measuring the slope of the position-time trace of the propellant positioning shaft, or 2) by monitoring, via a tachometer, the speed of the servomotor which controlled the velocity of the propellant.

In spite of the fact that the servo mechanism measurement technique yields extremely good results for near steady state linear burning rates, the inherent overshoot and the relatively large time constant of 50 milliseconds of the first order servo mechanism (9) make it impractical for unsteady applications.

Cineradiography, a method by which a moving picture record of fluoroscopic x-ray images is made, is a promising technique for the measurement of burning rates of solid rocket grains. Thiokol Chemical Corporation has conducted a study demonstrating the feasibility of such a system (10). In this investigation, static tests of a five inch diameter motor were conducted. The system, as shown in Figure 5, utilized a 300 kilovolt Norelco x-ray machine, which directed a beam through the motor forming a shadow image on the five inch diameter input screen of

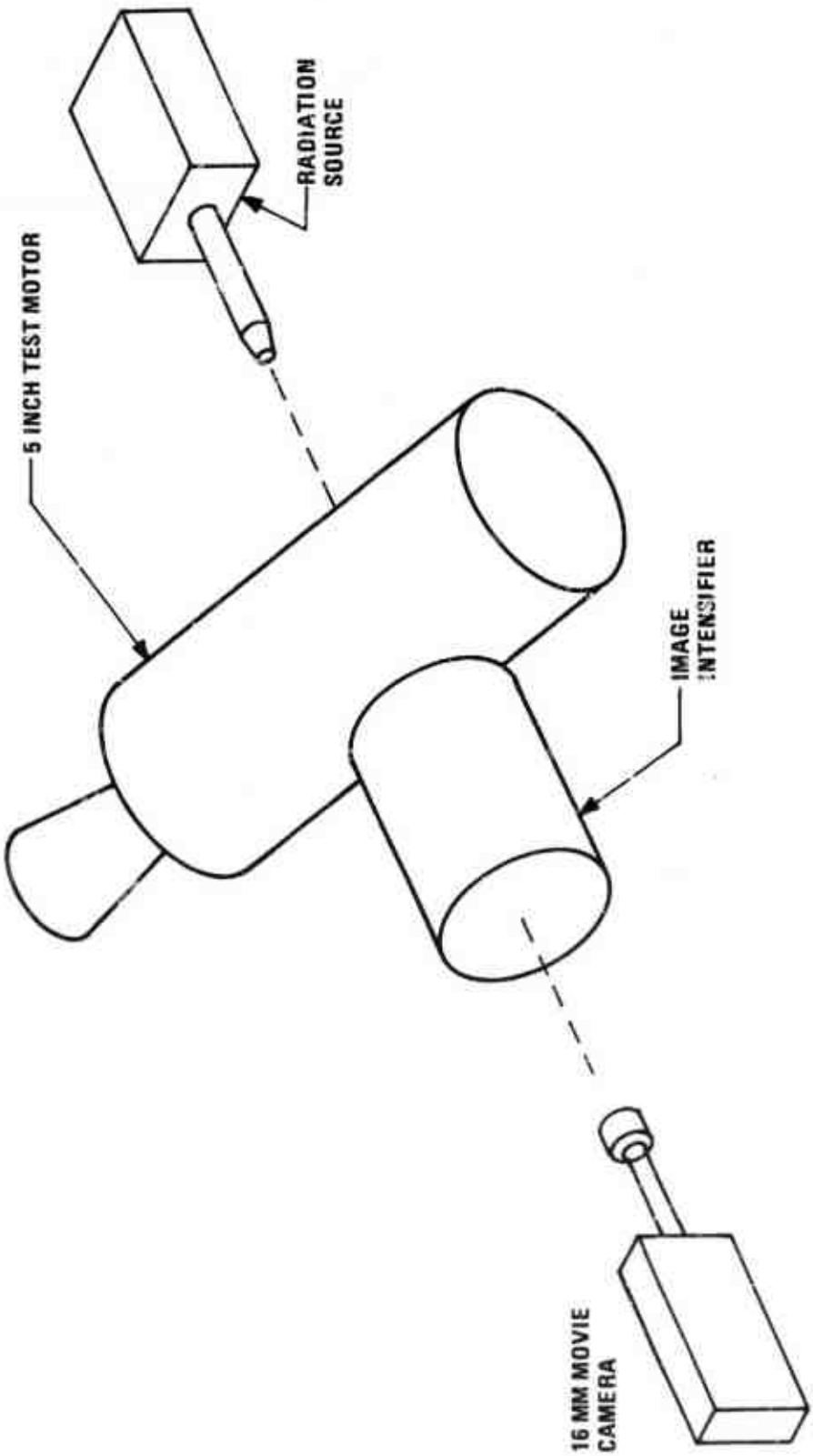

Figure 5. Cineradiographic Test Apparatus.

Norelco image intensifier. The intensifier converts this shadowy image into a highly intensified reproduction on the 0.63 inch diameter output screen. The image appearing on the output screen was photographed with a 16 millimeter Bell and Howell movie camera operating at eight frames per second. The results thus obtained were satisfactory, but higher frame rates are essential for transient burning rate data. By using the best image intensifiers available, film speeds of up to 100 frames per second can be achieved with this type of apparatus. The burning rate is determined by using a film reader to observe and measure the burning surface regression between each frame on the film.

In addition to burning rate measurements, this technique is adequate for monitoring small motors during static test firing in case unusual events occur and for determining erosion characteristics of propellants and chamber materials. Thus, cineradiography may ultimately become a very useful tool in solid rocket research. At present, though, it is not adequate to yield transient burning rate data, because of its lack of resolution, i.e. its ability to accurately locate the burning surface.

A method for continuous, high resolution measurement of the burning rate of solid propellants has been tested by researchers at the University of Waterloo in Ontario (11). This method consists of using a solid propellant strand as the dielectric material in a capacitor. This capacitor is used as part of the total capacitance of a parallel, resonant L-C circuit, as shown in Figure 6, oscillating at a center frequency of 10.7 megahertz. The change in resonant frequency is directly proportional to the change in circuit capacitance. In turn, the change

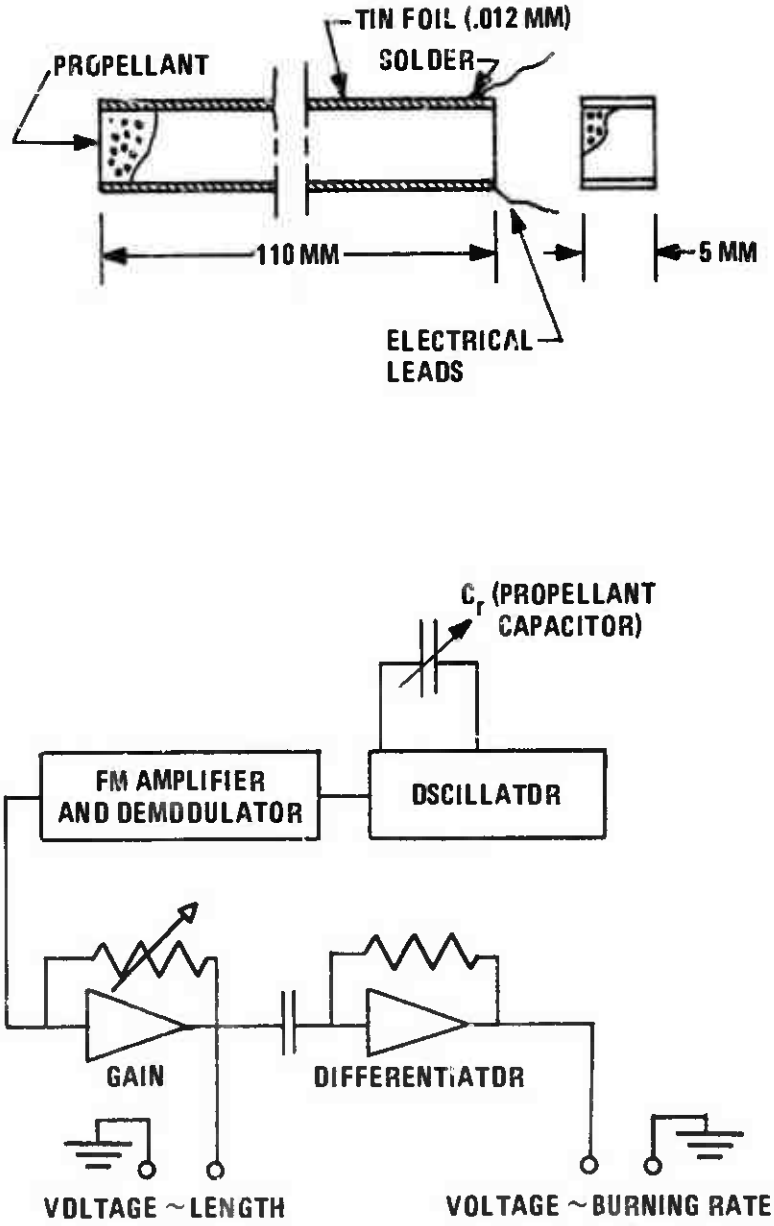

Figure 6. Propellant Strand Capacitor and Circuit Block Diagram.

in capacitance is proportional to the change in length of the strand, and the rate at which the capacitance changes with time yields the propellant burning rate. By conversion of the resonant frequency variation to a voltage variation, a signal directly proportional to the instantaneous length of the unburned portion of the strand was obtained. Simultaneous electrical differentiation of this voltage resulted in a signal directly proportional to the instantaneous burning rate of the propellant strand. The conversion of the resonant frequency variation of the L-C circuit containing the propellant capacitor was accomplished by the use of an FM intermediate frequency amplifier and demodulator. The resonant circuit was incorporated in a transistor oscillator, which supplied the frequency modulated signal to the FM amplifier and demodulator. A more recent study (12) utilized this capacitance method to take rapid depressurization data for several different solid propellants.

Through a brief analysis, it was deduced that the capacitance method has a length resolution capability on the order of five microns (11). However, this five micron ΔL is actually the magnitude of the error introduced through the instability of the constructed oscillator. This means that, neglecting all other sources of error, a five micron ΔL could be measured only to within plus or minus five microns, a 100 percent error. Thus, the minimum ΔL that can actually be measured with ten percent accuracy would be a 50 micron length change. Another source of error with this technique lies in the fact that the conductance of the flame itself must always be accounted for and the corrections which are derived from the theory involve many assumptions which are subject

to debate. This method appears to have good potential in the measurement of solid propellant burning rates, but the signal noise generated by the flame must always be dealt with.

An ultrasonic pulse-echo apparatus, illustrated in Figure 7, which has been shown to give excellent steady state burning rate results and should require little, if any, refinement in order to measure transient burning rates, was tested at NASA's Langley Research Center (13). The pulse-echo technique consists of transmitting a high frequency (20,000 Hz) sound pulse through a test specimen of propellant and recording the time required for that pulse to be reflected back from the burning surface to its original source. If the velocity of sound in the test specimen is known, a simple calculation gives the total distance traveled by the sound pulse. This technique is made possible by the step change in acoustic impediance between the solid propellant and its combustion gases, which causes most of the incident acoustic energy to be reflected back to the source. In this investigation (13), the rate at which the acoustic pulses are generated were selected by the operator from range of up to 1200 pulses per second. Each pulse emitted by the synchronizer initiated the operation of the pulse generator and the sweep circuit. The pulse generator then transmitted a high frequency electrical pulse to the ultrasonic transducer. This transducer embodied a piezoelectric crystal which converted the electrical pulse into an ultrasonic pulse. The ultrasonic wave passed through the test sample and was reflected from the various interfaces. When the reflected pulse arrived back at the transducer face, the same piezoelectric crystal converted the induced mechanical vibrations back into an electrical signal. The amplifier was

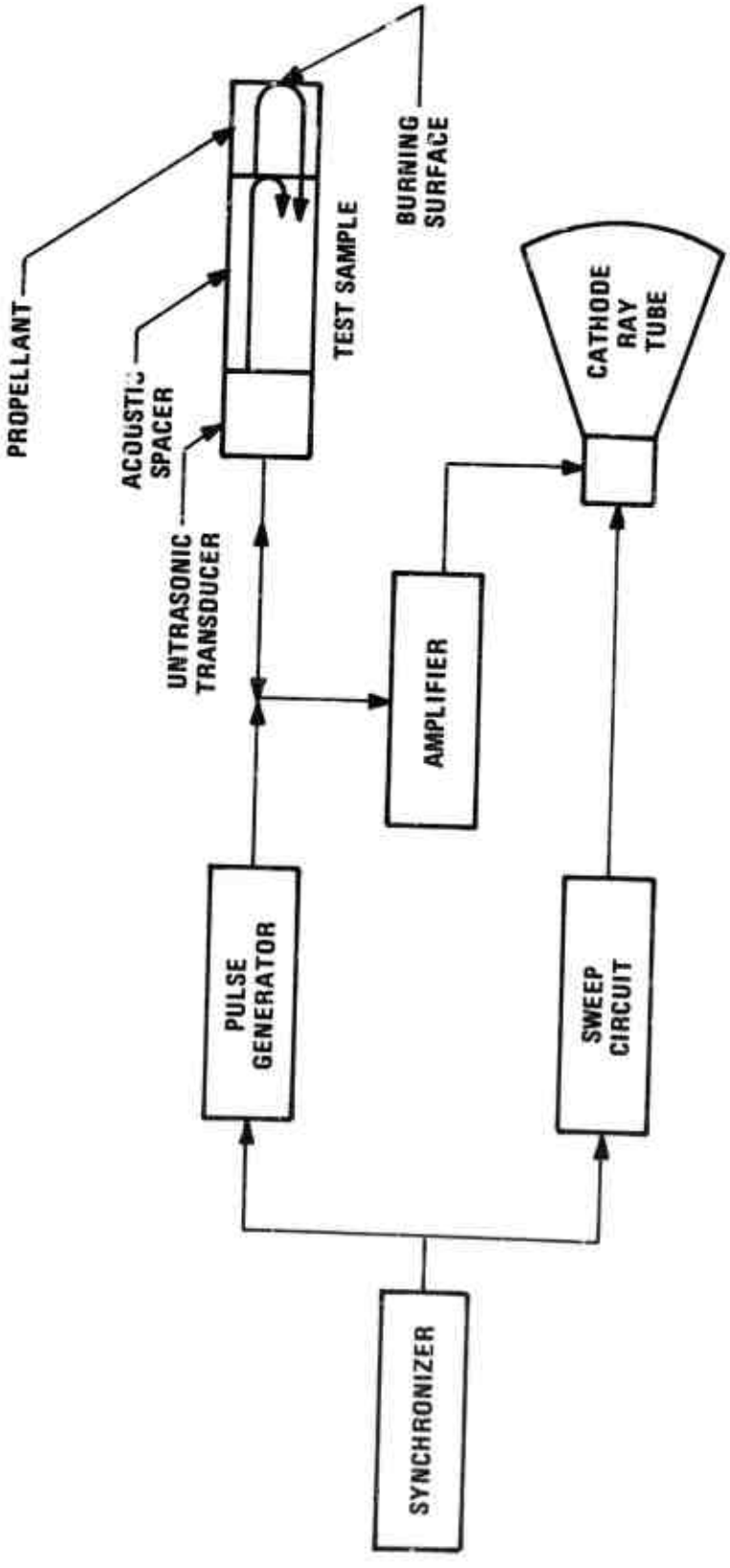

Figure 7. Schematic of Ultrasonic Pulse-Echo System.

then used to increase the electrical signals to a level that could be used to drive the vertical plates of the cathode ray tube. By utilizing a relatively high synchronizer pulse rate, it was possible to obtain an essentially continuous display of the distance traveled by the burning surface. High speed photography was then used to provide a time history of the display. Film readers permitted the acquisition of the required data which was then converted into a curve of propellant thickness burned versus time, the slope of which yields the burning rate.

Since it was not always possible to know the precise velocity of sound in the propellant, the instantaneous thickness of the propellant was found as follows. First, the length of the unburned propellant strand was measured. Second, the relative distance on the cathode ray tube between the reflections from the fixed interface (acoustic spacer rod-propellant) and from the moving interface (propellant-combustion gases) were noted with respect to time. This allowed a corresponding linear relationship to be established between the distance traveled by the signals on the tube and actual propellant length burned. Naturally, the main sources of error arise in measuring and interpreting the distances traveled by the signals on the tube. This fact limits the length resolution of the technique. However, the method already has excellent time response characteristics, and with improved data display and reduction equipment, could likely be used to obtain reliable transient burning rate data.

The first use of a microwave technique for the measurement of solid propellant burning rates was recorded by Giannini Controls in 1962 (14). In this demonstration a microwave beam was directed through a

propellant strand from the end opposite the burning surface as in Figure 8. In this arrangement, the microwave beam from the oscillator was first split into two signals, one which traveled away from the "T" down the control arm and the other which traveled down the measurement arm. The wave in the control arm was reflected by a sliding turner and traveled back to the "T" at the original frequency. The wave in the measurement arm was reflected by the burning surface and also traveled back to the "T". Thus, as the propellant strand burned and the microwave path length in the measurement arm decreased, an imbalance between the two reflected signals occurred at the "T". A signal proportional to this imbalance was sent by the "T" to the crystal detector. The resulting maxima and minima at the crystal detector occurred in successive quarter wavelength intervals. By recording the rate at which these maxima and minima occurred on an x-y recorder swept at one inch per second and by measuring the wavelength of the microwave beam in the propellant, it was possible to obtain the burning rate of the propellant strand.

A similar but slightly more refined microwave system was demonstrated by the Rohm and Haas Redstone Arsenal Division in Huntsville, Alabama (15). In this system it was recognized that reflections are not only caused by the burning surface but also by the interface between the air filled waveguide and the transition section leading into the propellant. For this reason, instead of assuming that all the reflected energy was coming from the burning surface, the Rohm and Haas system, shown in Figure 9, allowed the portion of the incident wave reflected by the fixed interfaces to mix with that reflected by the burning

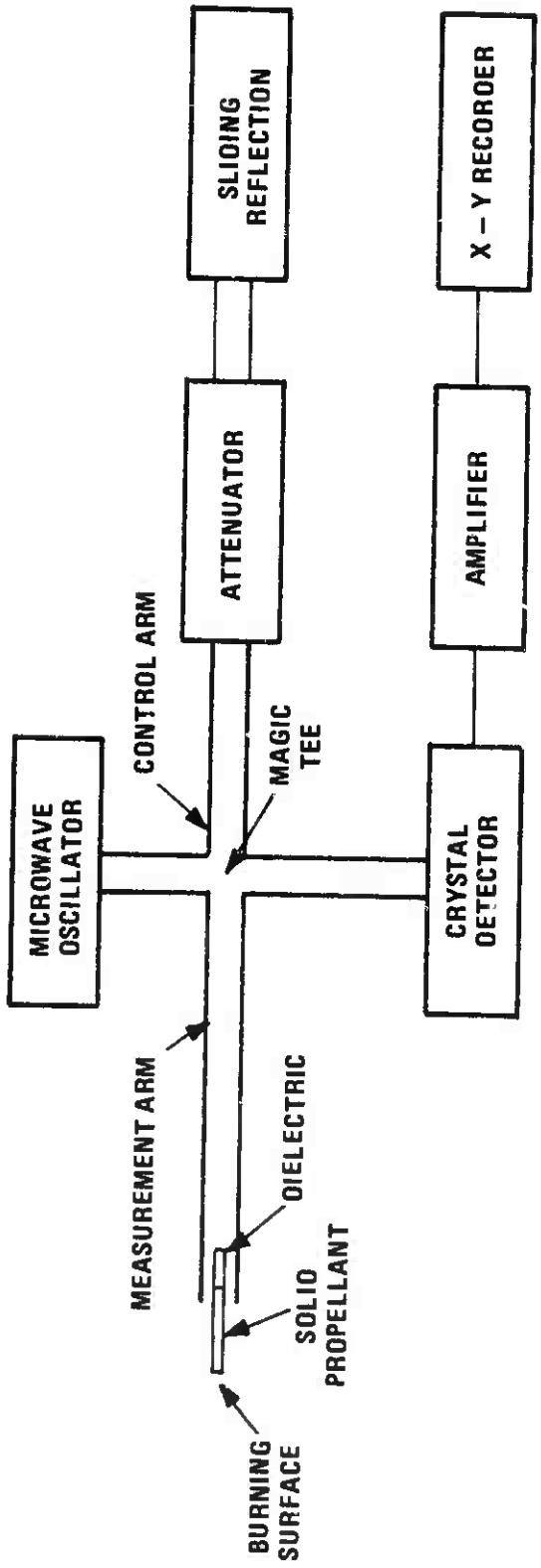

Figure 8. Schematic Diagram of Giannini Controls Microwave System.

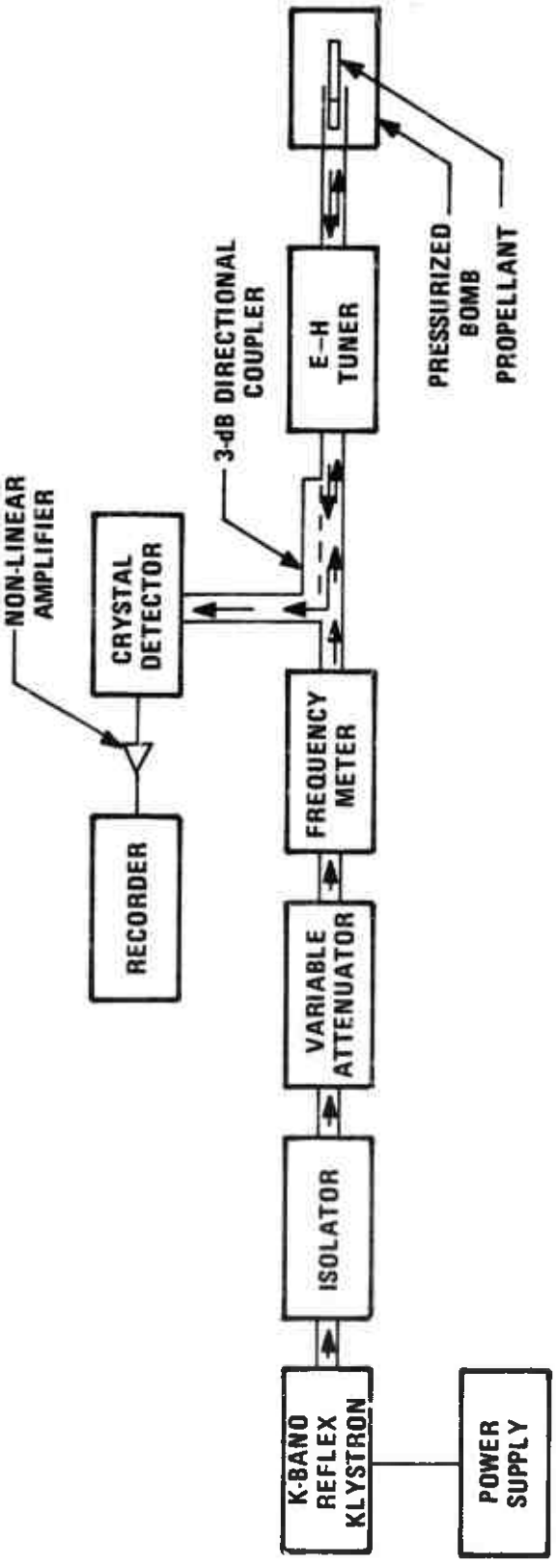

Figure 9. Schematic Diagram of Rohm and Haas Microwave System.

surface, thus yielding a truer indication of the burning rate when the analysis given below was employed.

The basic principle of both of the above microwave techniques is illustrated in Figures 10 and 11. A signal at a source frequency, f_i, is passed through a propellant strand from the end opposite the burning surface. It is reflected from the burning surface, and due to the motion of this surface, undergoes a doppler frequency shift, expressed as

$$f_r - f_i = f_i\left(\frac{2r/c}{1-r/c}\right) = \frac{2r}{\lambda_{p_g}}, \qquad (1)$$

where f_r is the frequency of the reflected signal, r is the burning surface velocity, and c is the speed of light. This frequency shift is commonly measured by allowing the reflected signal to mix with a signal of the incident frequency, resulting in a traveling wave with amplitude maxima (commonly known as beats), as shown in Figure 11. The frequency at which the beats occur is given by $f_r - f_i$.

Assuming a large burning rate of one inch per second and an incident frequency of 30 gigahertz (30×10^9 seconds^{-1}), the beat frequency is found to be about 10 beats per second (2). Since at least one half of a beat must be observed before the beat frequency can be determined, 50 milliseconds is the smallest time increment over which average burning rates may be obtained. At dP/dt values of 2000 psi per second, this yields burning rate data averaged over a 100 psi range, regardless of what the resolution capability may be. This simple fact renders this technique, often called the microwave interferometric approach, incapable of yielding accurate burning rate data during rapid pressure excursions. However, the microwave interferometric method, due to the simplicity of

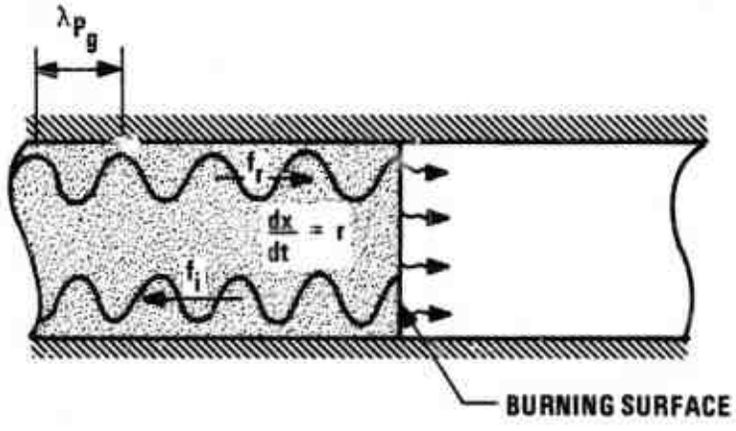

Figure 10. Doppler Shift Principle.

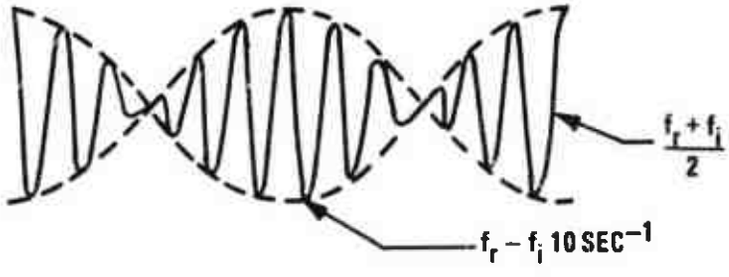

Figure 11. Determination of Doppler Shift by Superposition.

both its theory and its necessary equipment, is a very reliable method for burning rate measurements at near steady state conditions.

Summary

In the field of solid propellant technology, there is a great need for reliable unsteady state experimental data. Propellant characteristics must be known under various operating conditions for use in directly predicting the occurrence of combustion instability and in evaluating theoretical combustion models. Though, in the past, trial and error production methods have often eliminated instabilities, a better understanding of the behavior of propellants in unsteady environments is necessary before the phenomenon of instability can be entirely avoided.

Other than the microwave system to be described in the remainder of this thesis, only one technique, the propellant capacitance method, exhibits the fundamental potential to measure solid propellant burning rates under fully unsteady conditions. Several other experimental methods, including the microwave "interferometric", and the cineradiographic methods, have been found to yield excellent burning rate results at conditions near steady state, but have fundamental limitations which prevent their use in unsteady state experiments.

Under contract from the Air Force, a microwave apparatus, based on the system described in reference (2), has been assembled and used for the measurement of solid propellant burning rates. The objective of the investigation was to demonstrate the capability of the microwave continuous measurement technique by using it to measure the unsteady state burning rate of a CTPB composite solid propellant undergoing rapid depressurization.

Several preminary tests were conducted to determine the effects of propellant surface roughness on the resolution of the equipment. Also some steady state tests were made in order to compare the burning rates at particular pressures under steady and unsteady conditions. Further studies are continuing with the ultimate goal being to determine the response function, the complex quantity relating burning rate oscillations to pressure oscillations at a given frequency, of several different solid propellants to pressure disturbances of various frequencies.

CHAPTER II

MICROWAVES AND THE CONTINUOUS MEASUREMENT TECHNIQUE

Review of Microwave Theory

This section will briefly describe the basics of microwave propagation and introduce several terms that will appear later in the discussion.

Microwaves are electro-magnetic waves which propagate at the speed of light with frequencies between 0.1 and 30 gigahertz ($0.1\text{-}30 \times 10^9$ cycles per second) and have wavelengths much greater than the radiation of the visible spectrum.

Microwaves may travel in unbounded space or on conducting paths, whose form may be that of coaxial cables or metallic waveguides. The frequencies which may propagate in a given waveguide configuration are determined solely by the inside dimensions of the waveguide, whether it be rectangular or circular. The frequency below which propagation will not occur is called the "cut-off frequency". By operating a microwave waveguide system as near to the cut-off frequency as possible. it is relatively certain that only one mode (frequency) is propagating in the waveguide. The system under discussion utilizes X-Band waveguide and instrumentation. X-Band is the range of microwave frequencies from 8.2 to 12.4 GHz.

The actual theory of the propagation of the microwave in the waveguide is rather complicated (16). It is sufficient to say here that, when the system is operating near the cutoff frequency, only the lowest frequency mode is allowed to propagate down the waveguide. This lowest

mode, in most cases turns out to be what is referred to as the TE_{10} mode. "TE" stands for "transverse electric" and means that the electric field is everywhere transverse to the direction of propagation. The subscript indicates that there is one half wave variation of the electric field intensity along the narrow dimension of the waveguide, assuming a rectangular waveguide configuration is being used, and no half-wave variations of the electric field intensity along the narrow dimension of the waveguide. The TE_{10} mode has the longest operating guide wavelength and is designated as the dominant mode. For the dominant mode the cut-off wavelength (corresponding to the cutoff frequency) is given by

$$\lambda_c = 2a, \tag{2}$$

where a is the wide dimension of the rectangular waveguide.

The power of a microwave is often indicated in dBm, which is given by

$$P_{dBm} = 10 \log_{10}\left(\frac{P_{mW}}{1_{mW}}\right), \tag{3}$$

where P_{mW} is the power in milliwatts. When the power P_1 of one signal is referenced to the power P_2 of a second, the ratio may be expressed in dB, as

$$P_{dB} = 10 \log_{10}\left(\frac{P_{1mW}}{P_{2_{mW}}}\right). \tag{4}$$

In the transmission of microwaves it often becomes necessary to pass through attenuating materials or dielectrics. The properties of a dielectric are expressed in a complex quantity called the dielectric constant $\varepsilon/\varepsilon_o$, which is given by

$$\epsilon/\epsilon_o = \epsilon'/\epsilon_o + j\,\epsilon''/\epsilon_o. \qquad (5)$$

ϵ'/ϵ_o is the real part, which itself is often referred to as the dielectric constant, and ϵ''/ϵ_o is the imaginary part. The tangent of the phase angle ϕ is often used as a measure of attenuation, called the "loss tangent" and given by

$$\tan \phi = \epsilon''/\epsilon'. \qquad (6)$$

It should be emphasized at this point that when restricted by the conducting walls of a waveguide, the guide wavelengths and velocities of microwaves may be higher than their unbounded space values. These "stretched" parameters are called the "group wavelength" and "group velocity" respectively and are usually subscripted with "g". The equation for the "group wavelength" of a microwave propagating through a dielectric-filled rectangular waveguide as given in reference (17) is

$$\lambda_g = \lambda_o\left(\frac{\epsilon'}{\epsilon_o} - \frac{\lambda_o^2}{\lambda_c^2}\right)^{-\frac{1}{2}} \left\{ \frac{1}{2} + \frac{1}{2}\left[1 + \left(\frac{\frac{\epsilon''}{\epsilon_o}}{\frac{\epsilon'}{\epsilon_o}\frac{\lambda_g^2}{\lambda_c^2}}\right)^2\right]^{\frac{1}{2}}\right\}^{-\frac{1}{2}} \qquad (7)$$

where

λ_o = wavelength of wave of frequency w in free space

λ_c = cutoff wavelength of waveguide

λ_g = group wavelength of wave of frequency w in waveguide

ϵ'/ϵ_o = real part of dielectric constant

ϵ''/ϵ_o = imaginary part of dielectric constant.

In the remainder of this thesis, λ_g will refer to the group wavelength in X-Band waveguide filled with air ($\epsilon'/\epsilon_o = 1$ and $\tan \phi = 0.0$) and λ_{pg} will refer to the group wavelength in propellant-filled waveguide,

the propellant being a dielectric material.

Microwaves may be wholly or partially reflected by interfaces of materials of different dielectric constants. This fact is the basis for using a microwave to detect the position of the burning surface of a solid propellant strand. At the moving interface between the solid unburned propellant and its combustion gases, a portion of the incident power is reflected. However, by carefully designing the interface between the air-filled standard X-Band wave guide section and the propellant holder (an impedance matching process), it is possible to greatly reduce most reflections from this fixed interface. As a result, the majority of the reflected power returning from the combustion chamber is that reflected by the moving, burning surface.

Reflections on microwave transmission lines are often given in terms of the voltage standing wave ratio or VSWR, which is defined as

$$VSWR = \frac{E_i + E_r}{E_i - E_r} = \frac{E_{MAX}}{E_{MIN}}, \qquad (8)$$

where E_i is the voltage amplitude of the incident wave and E_r is the voltage amplitude of the reflected wave. The VSWR is thus simply a ratio between the maximum voltage (incident and reflected signals in phase) and the minimum voltage (incident and reflected signals 180 degrees out of phase) on a transmission line.

Microwave Continuous Measurement Technique

The problems encountered in the microwave interferometric approach are overcome in the present microwave technique by continuously measuring the phase angle between a source reference signal and the reflected signal. This is shown in the phasor diagram of Figure 12, where ϕ_a is

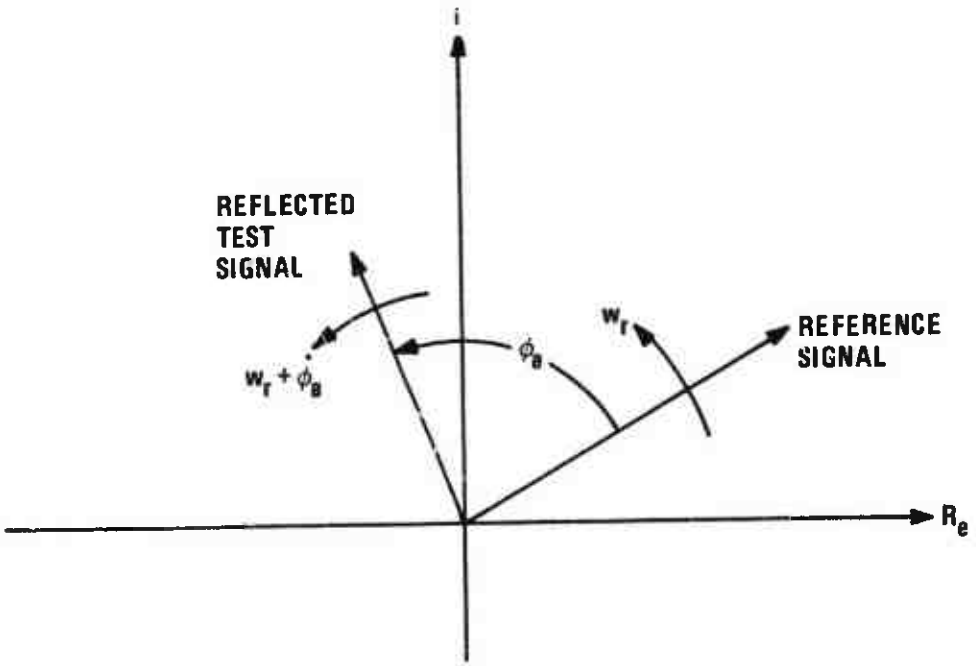

Figure 12. Phaser Diagram.

the angle to be measured. The doppler shift is equal to the derivative of this phase angle with respect to time as indicated by the following:

$$w_r = 360\ (f_i)\text{deg/sec} \tag{9}$$

and

$$w_r + \dot{\phi}_a = 360\ (f_r)\text{deg/sec.} \tag{10}$$

Subtracting equation (9) from (10) results in

$$\dot{\phi}_a = 360\ (f_r - f_i) \tag{11}$$

and from Equations (1) and (11)

$$r = \frac{\dot{\phi}_a \lambda_{pg}}{720}. \tag{12}$$

Thus, knowledge of the wavelength of the microwave in the propellant, which is easily measured, permits the determination of the burning rate. The distance traveled by the burning surface can be found by integrating Equation (12) to obtain

$$\Delta x = \frac{\Delta\phi_a \lambda_{pg}}{720},$$

where $\Delta\phi_a$ is the total change in phase angle.

In traveling into the propellant strand through the bomb window, shown in Figure 21, reflections from fixed discontinuities are created. Therefore, before each test an attempt is made to cancel all reflections (other than tha burning surface reflections) by tailoring the amplitude and phase of a signal at the source frequency and using it to cancel out the fixed reflections. This technique has succeeded in most cases in

reducing the fixed reflections to approximately 0.02 percent of the burning surface reflections. At this magnitude, it is not necessary to correct for these fixed reflections. However, it is interesting to note the effects they could have if they were large.

The effects of the fixed reflections can be seen and calculated by analysis of the phasor diagram shown in Figure 13. The quantity needed to determine the burning rate is ϕ_a and ϕ_m is the quantity actually measured. The fixed reflection is represented by vector A, rotating at the source radian frequency w_r; B is the vector representing the burning surface reflection rotating at a frequency of $w_r + \dot{\phi}_a$ with respect to a fixed axis or $\dot{\phi}_a$ with respect to the tip of A. The resultant test signal is represented by the vector C. The relation between ϕ_a and ϕ_m from geometry is

$$\phi_a = \phi_m \left[\frac{2C^2/B^2}{C^2/B^2 - A^2/B^2 - 1} \right] . \qquad (14)$$

Instrumentation is available which will measure the relative phase angle between two X-Band signals (8.2 - 12.4 GHz) to a 0.2 degree resolution. Using ϕ_a = 0.2 degrees and λ_{pg} = 1.0 inches, which is an average group wavelength of X-Band waves in propellant, the length resolution ΔL is approximately ten microns. This is well below the 64 micron resolution necessary for transient burning rate data averaged over a 50 psi pressure range.

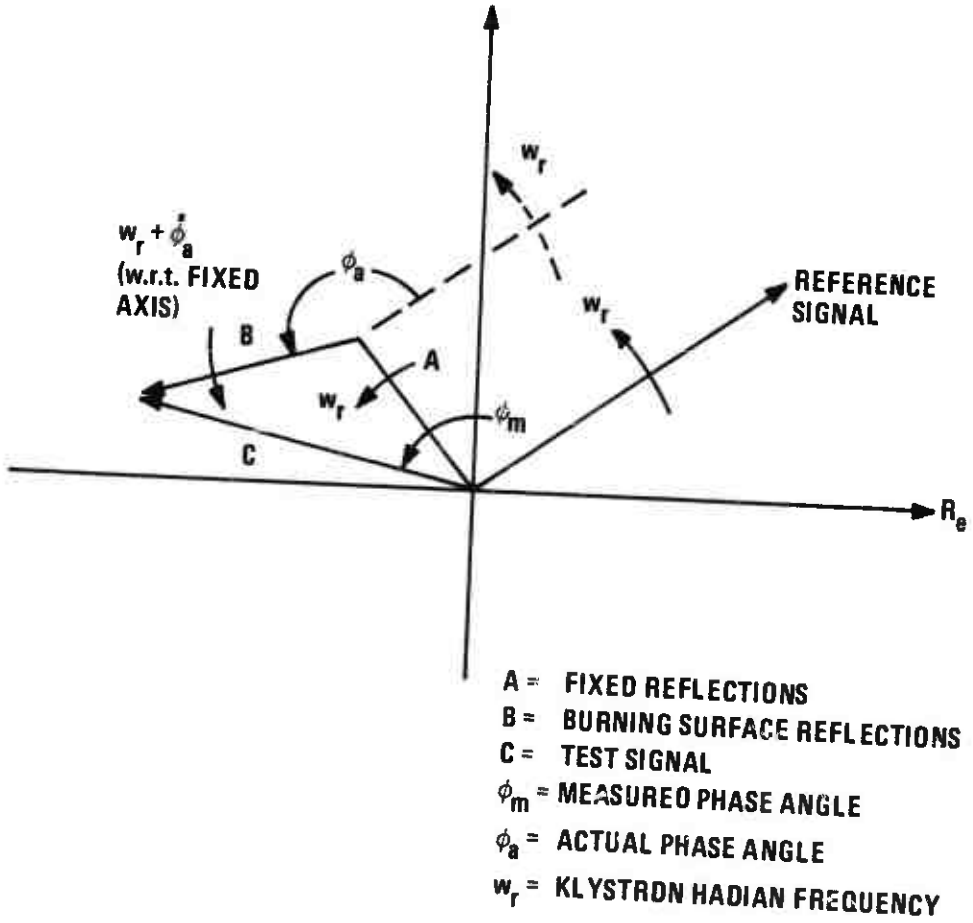

Figure 13. Phaser Diagram with Fixed Reflections.

CHAPTER III

THE INVESTIGATION

The test plan was divided into several phases. The first phase consisted of tests designed to determine the capabilities of the equipment before any propellant was actually ignited. The second phase involved some steady state burning rate tests at various pressures. The third phase entailed several unsteady burning rate tests under various rapid depressurization rates.

The first series of tests were intended to show how various types of burning surface roughness affect the measured phase angle as compared with a planar surface regressing perpendicular to the microwave beam. This had been a point of concern since the propellant strand was so long and thin (3 x 0.4 x 0.3 inches) and perfectly planar regression of the burning surface was not likely to occur in all cases.

A second investigation was then made to determine the magnitudes of fixed signals (or reflections) from within the microwave system itself (not from the transition section). These reflection tests along with the roughness tests mentioned above comprised the first phase of testing.

The second phase of testing consisted of six steady state burns at pressures of 0, 50, 100, 150, 200, and 300 psig and one slow depressurization burn from 300 to 0 psig. These tests had several purposes: 1) to test the equipment under actual combustion conditions by observing the effects of the fixed reflections (which are much harder to recognize under unsteady conditions), 2) to establish procedures for later testing,

3) to yield data with which to calculate λ_{pg} at various pressures, and 4) to yield steady state burning rates with which to compare the unsteady burning rates to be obtained from the rapid depressurization burns.

Four rapidly depressurized burns were conducted in the third test phase. The use of two different orifice plates allowed two tests at each of two different depressurization rates. The goals of these tests were: 1) to demonstrate the capability of the equipment to measure burning rates under unsteady conditions, and 2) to obtain unsteady burning rate data for comparison with steady state results.

Apparatus

The apparatus consisted of several major components. The microwave system and instrumentation generated and controlled the microwave signals and provided the data necessary to calculate the burning rate of the propellant strand. The pressure environment of the burning propellant was maintained by the bomb and the bomb control system. The data acquisition system tailored and recorded the data signals. Finally, the propellant mixing and casting apparatus was the equipment necessary to mix, cast, and cure the propellant samples. An overall view of the test apparatus excluding the bomb and the propellant casting equipment is given in Figure 14.

Microwave System and Equipment

A block diagram of the system used in the subject investigation is illustrated in Figure 15. A klystron, whose frequency is stabilized to one in 10^8 Hz per second provides a microwave signal. This signal passes through a directional coupler where ten percent of the power is

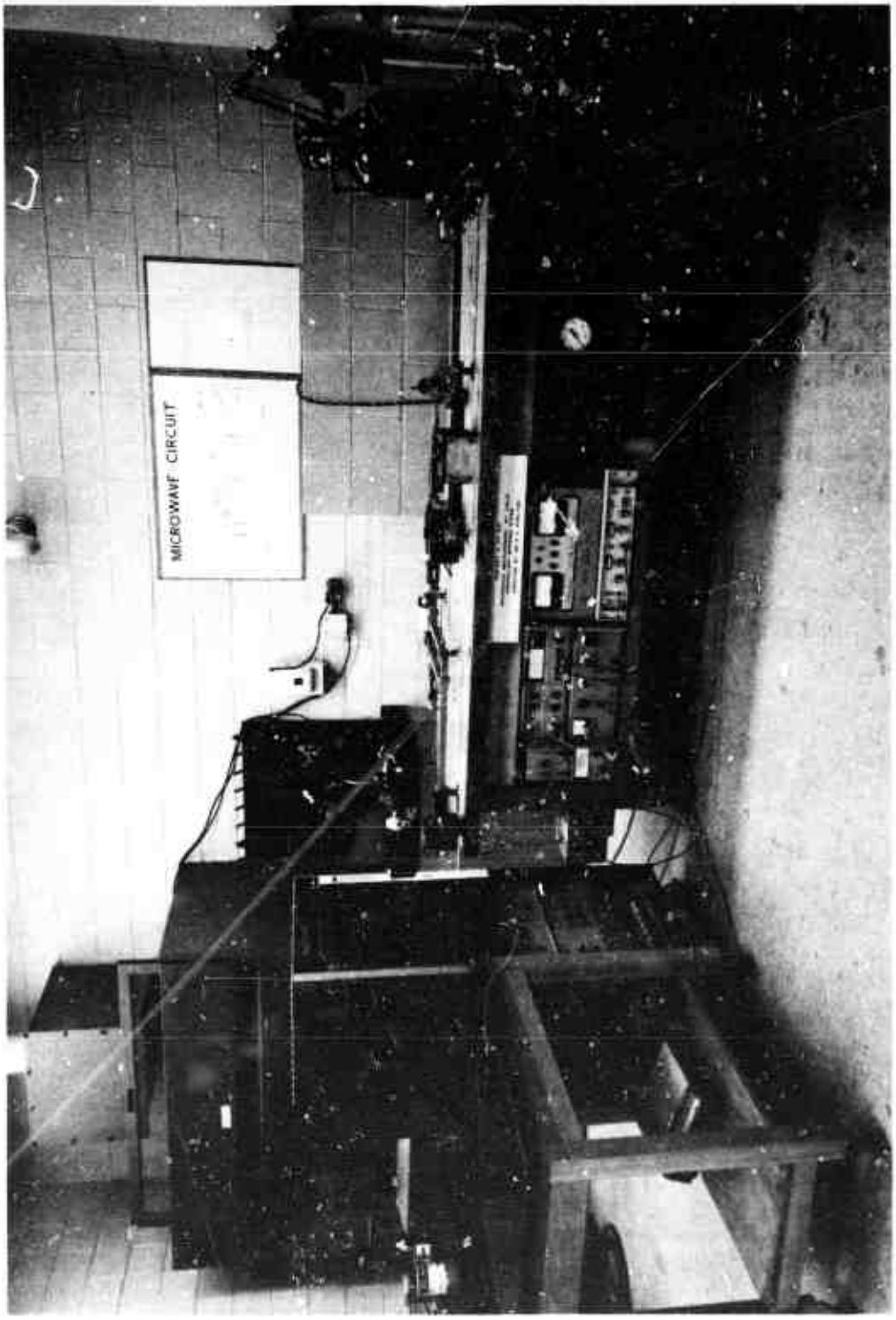

Figure 14. Control Panel and Instrumentation.

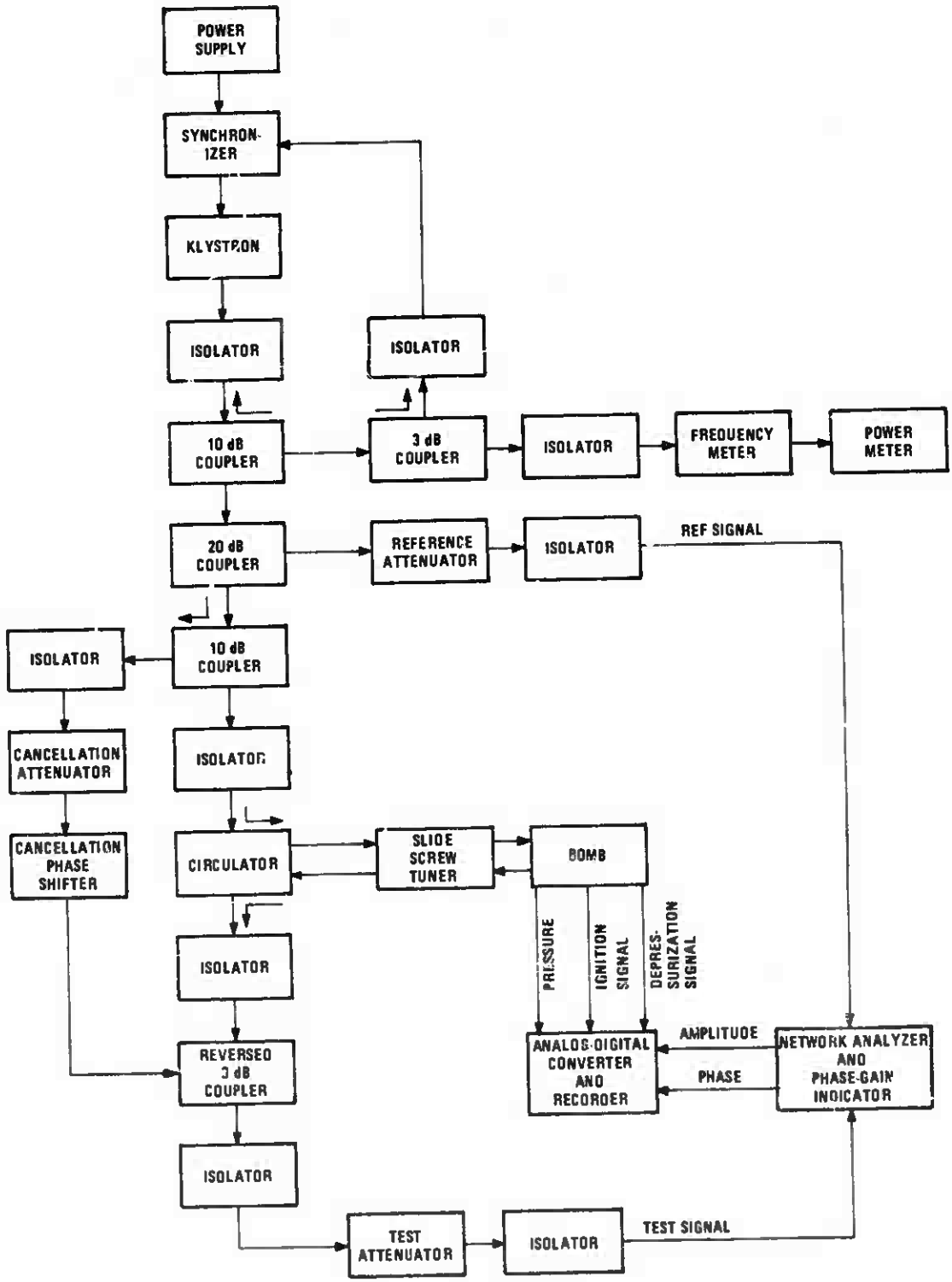

Figure 15. System Block Diagram.

diverted away. Part of this diverted signal paases to a aynchronizer, which compares its frequency with a crystal oscillator and appliea a correction to the klystron as necessary. The remainder of this diverted energy passes on to a frequency meter and then to a power meter for measurement of klystron power output. The original 90 percent of the klystron power which was not diverted passes further to another coupler where one percent is picked off to serve as a reference signal. This signal is sent on to the network analyzer. Further down the line another ten percent of the main signal is diverted to pass through a nulling loop designed to cancel out the fixed reflections from the waveguide-bomb interface. This signal is fed back into the main signal downstream of the bomb. The main signal passes on to a circulator which in turn passes the signal on to the bomb where it is reflected and undergoea a frequency shift. The reflected test signal travels back through the circulator, picks up the power diverted by the nulling loop at a reversed coupler, then passes on to the network analyzer for comparison with the reference signal. The network analyzer produces a voltage proportional to the relative phase angle and relative amplitude between the reference and test signals. These voltages along with the output of a pressure transducer and two other voltages signalling the ignition of the propellant and depressurization of the bomb are converted to digital signals and recorded on magnetic tape for later reduction by a computer.

This system incorporated some refinements over the system in reference (2). First, the extensive use of isolatora, which act as diodes allowing the microwave to pass in only one direction, eliminated many reflections that could have interfered with the results. Second, the

nulling loop was added and proved to be more efficient than the slide-screw tuner previously used to eliminate the fixed reflections generated at the waveguide-bomb interface.

Network Analyzer (Hewlett Packard Model 8410A and 8411A). The network analyzer is the heart of the system. It has the capability to measure the relative amplitude and phase of two RF signals over a frequency range of 0.11 to 12.4 GHz.

The network analyzer is provided with an amplitude control which can be used to adjust the gain of the test channel relative to the reference channel. The range of this gain is 69 dB in either 10 dB or 1 dB increments.

The network analyzer has a phase range from zero to 360 degrees and a vernier provides continuous adjustment over at least 90 degrees.

The maximum RF input to either channel is 50 mW and care must be taken not to approach this level.

Phase-Gain Indicator (Hewlett Packard Model 8413A). The phase-gain indicator, when used in conjunction with the network analyzer, provides a display of the relative amplitude and phase of two RF signals.

The phase-gain indicator is provided with a meter which has full scale readings of $\pm$3dB, $\pm$10dB, $\pm$30dB or $\pm$6, $\pm$18, $\pm$60, and $\pm$180 degrees depending on which meter function is selected. A phase-offset dial allows adjustment of the phase display in ten degree increments. In addition, the phase-gain indicator produces a voltage proportional to the relative amplitude (50 millivolts per dB) and to the relative phase (ten millivolts per degree) of the two signals being compared. These outputs were digitized and recorded on magnetic tape in the subject investigation.

Klystron Power Supply (Hewlett Packard Model 716B). The Model 716B Klystron Power Supply provides all necessary voltages for the operation of low power reflex klystrons. Beam and reflector voltages are closely regulated and continuously variable with calibrated controls. Beam voltage is variable from -250 to -800 volts with respect to chassis ground and reflector voltage is variable from zero to -800 volts with respect to the cathode. A standard 115 volt a.c. plug is provided in the rear of the power supply to operate a fan used to cool the klystron.

Synchronizer (Sage Laboratories Model 243). The Model 243 Microwave Oscillator Synchronizer is used to frequency-lock (stabilize the frequency) of the microwave oscillator (klystron). Locking is achieved at discrete fixed frequencies which are related to harmonics of a crystal reference. The synchronizer has a short-term stability of one in 10^8 per second and a long-term stability of one in 10^6 per week.

Power Meter (Hewlett Packard Model 432A). The power meter is used to monitor the klystron power output and, when used in conjunction with the frequency meter, to monitor the frequency of the klystron. The power meter is always used in conjunction with a thermister mount in the waveguide circuit.

The power meter has seven scale ranges from 0.01mW (-20 dBm) to 10mW (10dBm).

Waveguide Circuit Components. An overhead view of the microwave circuit is given in Figure 16. All components of the microwave circuitry were standard X-Band equipment, except for the tapered section leading from the X-Band guide into the bomb and the waveguide section which held the propellant. Preliminary tests of some samples supplied

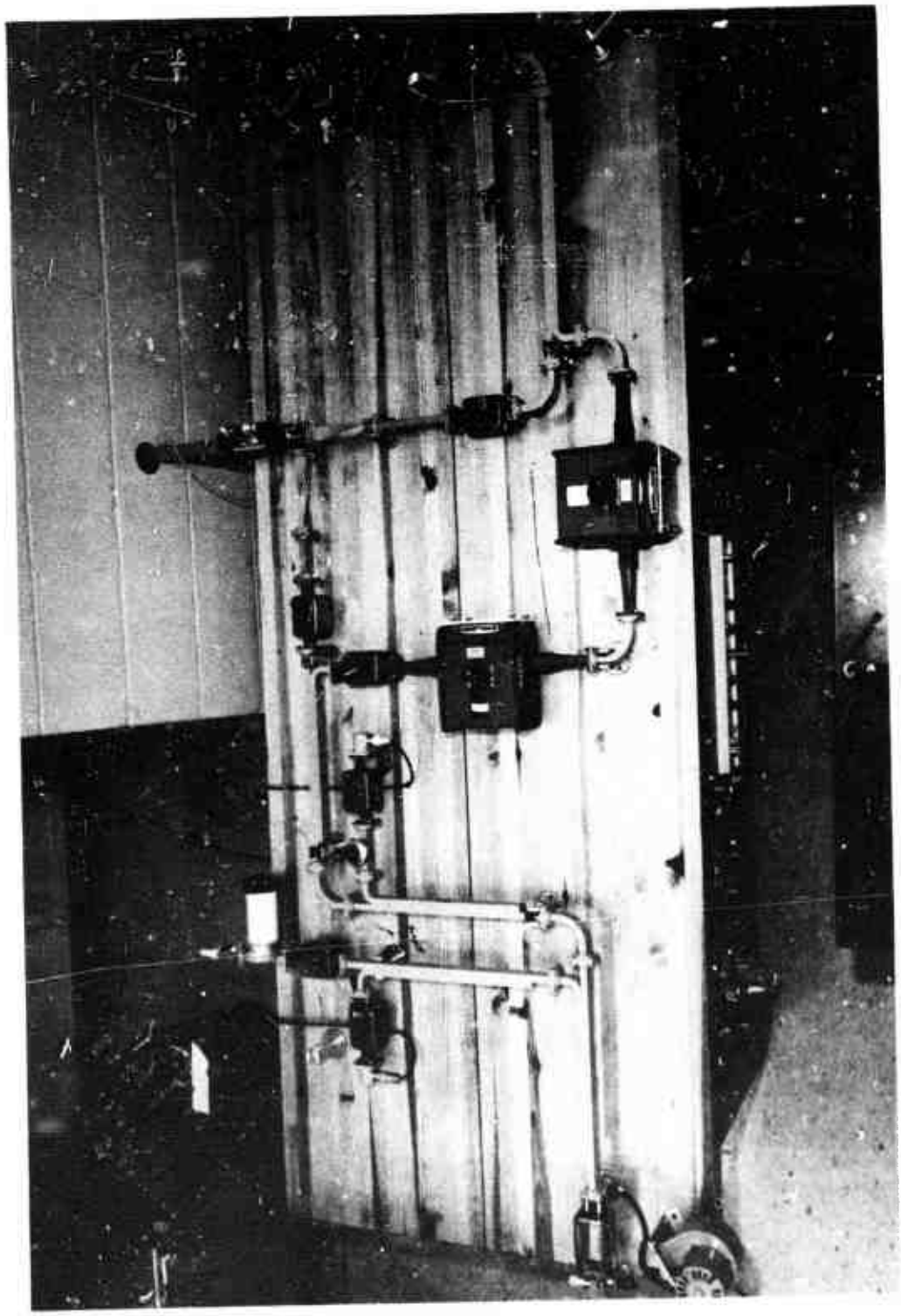

Figure 16. Microwave Circuit.

by the Jet Propulsion Lab indicated that non-aluminized CTPB propellant has a real dielectric constant of about 4.2 and a loss tangent of 0.008. With these figures in mind, microwave engineers at the Georgia Tech Engineering Experiment Station designed the transition section which adapted from the X-Band dimensions (0.9 x 0.4 inches inside dimensions) to a section, which when filled with a material whose dielectric constant is approximately four, would allow X-Band waves to propagate (Figure 17). It wasfound that inside dimensions for this test section should be 0.3 x 0.4 inches. As part of the impedance matching process a long thin taper of dielectric material was designed to provide a sealing window for the bomb and to provide a smooth transition from the air-filled X-Band waveguide to the propellant holder section, as shown in Figure 17.

The transition section waveguide which was cast out of copper, was mounted through the dielectric window retainer of the bomb with silver solder. The dielectric taper was then epoxied into the copper waveguide to provide the pressure seal between the bomb and the unpressurized X-Band waveguide circuit.

Before the transition section was actually used in burning rate tests, it was decided that aplot of reflection coefficient P which is related to VSWR by

$$VSWR = \frac{p + 1}{p - 1}, \tag{15}$$

at various frequencies should be obtained. This was necessary in order to determine the frequency at which fixed reflections were minimized. The plot shown in Figure 18 was produced. A scale is not indicated on the vertical axis of Figure 18 because it would vary with frequency. The plot is linear in reflection coefficient and the dotted line

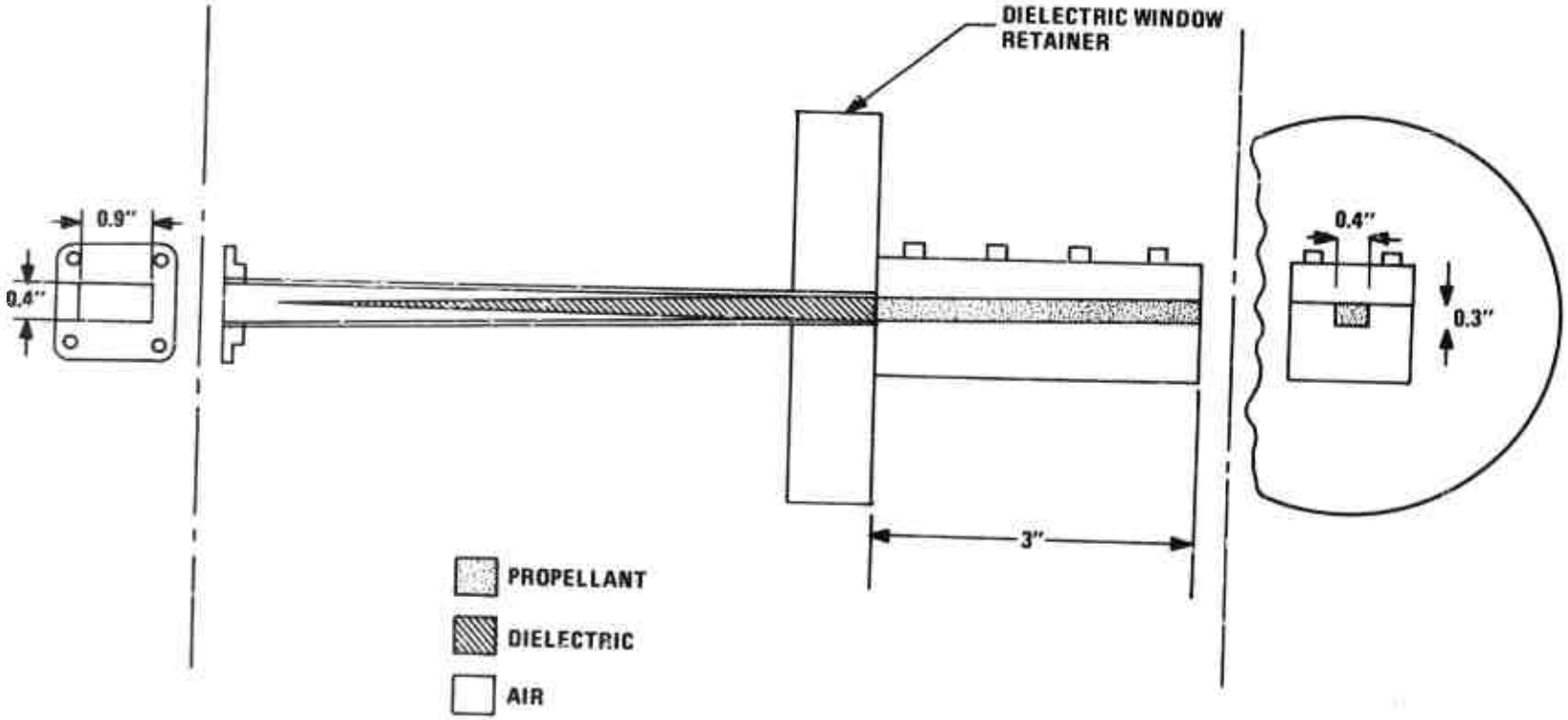

Figure 17. Microwave Electrical Path.

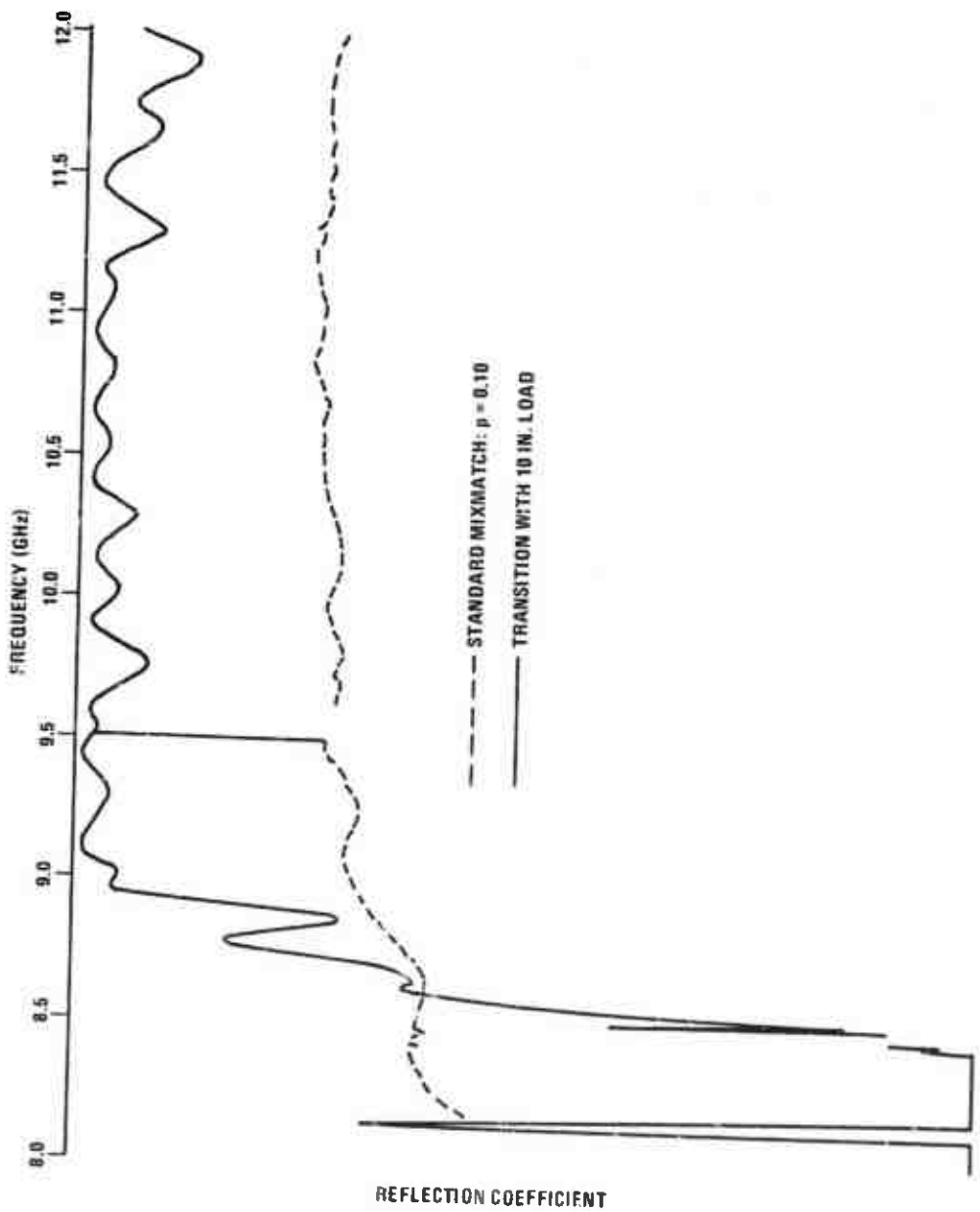

Figure 18. Plot of Transition VSWR vs. Frequency.

corresponds to p = 0.10.

Microwave engineers at the Engineering Experiment Station had calculated that at 9.6 GHz the possibility existed for higher order modes to propagate in the propellant. This precluded operation above 9.6 GHz. The high VSWR's and reflection coefficients indicated at frequencies below 9.0 GHz made it unadvisable to operate in that region also. The operating frequency of 9.13 GHz was finally chosen because it combined the good features of yielding a low VSWR, thereby minimizing fixed reflections, and being close to a harmonic of the crystal oscillator in the synchronizer, yielding good stability of the klystron signal.

Twelve propellant holder sections (Figure 19) were machined from aluminum. These were fashioned in two parts to provide ease of machining and cleaning. Four holes were provided in each end to provide alignment with four one-eighth inch dowel pins mounted on the stainless steel dielectric window retainer. Good alignment of the sample holder and dielectric window is essential since small misalignments can increase VSWR's substantially. Initially, the sample holders were made four inches long, but, in order to provide for easier casting of the propellent, the length was shortened to three inches.

Two loads were also constructed, see Figure 20, to aid in the cancellation of the fixed reflections from the waveguide transition. A load is a device which absorbs all, or essentially all, of the incident energy. The loads had the same internal dimensions of the sample holders but one load was 36 inches long and the other ten inches long. Both had tapers made of high loss material inbedded in one end of them. CTPB propellant was cast in both samples through the courtesy of Thiokol at Huntsville.

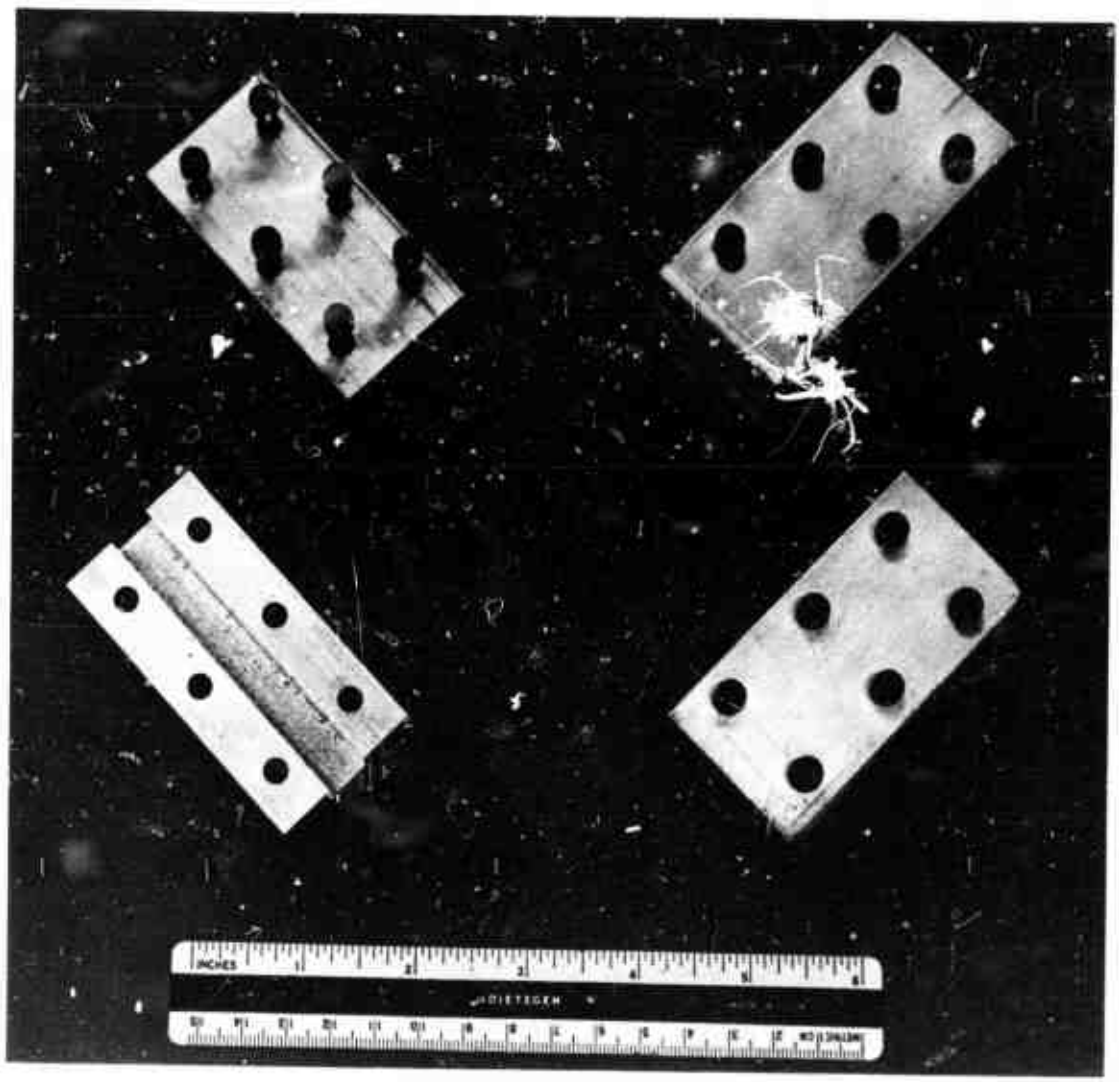

Figure 19. Sample Holder (Before and After Casting).

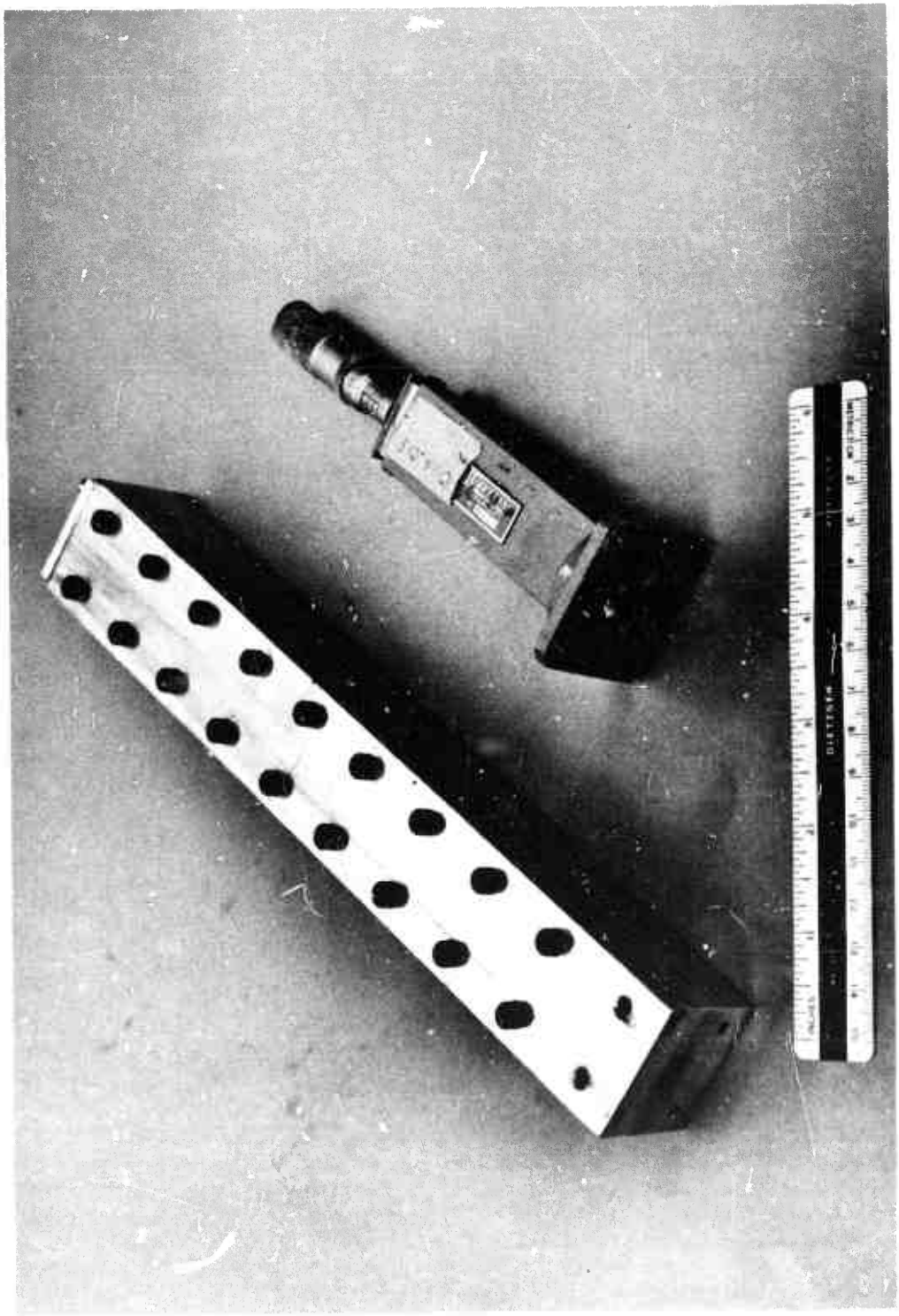

Figure 20. Ten Inch Load and Short.

Both loads were tested and it was found that the shorter load was the more efficient, possibly because bubbles had become imbedded in the longer load when it was cast. The shorter load was thus used in all subsequent testing.

A list of the standard components of waveguide circuitry and microwave instrumentation utilized in the investigation is given below.

List of Microwave Instrumentation:

1) Item: Network Analyzer
   Model: 8410A and 8411A
   Manufacturer: Hewlett-Packard, Palo Alto, California
   Time Constant: 6 μsec
   Frequency Range: 0.11 to 12.4 GHz
   Amplitude Range: 69 dB total in 10- and 1-dB steps
   Phase Range: zero to 360 in ten degree steps
   Inputs: 115 volts a.c., 70 watts

2) Item: Klystron Power Supply
   Model: 716B
   Manufacturer: Hewlett-Packard, Palo Alto, California
   Inputs: 115 volts a.c., approx. 200 watts
   Outputs: Reflector voltage 0-800 volts
   Beam Voltage 250-800 volts
   Filament Supply 6.3 volts d.c.
   Fan Supply 115 volts a.c.

3) Item: Phase-Gain Indicator
   Model: 8413A
   Manufacturer: Hewlett-Packard, Palo Alto, California
   Inputs: Internal connection with Network Analyzer HP8410A
   Outputs: 50 mv/dB, 10mv/deg
   Ranges: $\pm$3, $\pm$10, $\pm$30 dB, $\pm$6, $\pm$18, $\pm$60, $\pm$180 degrees

4) Item: Microwave Oscillator Synchronizer
   Model: 243
   Manufacturer: Sage Laboratories Instrument Division, Natick, Mass.
   Inputs: Line-115 volts a.c.
   R.F. Input-20 dBm at X-Band
   Outputs: Klystron Reflector 2000 volts d.c. maximum and up to 25 ma
   Frequency Range: 1.0 to 15.0 GHz
   Crystal Reference: 100 MHz crystal with lockpoints every 60 MHz and 40 MHz alternately
   Stability: one part in 10^8 per second

5) Item: Power Meter
   Model: 432A

Manufacturer: Hewlett-Packard, Palo Alto, California
Inputs: Line 115 volt a.c.
Ranges: 10, 30, 100, and 300 watts
1, 3, and 10 mW

List of Waveguide Circuit Components:

Quantity	Item	Manufacturer
2	Type 674-3 3dB Directional Couplers	Waveline, Inc. W. Caldwell, N. J.
2	Type 674-10 10dB Directional Couplers	"
1	Type 674-20 20dB Directional Couplers	"
2	Type 611 Shielded Variable Calibrated Attenuators	"
2	Type 690-2 90 Degree Waveguide Twist Sections	"
7	Type 632-2 E-Plane Waveguide Elbows	"
1	Type 633-2 H-Plane Waveguide Elbows	"
3	Type 601-NF Waveguide to Coaxial Adapters	"
1	Type 698-DR Frequency Meter	"
1	Model X114LT Waveguide Circulator	E&M Laboratories Westlake Village, California
8	Model X78LI Waveguide Isolator	"

Waveguide Circuitry (continued)

Quantity	Item	Manufacturer
1	Model X382A Variable Attenuator	Hewlett-Packard Palo Alto, Calif.
1	Model X885A Phase Shifter	"
1	Model X870A Slide Screw Tuner	"
1	Model X486A Thermistor Mount	"
1	Model X13 CW Klystron	Varian Associates Eastern Tube Division Beverly, Massachusetts

The Bomb

The bomb is a sealed pressure vessel (Figure 21, 22) designed to operate safely at pressures up to 10,000 psi. The main components of the bomb were manufactured from type 321-347 stainless steel. Stainless steel was chosen due to the extreme corrosiveness of the propellant and its combustion gases.

The center portion of the bomb was bored out to a diameter of three inches from a five inch outside diameter round bar. Another section of five inch outside diameter stock provided the discs which form the ends of the cylinder. The threaded retainers which hold these caps in place were turned from seven inch outside diameter stock.

The microwave taper section was mounted permanently (soldered) to the dielectric window retainer. A tapped hole was also provided in this retainer to accommodate a Teledyne igniter plug which provided the leads for the ignition circuitry.

The other end cap was designed to hold an orifice plate (Figure 23),

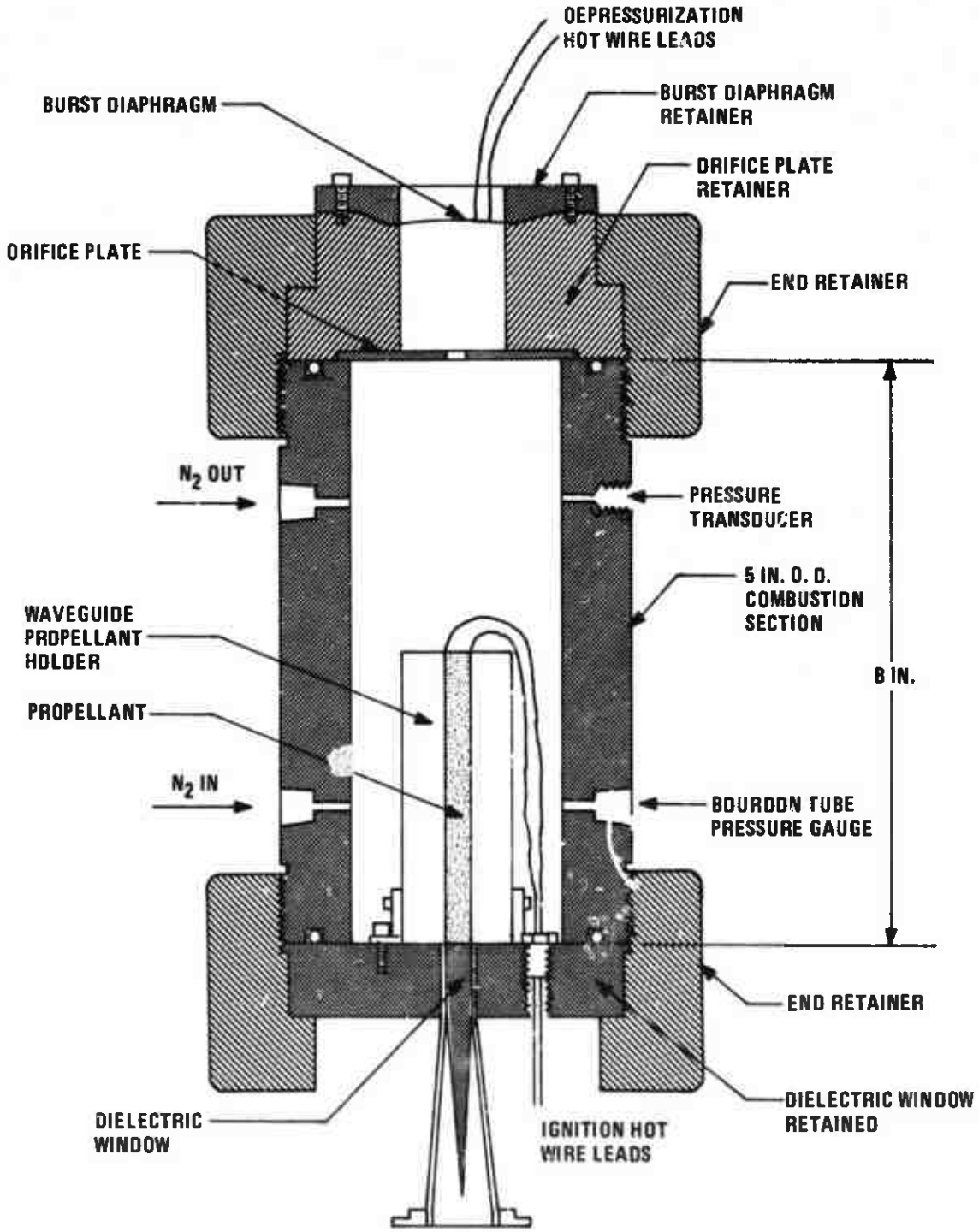

Figure 21. Diagram of Microwave Bomb.

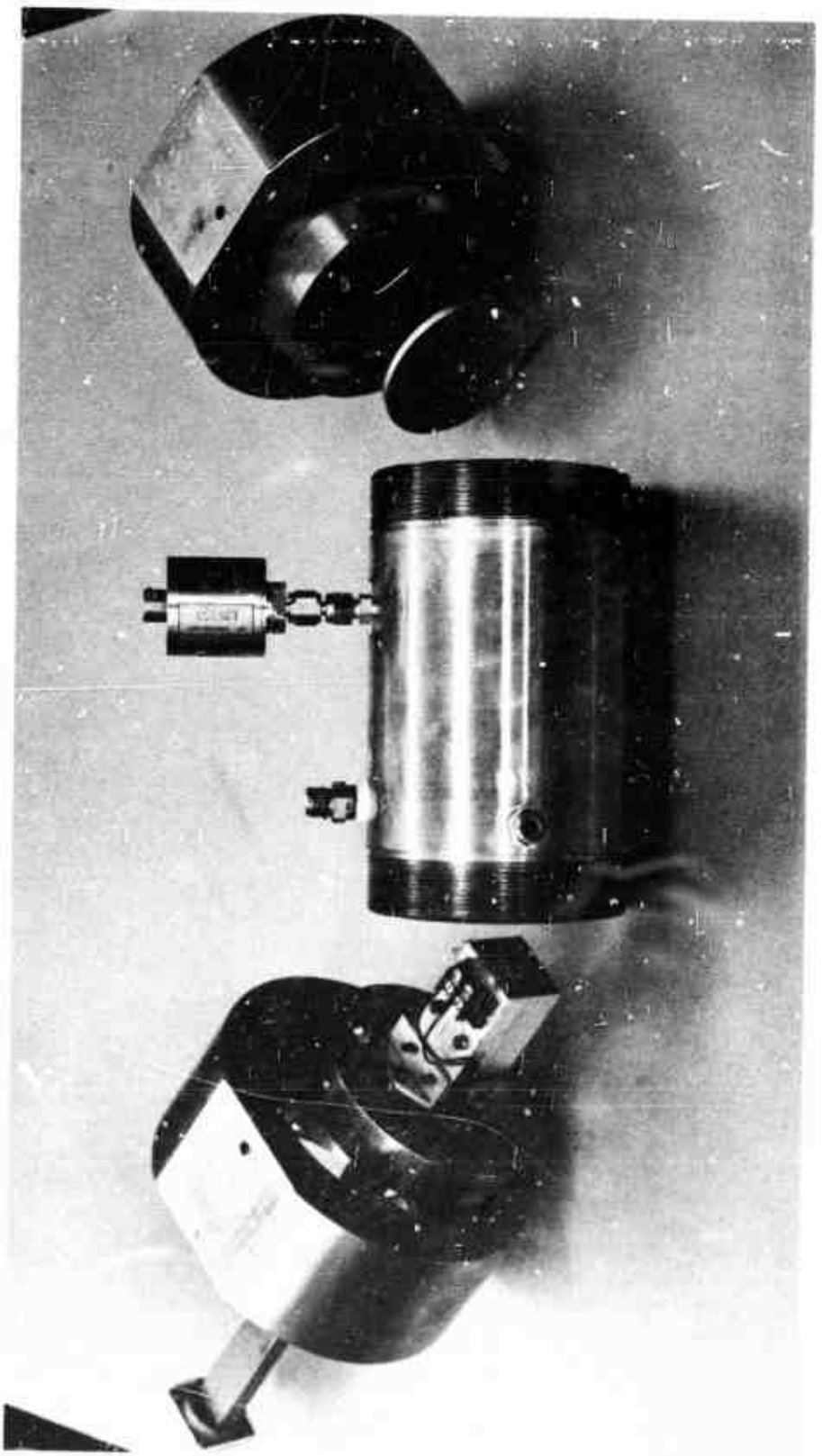

Figure 22. Exploded View of Bomb.

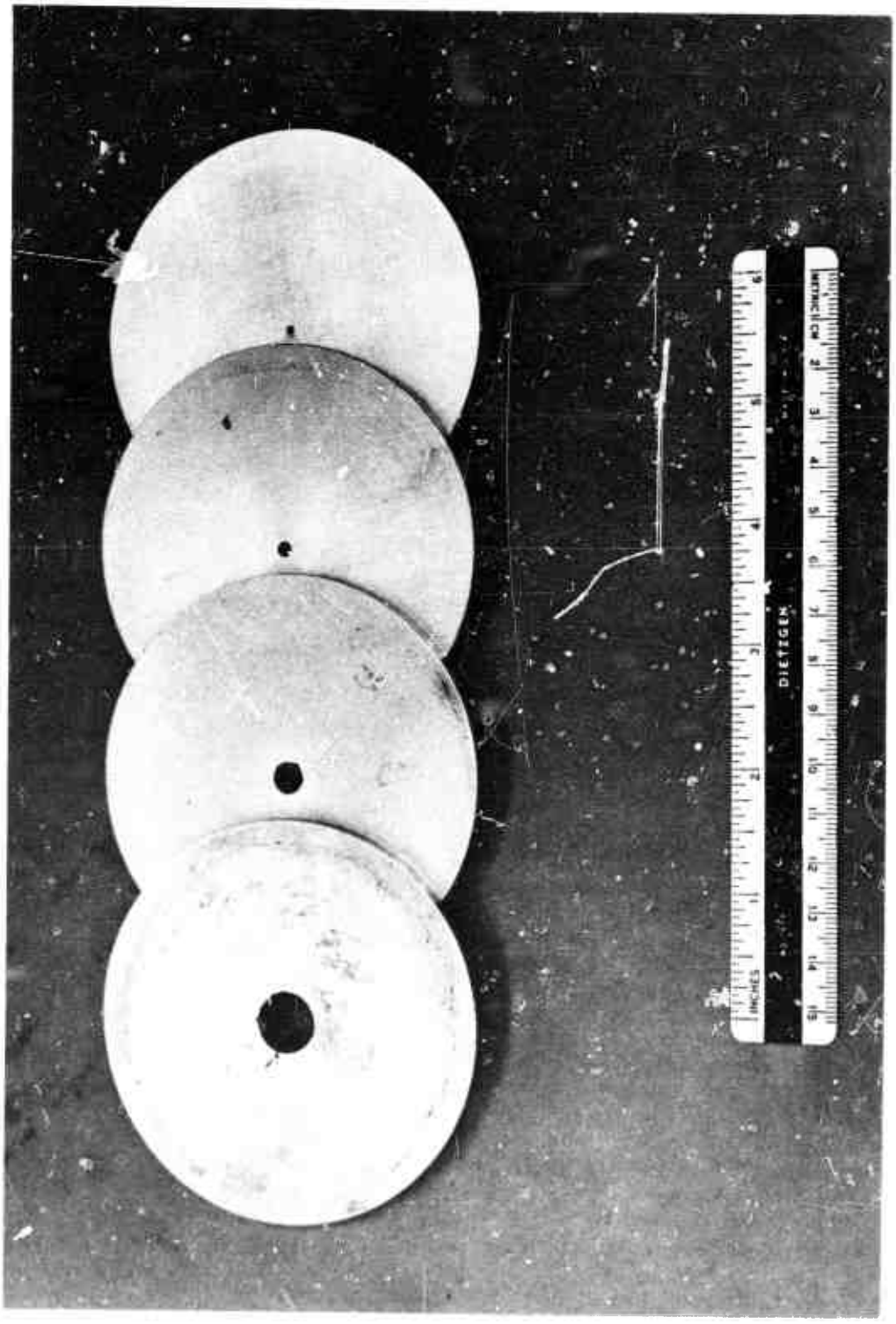

Figure 23. Orifice Plates.

which was formed from aluminum in several different orifice sizes, to provide for different rates of depressurization. This end cap also held the burst diaphragm (Figure 24), which is a multi-layered mylar disc ruptured on command by a bare nickel chromium 30 gauge hot wire. This rapid decompression system was first employed in reference (18).

Pressure seals were accomplished using "O"-rings mounted in grooves on the ends of the center section of the bomb.

The bomb itself was mounted on a stand (Figure 25), which was made from carbon steel angle iron (2 x 2 x 3/16 inches) and bolted to the floor to reduce mechanical vibration feedback to the microwave system during firing and, in particular, during depressurization.

To protect the operator an L-shaped wall was formed from 8 x 8 x 16 inch concrete blocks reinforced with iron rod and filled with cement. A two inch diameter hole was retained to provide a passageway for the microwave circuit. Later, three one-half inch diameter holes were drilled through the wall to provide for the stainless steel tubes leading to and from the bomb.

Bomb Control System

The bomb control system was responsible for controlling the test sequence and consisted of the ignition and depressurization electrical circuits and the pressurizing and purging flow systems.

During a test run, the bomb was initially pressurized and continuously purged with nitrogen provided by a standard 2000 psi tank. The flow system is illustrated in Figure 26. Two pressure regulators, a Matheson Gas Products Model 3-580 at the tank and an Accessary Products Company Series 1342 on the line leading to the bomb, were used to maintain

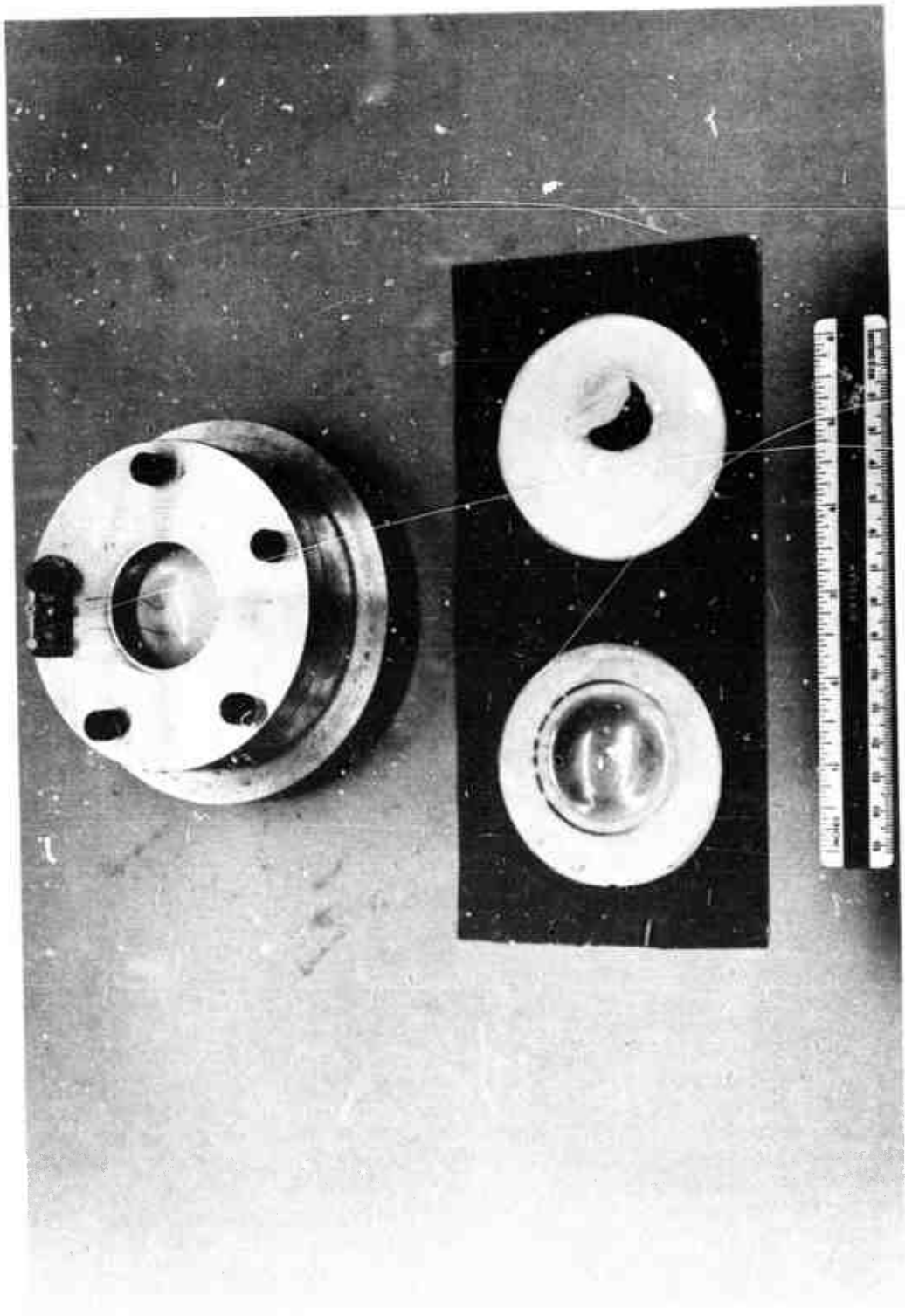

Figure 24. Burst Diaphragm and Retainer.

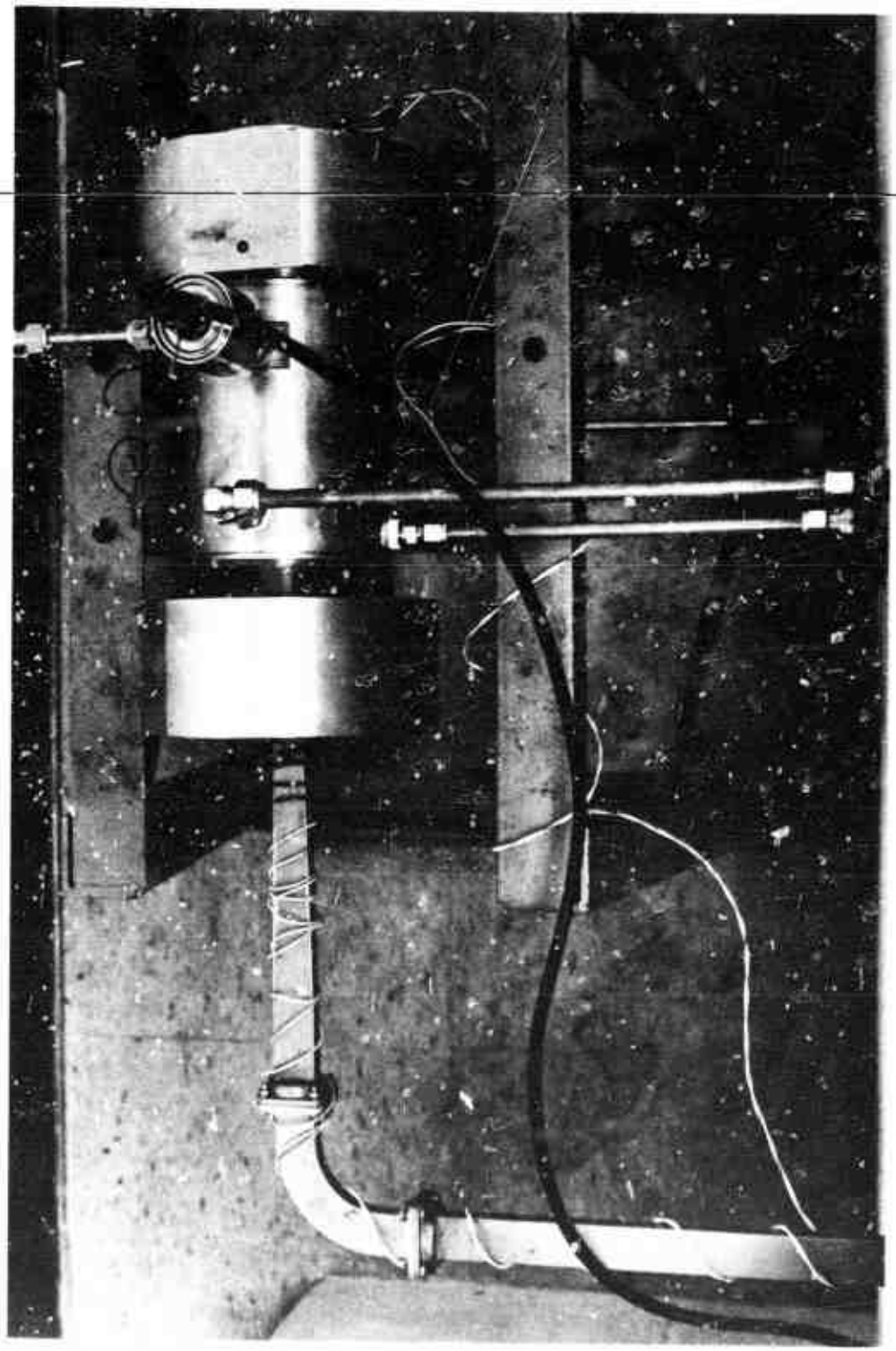

Figure 25. Bomb (Assembled) and Stand.

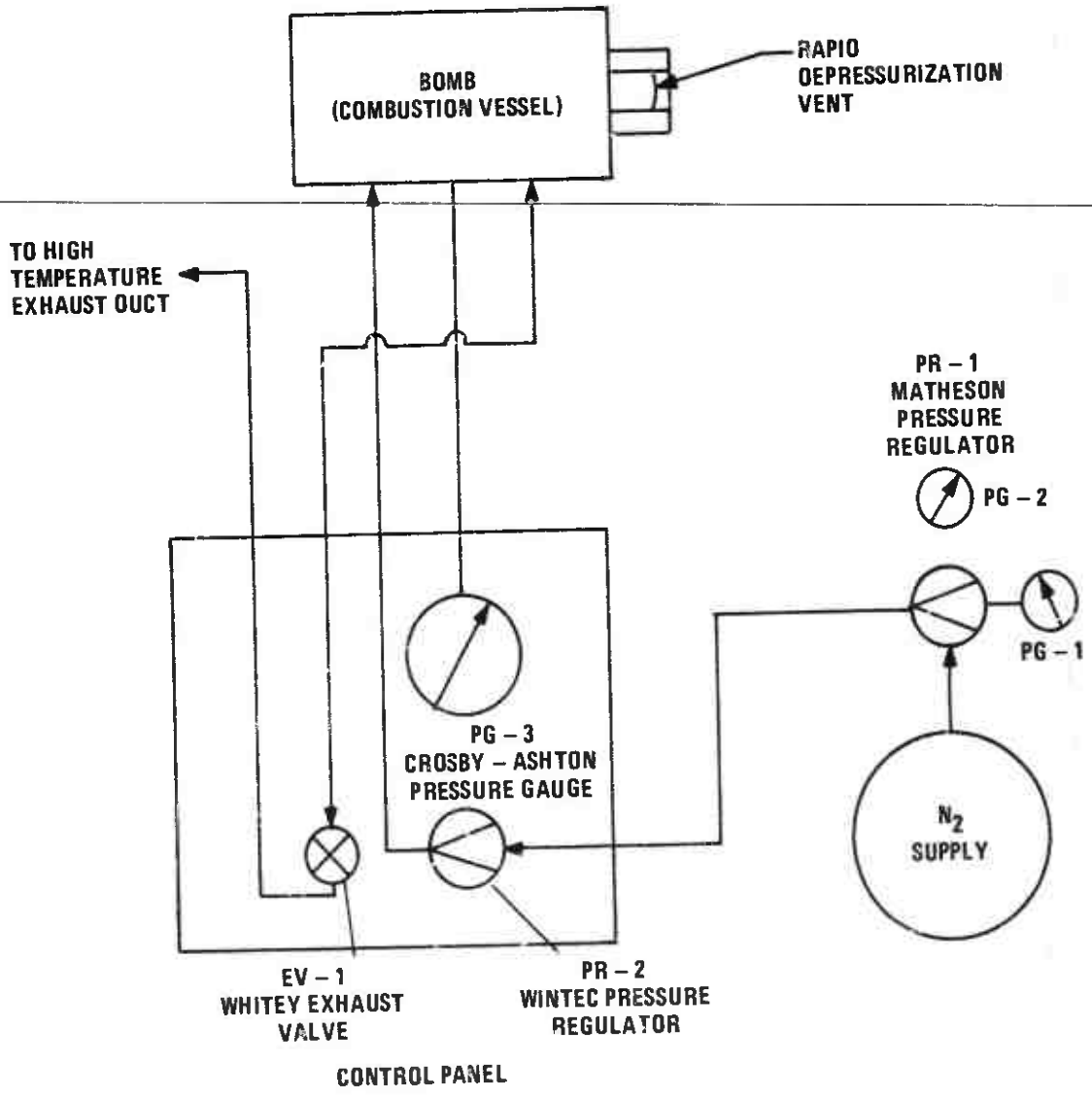

Figure 26. Schematic of Flow System.

the bomb pressure at the desired level until depressurization was induced. All tube connections were provided by Crawford Swagelock Type 316 stainless steel tube fittings. Stainless steel tubing with an outside diameter of 3/8 inches and a wall thickness of 0.065 inches was used throughout. The exhaust flow was regulated by a Whitey 16DK-316 shut-off valve and passed on to a high temperature exhaust duct leading to the exterior of the building. A standard Crosby-Ashton 0-1000 psi bourdon tube pressure gauge was utilized in addition to a Statham Model PA 826-IM Pressure Transducer. The bourdon tube gauge provided direct information of the pressure level in the bomb to the operator, while the transducer signal was not monitored directly, but simply recorded in real time on the magnetic tape recorder and later read back by a computer.

The power supply for the ignition and depressurization circuitry was an American Monarch Battery Eliminator capable of a d.c. output of 48 volts and 12 amps. The power supply was regulated by means of a 3.75 amp variac. A wiring diagram is given in Figure 27. Two type BNC plugs provided outlets to the recorder. The lights were used to indicate the completion of the circuit to the hot wires. The voltage across the light was in turn converted to a digital signal and recorded along with all other data to indicate when each particular hot wire circuit was activated. Bare nickel chromium 30 gauge wire was used as the hot wire in both circuits. Prior to ignition, the ignition hot wire was pressed into a small slot cut into the appropriate end of the propellant strand. The depressurization circuit was readied by running the hot wire under the outer layer of the multi-layered mylar burst diaphragm.

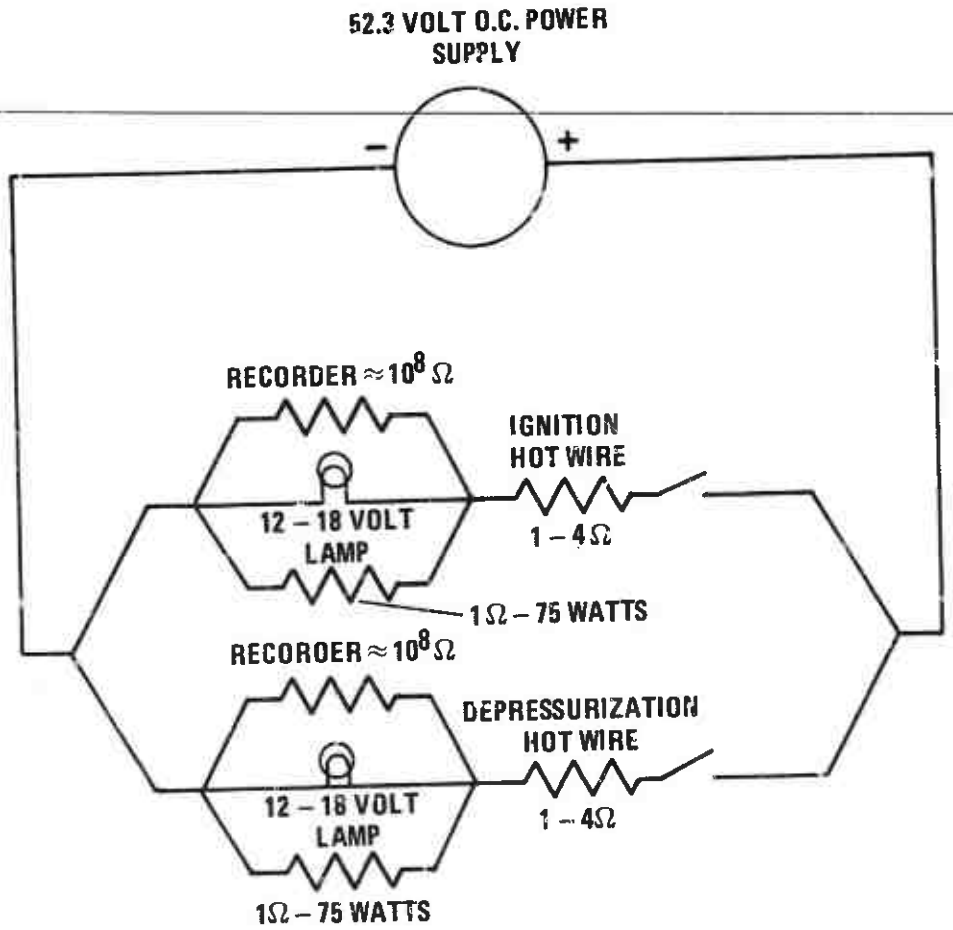

Figure 27. Control Panel Wiring Diagram.

Data Acquisition

Since a prerequisite for obtaining unsteady state burning rate data is the ability to reduce to the order of several milliseconds the time interval over which the burning rate is observed, large amounts of data must be recorded, even when the duration of the burn is only several seconds. For most purposes an oscillograph might accomplish the job. However, since the output of the network analyzer is ϕ_a, and $\dot{\phi}_a$ is the quantity necessary to calculate the burning rate r, it would be necessary to first electronically differentiate ϕ_a and record the result on the oscillograph. This electronic differentiation could lead to large errors, however, due to the small amounts of noise always present, in the ϕ_a signal, and graphical differentiation of a graph of ϕ_a was out of the question. Numerical differentiation of distinct values of ϕ_a recorded in known time increments was much more desirable.

This could possibly be accomplished by recording the voltage signals on an analog type recorder, converting these signals to digital signals, and recording this digital information on magnetic tape for reduction by a computer.

However, noise levels on analog tape recorders are typically in the -40dB range, which means that the voltage amplitude of the noise is approximately one percent of the true voltage signal. Since the output of the network analyzer is accurate to within 0.2 degrees (about 0.1 percent of full scale), the use of an analog recorder would nullify the accuracy of the network analyzer.

Considering all the above facts, it was decided that if an analog converter and recorder system could be purchased for a reasonable price,

it would be far superior to any other type of data system. Such a system was found in the Model 120-141 Data Acquisition System manufactured by Datum, Inc. of Anaheim, California.

The Model 120-141 system (Figure 28), consists of an analog to digital converter, formatter, and a synchronous write tape transport. The converter and formatter has the capability of scanning, converting, and passing on to the recorder the information up to 20 data channels at the rate of one channel every 200 microseconds. The tape transport is a seven track system compatible with the most modern high speed computers. The tape transport writes the data in high density (800 characters per inch) on standard magnetic tape.

The converter takes an analog input of minus ten to plus ten volts and changes this to an integer (in digital form) from zero to 4096, which is recorded on the magnetic tape. The system has the ability to scan each channel up to 7999 times per record (a record being the length of tape read into core at one time by the computer).

In the subject investigation, five channels of the data acquisition system were utilized. These five signals represented the relative phase angle and relative amplitude outputs of the phase-gain indicator, the output of the Statham pressure transducer, and the two signals representing the ignition and depressurization sequences.

The full scale phase output of the phase-gain indicator is only ± 1.8 volts. Therefore, in order to make full use of the ± 10 volt full scale ability of the analog-digital converter and recorder, hereafter referred to as the ADCR, it was necessary to amplify the voltage signal by a factor of five. For this purpose a Hewlett-Packard Model 467A

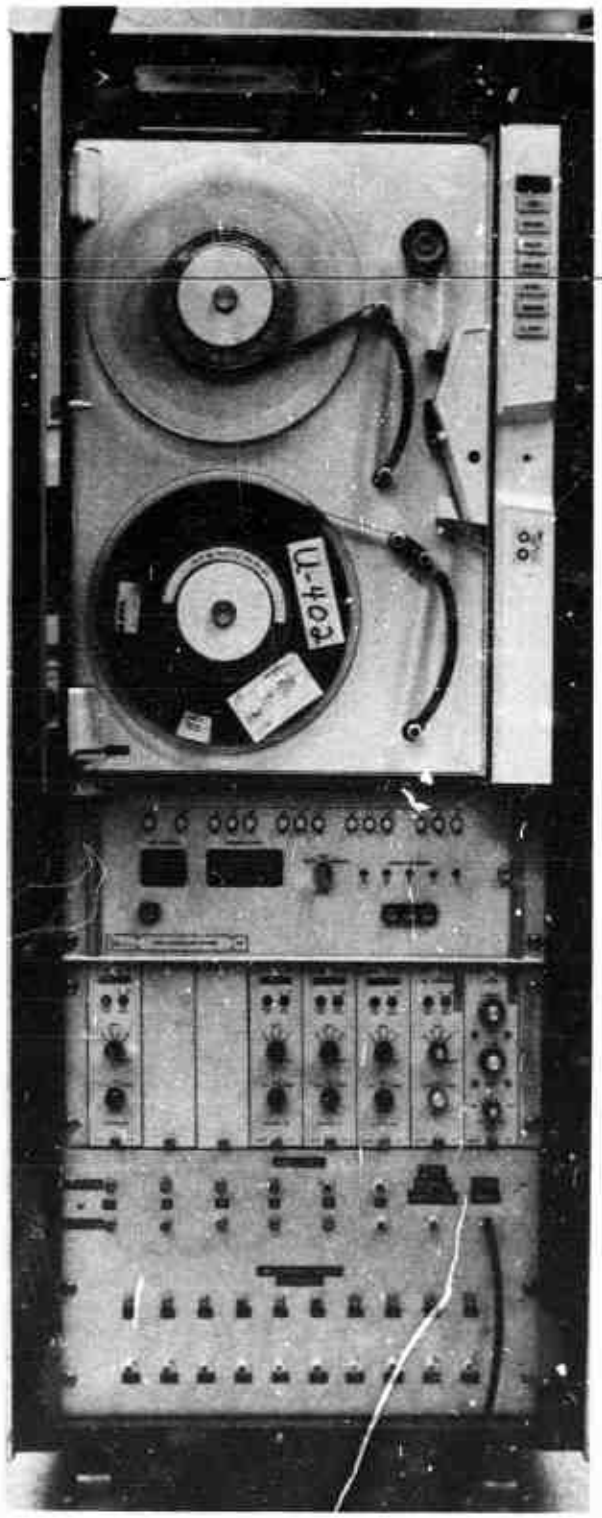

Figure 28. Model 120-141 Data Acquisition System.

Amplifier/Supply was obtained. This unit has four fixed gain settings of one, two, five, and ten, and for input signals from d.c. to 10KHz, has an accuracy of $\pm$0.3 percent. The power supply with outputs of $\pm$1, $\pm$2, $\pm$4, $\pm$10, and $\pm$20 volt ranges proved stable enough to use in calibrating the full scale readings of the ADCR.

Due to the excessive noise initially encountered on the phase channel, a filter was obtained to reduce high frequency oscillations of the phase channel to an acceptable level. The filter, an AP Model 245-5 operated in the "low-pass" mode, was used to filter out all oscillations above 50 Hz of the amplified phase signal before the signal was recorded.

In addition to the ADCR, a Hewlett Packard Model 716 Moseley Plotter was used to record the unamplified and unfiltered phase output. This was done to obtain a quick visual check on the progress of a test and to provide data with which to calculate λ_{pg} during steady state burn tests. The x-axis of the plotter was swept at five seconds per inch and the y-axis sensitivity was set at one volt per inch.

The power supply for the Statham Model PA-826-IM 0-1000 psi Pressure Transducer was a Honeywell Accudata 105 Gage Control Unit which provides a 3-12 volt supply for bridge excitation and a ten-turn potentiometer for balance. A Honeywell Accudata 120 DC Amplifier with a variable gain of 10 to 1000 was used to amplify the signal from the pressure transducer and gage control unit prior to recording it on the ADCR.

List of Data Acquisition Equipment:

1) Item: Data Acquisition System (Analog-Digital Converter and Recorder)
   Model 120-141
   Manufacturer: Datum, Inc., Anaheim, California
   Tape Specifications: Seven Track, 12-Bit Binary, Univac and IBM Compatible
   Tape Speed: 12.5 ips

Character Density: 800 cpi
Scan Rate: 200 μsec/channel
Power Requirements: 120 volts a.c.

2) Item: Honeywell Statham Pressure Transducer
Model: PA-826-1M
Manufacturer: Honeywell Test Instruments Division, Denver, Colorado
Excitation: 10 volts d.c.
Full Scale Output: 3mV/V (open circuit)
Range: 0-1000 psia
Bridge Resistance: 350 ohms

3) Item: Honeywell Accudata DC Amplifier
Model: 120-1
Manufacturer: Honeywell Test Instruments Div., Denver, Colorado
Gains: x10 to x1000 in eight calibrated steps, plus vernier
Input: 2.5mV to 250mV
Outputs: 50 ma at 44 volts d.c. to power gage unit, ±2.5 volts and/or 65 ma DC
Noise: Less than 5 μv rms RTI + 500 μv rms at output
Power Requirement: 120 volts a.c.

4) Item: Honeywell Accudata Gage Control Unit
Model: 150-3
Manufacturer: Honeywell Test Instruments Div., Denver, Colorado
Excitation Voltage: 3.5 to 11.5 volts
Balance: 10-turn potentiometer
Power Requirement: 44 volts d.c. from Accudata 120 Amplifier

5) Item: APVC Variable Filter
Model: 245-5
Manufacturer: A.P. Circuit Corp., New York, N. Y.
Modes: Low Pass, High Pass, Band Pass
Attenuation Slope: 24dB/octave
Tuning Range: 0.2Hz - 20kHz
Power Requirement: 4-4.2 volt Batteries

6) Item: Moseley X-Y Recorder
Model: 7035A
Manufacturer: Hewlett-Packard, Palo Alto, California
Axis Sensitivities: 1mV/in. to 10V/in.
Power Requirement: 120 volts a.c.

7) Item: Mosley Time Base
Model: 17108A
Manufacturer: Hewlett-Packard, Palo Alto, California
Sweep Rates: 0.5, 1, 5, 10, 50 seconds/in.
Power Requirement: 1-12.6 volt battery

8) Item: Amplifier/Power Supply
Model: 467A
Manufacturer: Hewlett-Packard, Palo Alto, California
Gaines: x1, x2, x5, x10, Variable
Output Voltages: ±1, ±2, ±4, ±10, VDC
Noise: Less than 5mV peak to peak
Power Requirement: 115 volts a.c.

Propellant Mixing and Casting Apparatus

In order to insure that as few bubbles and impurities as possible would get into the propellant it was decided that a vacuum box should be obtained in which the bubbles could be drawn out of the propellant mixture before casting. Also, an oven in which the propellant samples could be allowed to cure (a process accelerated greatly by heat) was needed. A vacuum oven (Figure 29) manufactured by Fisher Scientific Company was purchased to meet both these needs. The vacuum oven came equipped with outlets for a vacuum pump, a vacuum gauge, a thermostat type heating control, and a glass window on the door which eliminated the necessity to release the vacuum while checking on the samples.

In addition to the vacuum oven, a scale (0.1 gram accuracy), spatulae, and several beakers were all that was required to mix and cast the propellant (Figure 29).

Many of the chemicals required for the subject investigation were provided through the courtesy of the Thiokol Chemical Corporation. These included a supply of the CTPB binder (Thiokol brand HC-434), supplies of ground AP and "as received" AP, and a small supply of the curing agent (Thiokol trade name MAPO). Later a gallon can of HC-434 was also purchased from Thiokol. Methylene Chloride was used to clean the equipment after the mixing process.

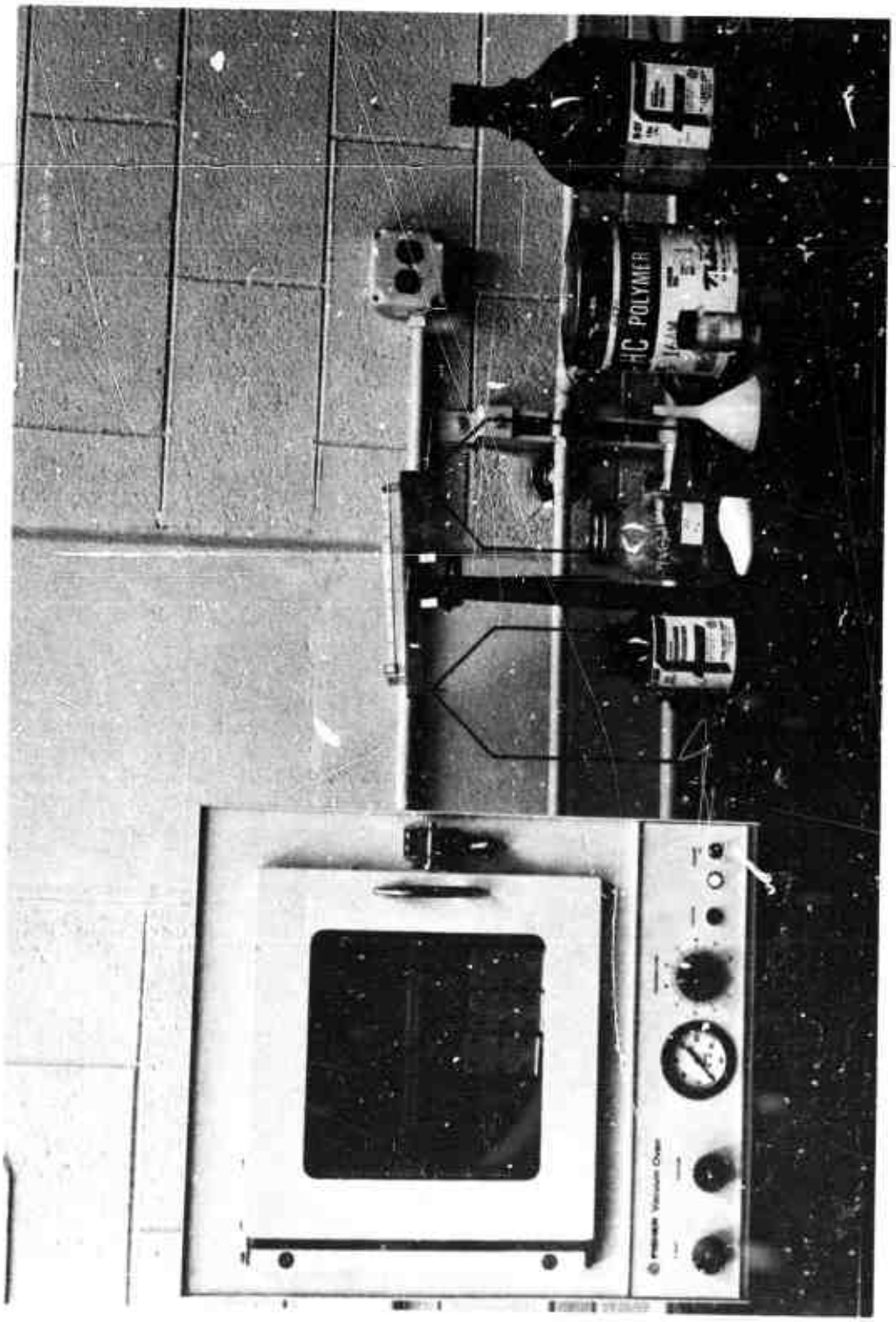

Figure 29. Propellant Mixing and Casting Apparatus.

Procedures

Roughness and Fixed Reflection Tests

The first series of tests were designed to indicate how the burning rate sensing equipment would respond to the roughness of the burning surface. To this end, several strands of a solid material with a dielectric constant of 4.0 were used in place of the propellant strand.

Three possible types of surface roughness were considered: pocketing (rapid local burning leading to distinct cavities in the burning surface), general roughness (in the form of distinct scoring of the surface), and regression of the burning surface in a direction not perpendicular to the incident microwave beam. These conditions were simulated by drilling holes, filling groves, and filling a distinct slant respectively in one end, representing the propellant's burning surface, of a strand of dielectric material (Figure 30).

In these tests the transition section was mounted on the end of the microwave circuit and a sample holder was positioned on the stainless steel dielectric window retainer. No attempt was made to cancel the fixed reflections from the transition, in fact the cancellation attenuator was set at maximum attenuation. The operating frequency was 9.47 GHz (these tests were made before it was known that the VSWR of the transition was rather high below 9.0 GHz). At any rate, the effect of the fixed reflections was the same for each test and thus was of little consequence.

The procedure for these tests follows. With the microwave equipment operating and the klystron frequency locked, the phase-gain indicator was adjusted to yield a relative phase angle indication of zero.

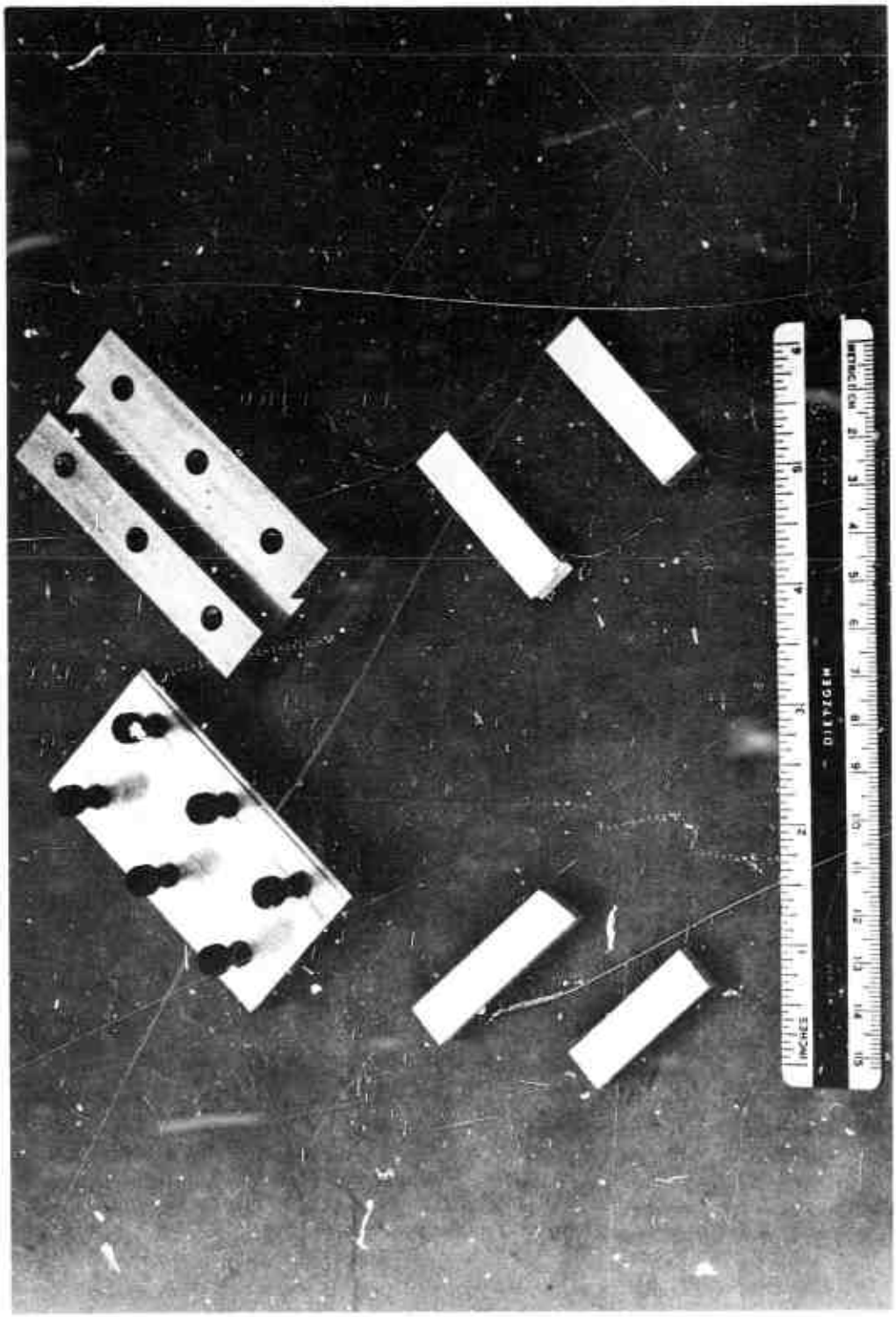

Figure 30. Dielectric Samples for Surface Roughness Tests.

Two strands of the dielectric were cut to equal lengths and filed smooth on both ends. Both strands were weighed on an analytical balance and their lengths were measured on a vernier caliper. Each strand was placed in the sample holder waveguide section in turn and three measurements were taken of the resulting phase and amplitude shift. One strand was then either drilled to a known depth, scored to a known depth, or filed to a known angle. This strand was then reweighed to determine the mass of material removed.

The second strand was then cut and filed so that this same amount of material was removed. In this case both ends of the strand remained smooth and parallel. Each strand was then placed in turn in the sample holder and three readings were again made of the resulting phase and amplitude shift. The process was then repeated until sufficient data was obtained to draw some conclusions.

After the roughness tests were completed, another short series of tests were made to determine the magnitudes of any fixed reflections coming from sources within the system other than the transition section itself. This was accomplished by fastening a short, which reflects all incident microwave energy, in place of the transition and plotting the relative phase and amplitude outputs as the short was moved out at a constant speed. Since the phasor representing the moving reflections rotates about the end of the phasor corresponding to the fixed reflections in the phasor diagram of Figure 13, it can be seen that when the magnitude of the fixed reflections are great, the phase angle changes at various rates even though the moving surface may travel at constant speed. Another effect of the fixed reflections is a fluctuation of the relative amplitude

output of the network analyzer as the moving and fixed reflections alternately cancel and reinforce each other. It was suspected that any reflections, if they did exist, were frequency dependent. Therefore, the tests were carried out at 8.53, 9.03, 9.53, and 10.03 GHz, which were the synchronizer lock frequencies closest to 8.50, 9.00, 9.50, and 10.00 GHz respectively.

Burning Rate Tests

The procedure for both the steady and unsteady burning rate tests is basically the same. Thus, only the steps of the rapid depressurization tests will be discussed in detail.

The first step was to cast the propellant in the waveguide sample holder (refer to the section covering the procedure for propellant mixing and casting). The residue from the propellant was discovered to be so corrosive that the sample holders, the sample holder brackets, and the orifice plates, all of which were machined from aluminum, could not be left uncleaned overnight without becoming severely pitted. Thus, it became necessary to completely clean the bomb after each day's testing, and it was found more convenient to cast enough samples to make several tests in one day.

During the tests channels zero through four of the ADCR recorded the relative phase angle and relative amplitude outputs of the network analyzer, the amplified output of the Statham pressure transducer, and the ignition and depressurization signals respectively. Channel five was shorted. The phase signal was first passed through a filter operating in the "low pass" mode and filtering out all noise above 50Hz. The output of this filter was then amplified by a factor of five in the

Hewlett-Packard Amplifier-Power Supply before recording on the ADCR. The phase signal at the recorder thus had an amplitude of ± 9 volts. The unamplified and unfiltered phase signal directly from the network analyzer was recorded on the X-Y plotter, which was operated with a y-axis sensitivity of one volt per inch and an x-axis sweep time of five seconds per inch. The amplitude signal was taken directly from the net-work analyzer and recorded on the ADCR. The pressure signal from the Honeywell Gage Control Unit was amplified 500 times in the Honeywell 120 DC Amplifier before it was recorded. The ignition and depressurization signals were simply the voltages across the lights indicating the completion of each circuit respectively.

Before going further with the test procedure, it was first necessary to set the excitation and balance of the pressure transducer. No voltmeters were necessary to accomplish the adjustment, since the ADCR when operated in the "manual" mode provides a convenient voltmeter in itself. Using the "display channel" switches of the ADCR the input to any channel could be displayed on the binary lights. A coaxial wire was then run from the input plug of the ADCR channel to the excitation test points of the gage control unit. Since the full scale capability of the ADCR is ten volts, the balance was adjusted until the last light of the ADCR binary display flickered on. The excitation voltage was thus set at ten volts. Since the least count of the ADCR was five millivolts, it was necessary to set the balance by using the amplified signal output of the gage control unit. This output was fed into channel "two" of the ADCR and the balance was adjusted until all lights on the display barely flickered on, thus indicating negative zero volts. The

above steps were carried out before the bomb was pressurized.

The microwave equipment was then turned on and allowed to warm up. After the equipment had been adjusted several times to operate at a certain frequency, it would as a rule come to the operating frequency automatically. If it became necessary to change the klystron frequency, the phase-locking procedure given in Appendix B was followed.

The bomb transition section was removed from the circuit and a short was put in its place. The short reflects essentially all of the incident microwave energy. With the cancellation attenuator set at "maximum" attenuation and with the "reference channel level" of the network analyzer centered in the "operate" region by adjusting the reference attenuator, the test attenuator was then also adjusted until a relative amplitude output of zero was indicated on the network analyzer. This procedure was followed to allow maximum test signal level without danger of overloading the network analyzer.

The short was then removed from the circuit and the transition section with the ten inch load attached was replaced. At least a 25dB drop in the test signal level was immediately evident on the network analyzer. This amplitude decline was due to the load's absorbing all energy passing through the transition section. If less than a 25dB drop was indicated, the load was checked for proper alignment. At this point the test signal consisted almost totally of the undesirable fixed reflections from the transition. Then by adjusting the cancellation attenuator and the cancellation phase shifter, it was possible to bring the test signal level to a point where its amplitude was 75dB less than the reference signal level. At this point the test channel power was about 0.02 percent of

the reference channel power and it could be assumed that all fixed reflections from the interface were essentially eliminated.

Before replacing the load with the propellant sample holder, it was then necessary to make other preparations. A data sheet was prepared, which listed the pertinent equipment settings and other test information. Some calibration had to be reserved until the last moment before firing because of a tendency of the phase output to change slightly under pressure. At this point if the test was to involve rapid depressurization, the burst diaphragm was readied. Five two inch diameter discs of 0.005 inch mylar were cut. About five inches of 30 gauge nichrome hot wire was cut and placed through two holes on the outer mylar of the diaphragm. The mylar layers were then sealed between the orifice plate retainer and burst diaphragm retainer. One screw was used to mount two small terminal about which the two ends of the hot wire were wound. The wires of the rapid depressurization circuit were fastened to the bases of these terminals. The burst diaphragm end of the bomb, however, was not sealed until after the transition section with the sample holder was mounted and sealed on the other end of the bomb.

The next steps were carried out as rapidly as possible due to the tendency of the equipment to drift slightly after tuning out the fixed reflections. The transition and load were removed from the circuit and the load was removed from the dielectric window. A small amount of Dow Corning DC-4 silicone dielectric lubricant was placed on the end of the propellant sample which was to mate with the dielectric window. Care was taken to avoid using excess lubricant which might impair electrical contact between the transition and sample holder. The sample holder was

then mounted on the dielectric window by aligning the dowel pins with the four holes on the end of the sample holder and using a rubber mallet to tap the sample holder until it was tight against the dielectric window. Set screws on the sample mounting brackets were then tightened on the sample holder. One screw on the end of the sample holder was used to mount the two terminals to which the ignition wires leading through the pressure sealing electrical plug to the outside of the bomb were connected. Using a single edge razor blade, a small slit was cut across the exposed face of the propellant strand. About four inches of the nichrome hot wire was prepared and the center portion of the wire was pushed into the slit in the propellant leaving the two ends of the wire protruding. These loose ends were then wound around the ignition posts on the top of the sample holder. It was found necessary to use a strip of ordinary cellophane tape to bind the wires tight against the end of the sample holder while care was taken to keep the two leads separate and to keep them from actually touching the aluminum sample holder (Figure 31). The transition and sample holder were then sealed into the appropriate end of the bomb by tightening one of the end retainers down around the flange of the dielectric window retainer. The ignition wire was then checked for proper positioning by a glance through the open end of the bomb. The transition was then mated to the microwave circuit and the external ignition lead wires were joined with the rest of the ignition circuit. Finally, after selecting the proper size orifice plate and mounting it on the inside of the orifice plate retainer, the burst diaphragm and orifice plate were sealed into the bomb by tightening the other end retainer on the flange of the orifice plate retainer. The

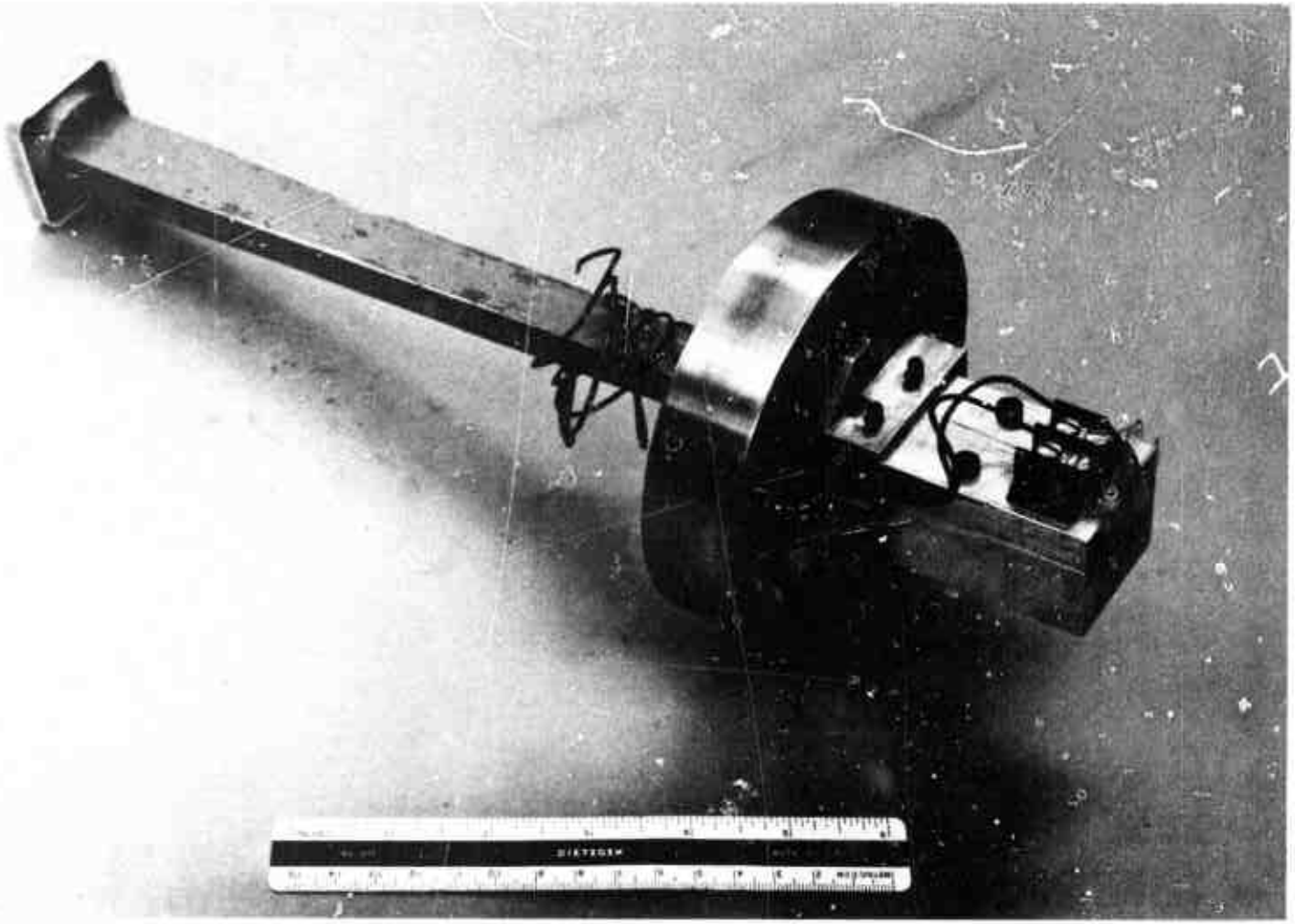

Figure 31. Transition Section with Sample Holder Attached.

bomb itself was then ready for firing.

All equipment was then checked for proper adjustment. The ADCR was loaded with a magnetic tape. The "last channel" thumbwheel switch of the ADCR was set at "five" and the "scans per record" thumbwheel switch was turned to "6000". The ADCR was turned to the "auto" mode, which allows one to start recording data by pushing the "start" button on the ADCR control panel.

After checking both the ignition and depressurization switches to make certain they were in the "off" position, the power supply for these circuits was activated. All readings except the "phase offset" output of the network analyzer were then recorded.

The next step was to bring the bomb up to operating pressure. It was determined that a nitrogen flow rate of at least ten cubic feet per minute was sufficient to purge the bomb of exhaust gases. Refer to Figure 26 for aid in understanding the following discussion. First, the exhaust valve EV-1 was opened all the way (it was found necessary to always keep the valve completely open during testing in order to reduce the amount of propellant residue caught in its passages). The shut off valve on the nitrogen tank was opened and the pressure was checked on the upstream gauge PG-1 of the pressure regulator PR-1. If tank pressure was found to be less than 400 psi, the tank was replaced by a full one. The pressure regulator PR-2 on the control panel was opened and the shut-off valve on the down stream side of PR-1 was opened. PR-1 was then adjusted to yield a pressure of 400 psi on gauge PG-2 and, finally, pressure regulator PR-1 was adjusted to yield the appropriate bomb pressure up to 300 psig, as indicated on gauge PG-3 on the control panel.

A final adjustment of the phase output was made and the "phase offset" setting of the network analyzer was recorded. The sweep of the X-Y plotter and the "start" button of the ADCR were activated simultaneously. After a quick check to make sure both were running properly, the ignition switch was thrown. If the light which indicated the completion of the ignition circuit did not come on, a quick glance at the X-Y plotter could determine whether ignition had occurred. If the characteristic sawtooth curve of the phase angle plot was being traced out by the plotter, the propellant had ignited. Otherwise, if a quick check did not reveal the source of the problem the test was halted.

It was known that approximately every 7.2 seconds, the ADCR would write an inter-record gap on the magnetic tape. These gaps consisted about 48 milliseconds of time in which no data was being written on the tape. To avoid depressurization during an inter-record gap or during a discontinuity in the phase signal (as the phase angle shifts from + 180 to - 180 degrees), it was found most convenient to mark the graph paper on the X-Y plotter at the points in time at which the inter-record gaps would occur. Then, the operator, by following the phase angle versus time plot as it was being traced out, could determine the best possible time to activate the depressurization circuit, the ideal point being in the center of the magnetic tape data record as the phase angle passes through the zero point.

After depressurization, if extinction of the propellant did not occur, the test was continued until burning ceased as indicated by the constant phase angle output on the plotter. The data receiving equipment was allowed to run for several seconds longer. After halting the

plotter and ADCR, the final phase angle and final amplitude outputs were recorded before the bomb was opened. It was found desirable to allow the nitrogen to continue to purge the bomb for ten to fifteen seconds to help remove all toxic gases. The shut off valve on the nitrogen tank was then moved to the fully closed position.

If another test was to be run, one "end-of-file" mark was put on the tape and the tape transport's power was left on (the tape unit should never be turned off in the middle of a tape or the position will be lost). If no other tests were to be run that day, one "end-of-file" mark was placed on the tape and the tape was then rewound and removed from the transport.

Immediately after the last test each day, it was necessary to completely clean the bomb and sample holder. Both ends of the bomb were removed. The sample holder was removed from the transition section and the exposed face of the dielectric window was cleaned with methylene chloride. Care was taken not to use too much solvent, as it can dissolve the window or the epoxy holding it in place. The sample holder, mounting brackets, and all screws were removed and dropped in beakers of the solvent, while the inside of the bomb was scrubbed with a toothbrush dipped in solvent or a steel wool soap pad and wiped clean with a hand towel. The sample holder, mounting brackets, and orifice plate (all aluminum pieces) were then scurbbed with a steel wool soap pad to remove all residue. All steel screws were scrubbed with steel wool and then allowed to soak in household oil to prevent rust. The tubing of the exhaust line was opened at several places and 75 psi air was forced through to aid in removing the propellant residue.

After each day's testing the magnetic tape on which the data was written was carried to the Georgia Tech Rich Electric Computer Center and placed in the tape library of the Univac 1108 computer. A program punched on cards (see Appendix A) was used to reduce, print, and/or plot the data as desired. The plots presented in this thesis were redrawn to make them suitable for reproduction.

Propellant Mixing and Casting

In the subject investigation, the propellant used was carboxyl terminated poly-butadiene (CTPB) with ammonium perchlorate (AP) oxider. HC binder (Thiokol trade name for CTPB) was first mixed with a small amount of MAPO in the respective amounts of 94 to 6 percent by weight. A second mixture was made in which 200 micron (particle size) AP was mixed with 16 micron AP in the ratio of two parts to one. Finally, the AP mixture was added to the binder mixture with the oxidizer making up 75 percent by weight of the final mixture A typical formulation thus consisted of

10 grams of HC

0.65 grams of MAPO

10.65 grams of 16 micron AP

21.3 grams of 200 micron AP,

where all amounts were weighed to the nearest 0.1 gram.

The above ingredients were mixed in a beaker and then placed in a vacuum oven pre-heated to 65 degrees Centigrade for approximately 45 minutes. In the meantime the sample holders were also heated. These steps were taken to reduce the difficulty of casting the propellant in the sample holder and to remove the air bubbles, which entered during

mixing, from the propellant mixture.

A small one-eighth inch thick plate of teflon was then attached to one end of each sample holder, as shown in Figure 19. This procedure was followed for three purposes: 1) it allowed the sample holders to stand on one end to facilitate casting and curing without spillage of the propellant, 2) it provided a smooth surface for mating with the dielectric window, and 3) the propellant mixture did not bind to the teflon (it was found to bind quite readily to the sides of the aluminum sample holder). The propellant was then allowed to flow into the sample holders from a micro-spatula. Care was taken not to allow the propellant to touch the walls of the sample holder. When the sample holders were about 3/4 full, they and the remaining propellant mixture were placed back in the vacuum oven for an additional 30 minutes. The sample holders were then filled to the top with the remaining propellant formulation and placed back in the oven, although not under a vacuum. They were then allowed to cure at 65 degrees Centigrade for three days.

After curing, the sample holders were removed from the oven and any excess propellant on the top end of each holder was trimmed away. The teflon plate was then removed and the sample, after cooling, was then ready for use.

Much effort was put into removing all bubbles from each sample. Any imbedded bubbles could have caused reflections and thus errors in the determination of the burning rate.

CHAPTER IV

RESULTS

Surface Roughness

Results of the surface roughness tests are summarized in the graphs of Figures 32, 33, and 34. Figure 32 compares the phase angle change $\Delta\emptyset$ caused by drilling holes with equal width and depth in one strand, to the $\Delta\emptyset$ resulting from removing the same amount of material from a second strand, whose end was maintained square and smooth. Figures 33 and 34 do likewise for a grooved strand and for a strand cut off at an angle respectively.

The graphs clearly indicate that the errors between either the drilled strand and the smooth strand, or the grooved strand and the smooth strand are quite large. Thus, were those types and depths of surface roughness to appear one could expect large errors (up to about 60 percent) in the measured burning rate.

However, from Figure 34 the errors caused by a slanted burning surface are seen to be only slightly more than ten percent. Figure 35 shows two propellant samples which were extinguished during rapid depressurization. The strand on the right apparently was burning nearly perpendicular to the axis of the sample holder. The strand on the left had begun to burn at a slight angle (less than the angles included in the graph in Figure 34). Several other extinguished samples were observed and, though most burned at slight angles to the incident microwave beam, none was found to exhibit pitting deeper than about 0.005 inches or to

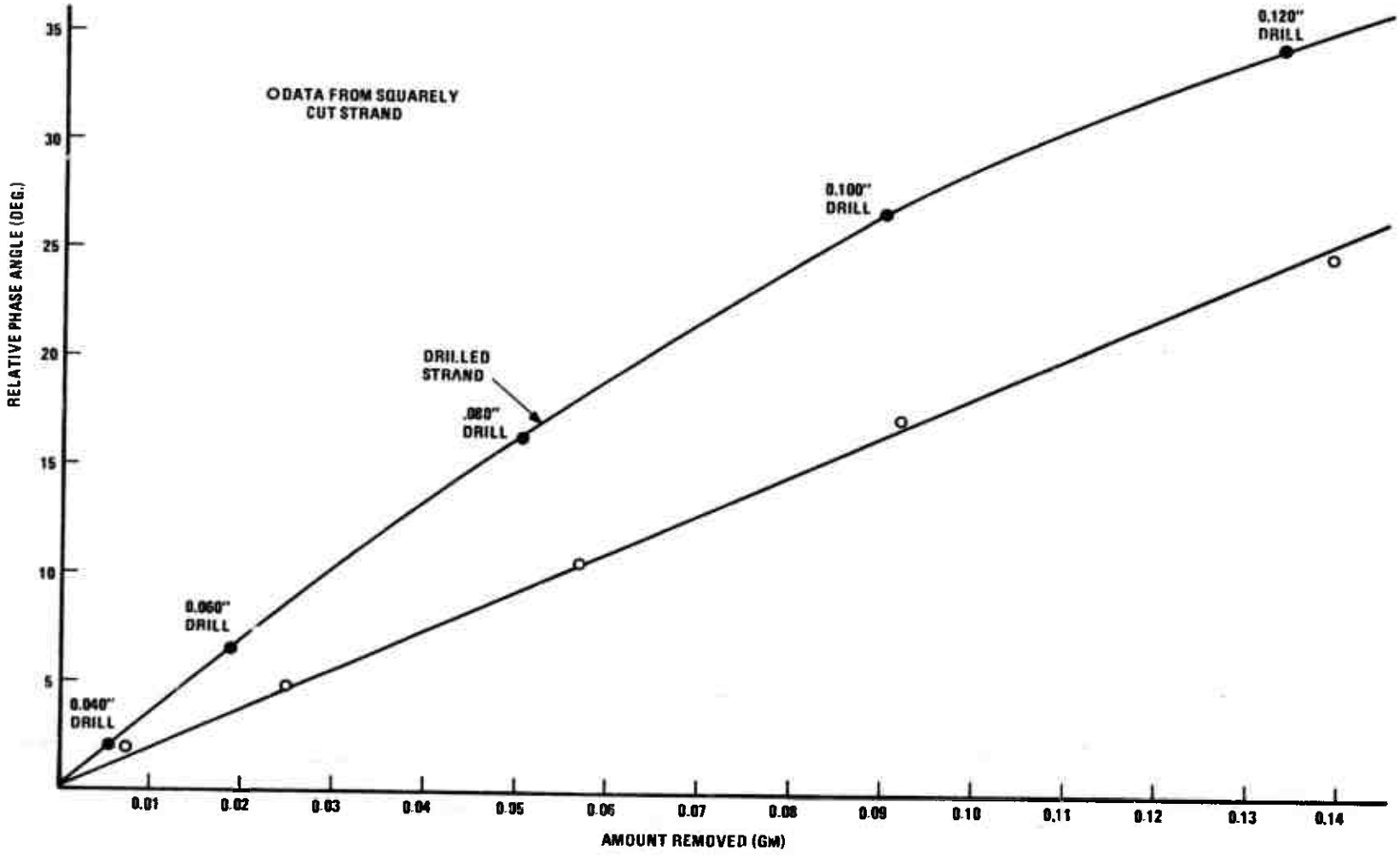

Figure 32. Comparison of Phase Angle Change $\Delta\phi$ for Drilled Strand and Squarely Cut Strand.

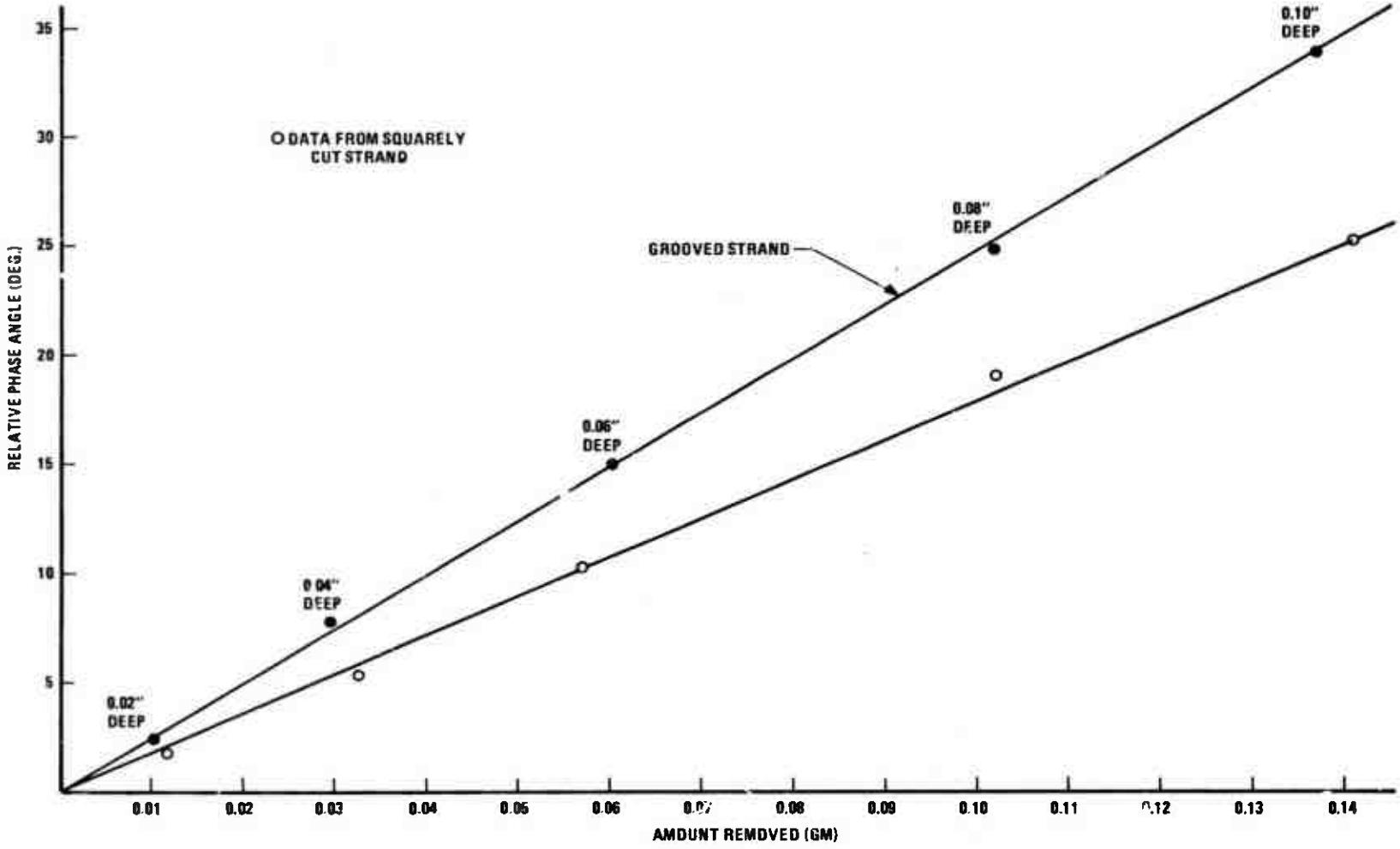

Figure 33. Comparison of Phase Angle Change $\Delta\phi$ for Grooved Strand and Squarely Cut Strand.

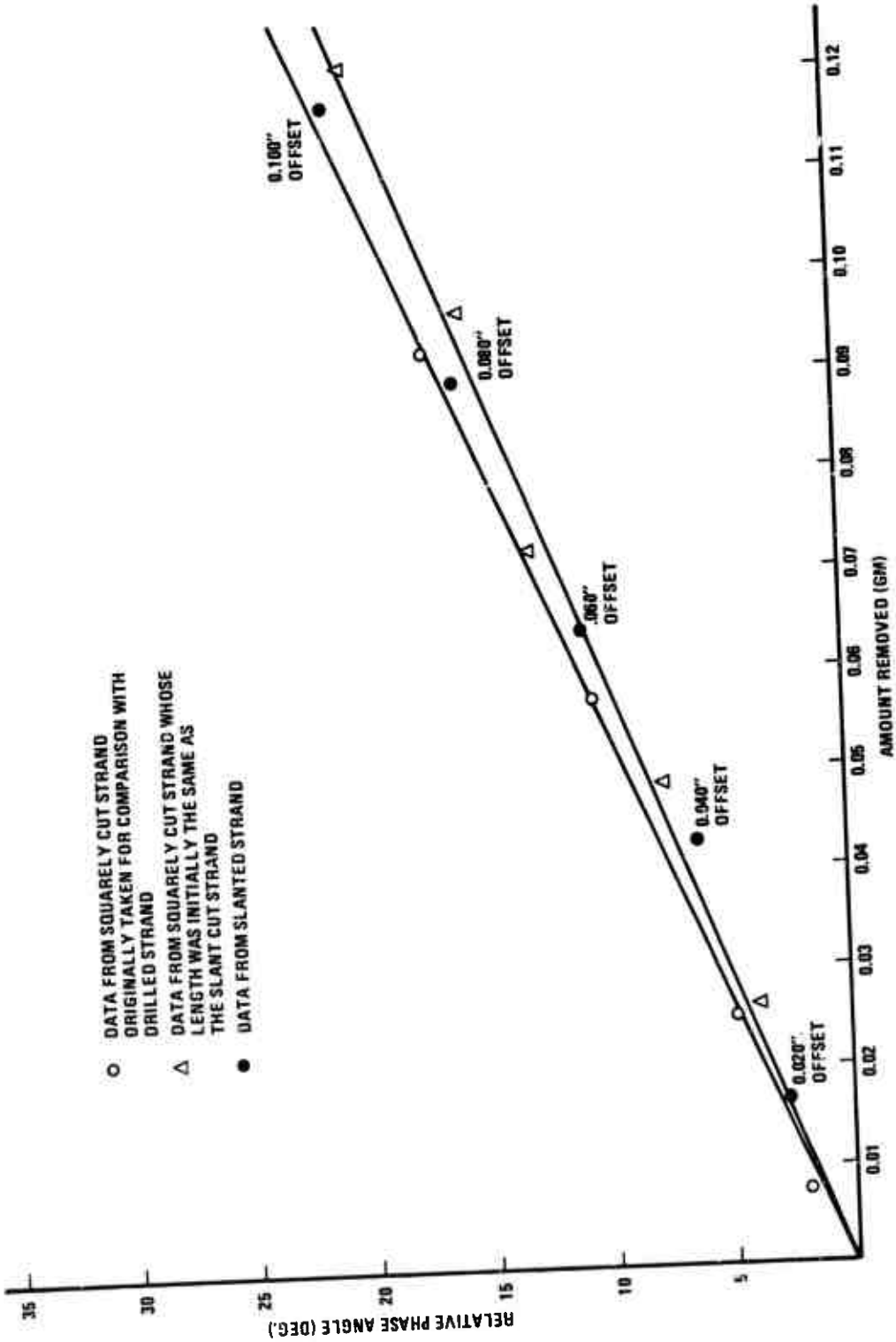

Figure 34. Comparison of Phase Angle Change $\Delta\phi$ for Slant Cut and Squarely Cut Strand.

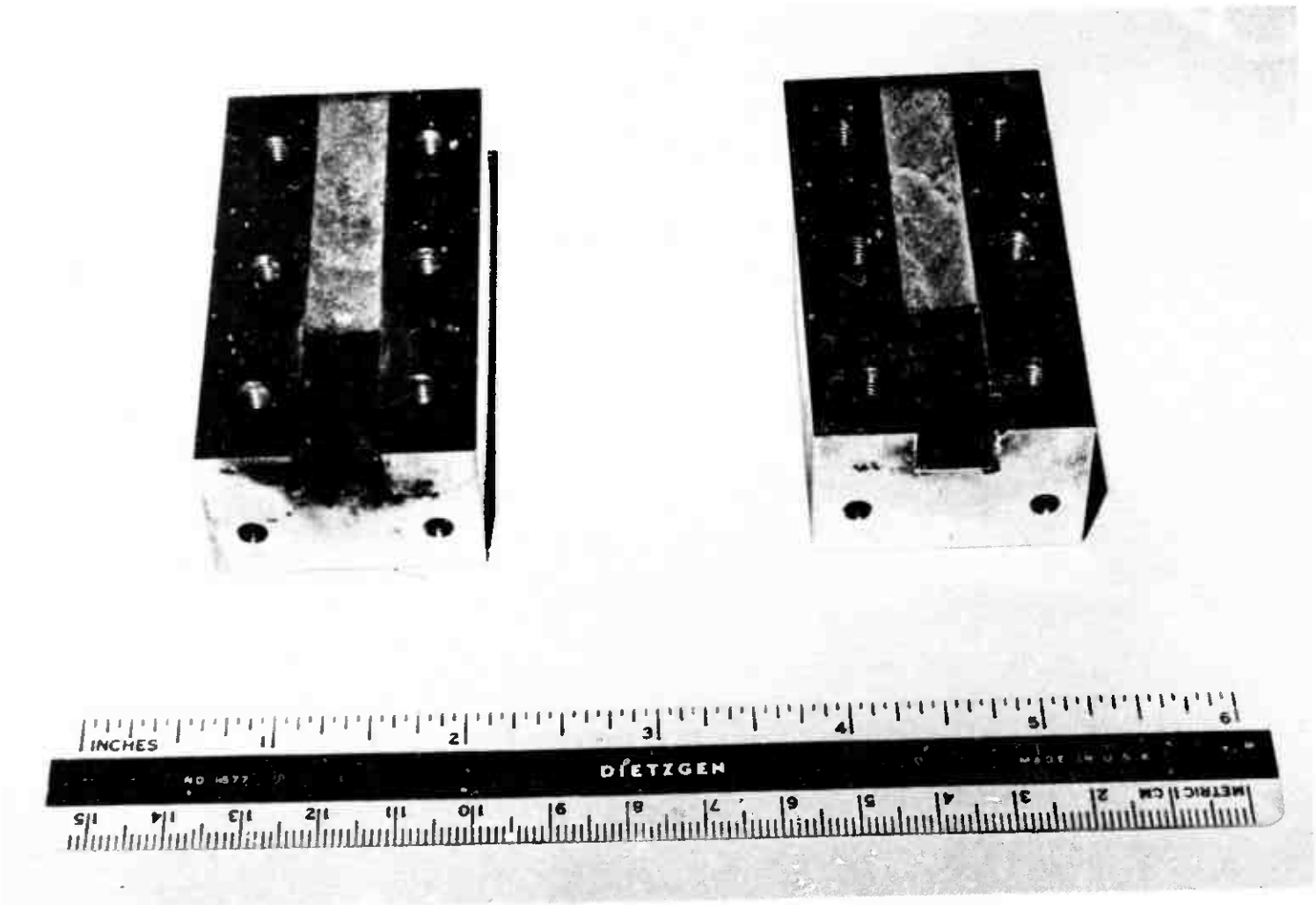

Figure 35. Extinguished Propellant Samples.

burn at angles in excess of the cases considered in Figure 34. Thus, one may conclude that in the majority of cases the system exhibits less than a ten percent error due to surface roughness.

Fixed Reflections

The series of tests to determine the magnitudes of fixed reflections other than those emanating from the propellant surface indicated that rather large reflections of some sort were present at 8.53 GHz, while their presence was essentially undetectable at 9.03 GHz and above. The data from these tests have not been reproduced here.

The magnitude of the fixed signal detected at 8.53 GHz was too large to assume the signal was being created by some misalignment of waveguide components between the circulator and the bomb. Also, the generous use of isolators between the circulator and the test signal pickup precluded the idea that the signal might be a second reflection (e.g., a signal reflected first by the test signal pickup and then reflected again by the circulator so as to be traveling once again in the original forward direction).

It was concluded that the reflections present at 8.53 GHz were the result of a decreasing directivity of the circulator with decreasing frequency. This means that at 8.53 GHz a significant portion of the main signal, which was supposed to be directed into the bomb by the circulator, was actually leaking into the test signal arm and, having escaped any reflection by the moving surface, appeared as a fixed reflection (oscillating at the source frequency). The fact that these signals were undetectable at and above 9.03 GHz caused them to be of little concern, since 9.13 GHz had already been singled out as the

operating frequency for the burning rate tests for different reasons altogether (see section on Microwave Circuitry apparatus in Chapter III).

Steady State Tests

The steady state tests in general yielded good burning rate results, though some tests indicated the presence of some significant fixed reflections. Figures 36 and 37 were reproduced from the X-Y plotter trace of the phase angle versus time during steady state tests at 50 psig and 300 psig. The slope of the graph (excluding phase discontinuities in jumping from +180 to -180 degrees) is proportional to the burning rate. The propellant sample in the test of Figure 36 was three inches long, and in the test of Figure 37 was four inches long. A $\Delta\emptyset$ of 720^{o} on the graph corresponds to one wavelength in the propellant. Thus, it can be seen that in both cases the wavelength λ_{pg} was very close to one inch if one excludes the initial transients visible particularly on Figure 36.

An explanation of a possible source for these initial transients is in order. It was initially found convenient, when positioning the ignition hot wire in the propellant, to leave a small amount of excess propellant protruding from the end of the sample holder. The possible effects of this procedure were not considered at the time. However, the propellant outside the waveguide can act as a microwave horn and enables part of the incident energy to propagate past the end of the sample holder into the interior of the bomb. This was first discovered when, after fastening a sample holder to one end of the bomb, the orifice plate was brought up to the other end, causing both a phase and amplitude change on the equipment output. This was because part of the energy escaping the sample holder was being reflected back into the sample holder by the

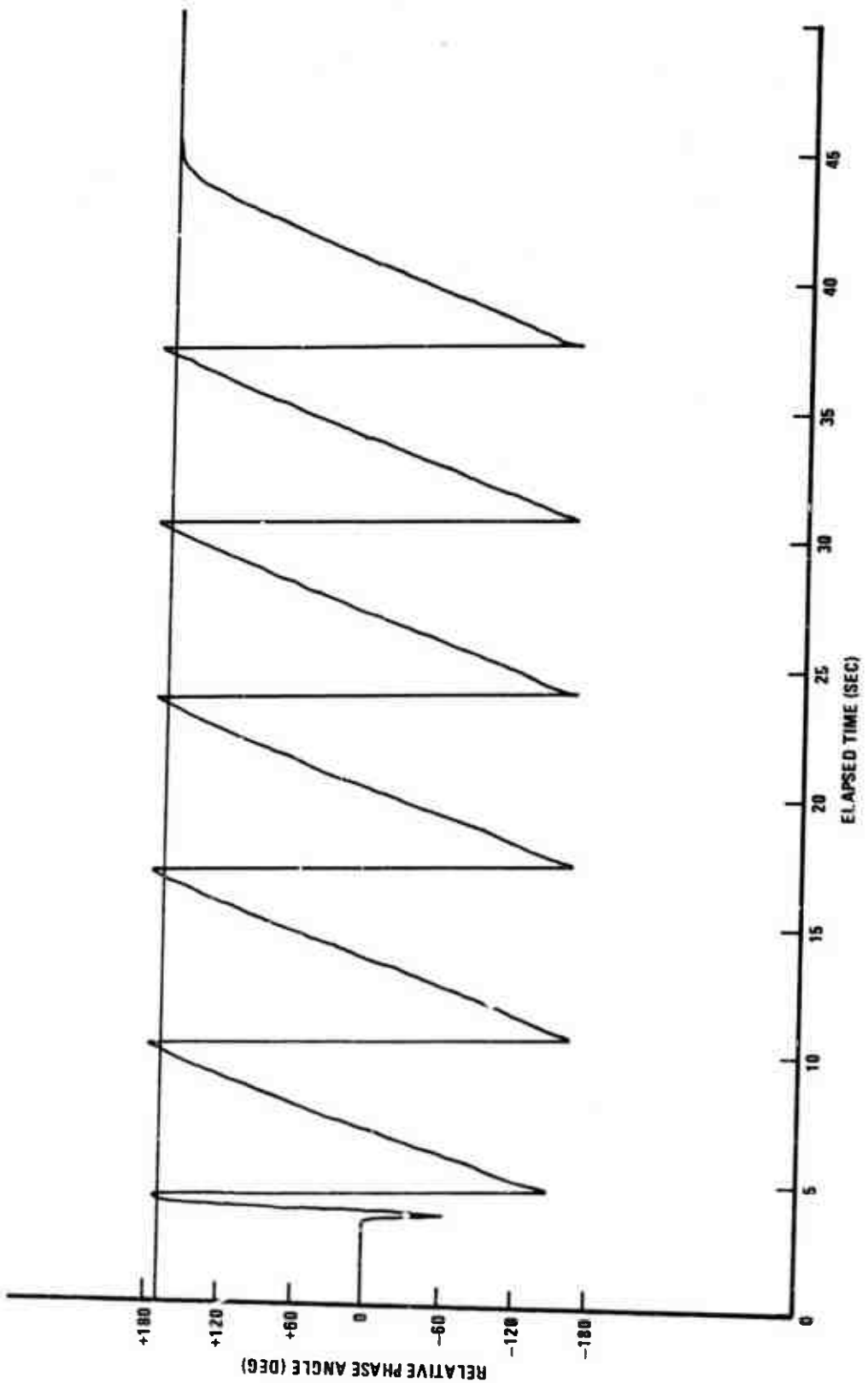

Figure 36. Phase Angle vs. Time for Three Inch Strand Burned at 50 psig.

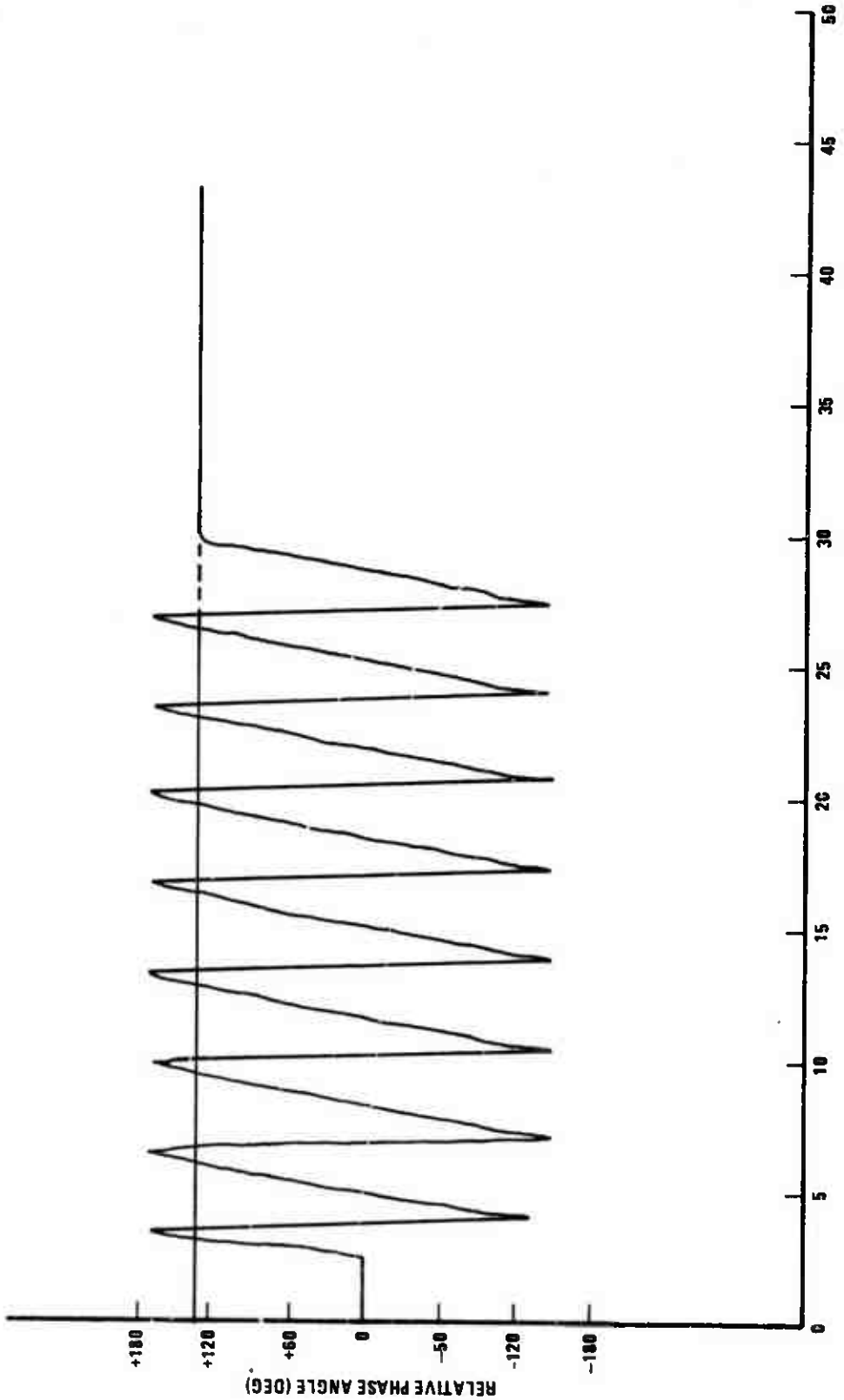

Figure 37. Phase Angle vs. Time for Four Inch Strand Burned at 300 psig.

orifice plate. The wavelength of the microwave in the excess propellant outside the sample holder is much shorter than inside the sample holder and, as this excess propellant burns, the phase angle changes very rapidly at first (although the burning rate is essentially the same inside and outside the waveguide). Thus, if one neglects the initial effects of this excess propellant by knowing the length of the propellant strand and the time for it to burn (the plotter was always swept at five seconds per inch), it is possible to calculate a fairly accurate average burning rate for these steady state burns.

Burning rates were calculated according to the above procedure for each of the constant pressure burns to produce the plot of burning rate versus pressure shown in Figure 38. The results of the slow depressurization test were taken from the graph of Figure 39, which was redrawn from the original computer plot to damp out the high frequency noise. There is good agreement between the constant pressure and slow depressurization results demonstrating the accuracy of the technique. The data can be reduced to the simple relation between burning rate and pressure,

$$r \text{ in/sec} = 0.04\ P_{atm}^{0.4}\ , \qquad (16)$$

which is in good agreement with the results for other similar propellant formulations.

Figure 40 was redrawn very nearly as the computer interpreted the data for a constant pressure (in this case atmospheric) burn. The upper line represents the relative amplitude between the reference and test signals and the lower line represents the burning rate.

Figure 40 illustrates many problems that were initially encountered, but also provides some answers to some persistent questions about the

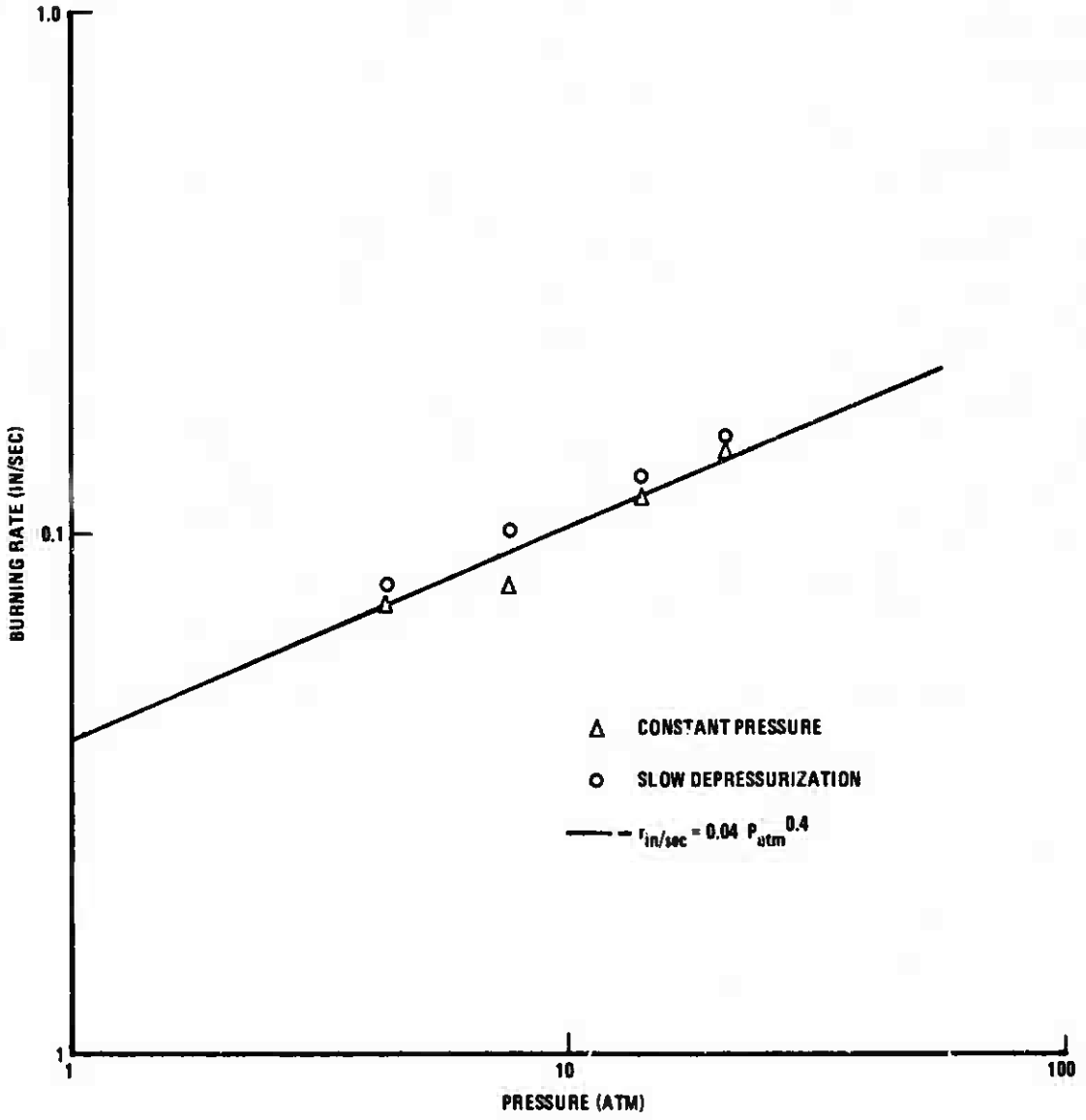

Figure 38. Steady State Burning Rates vs. Pressure.

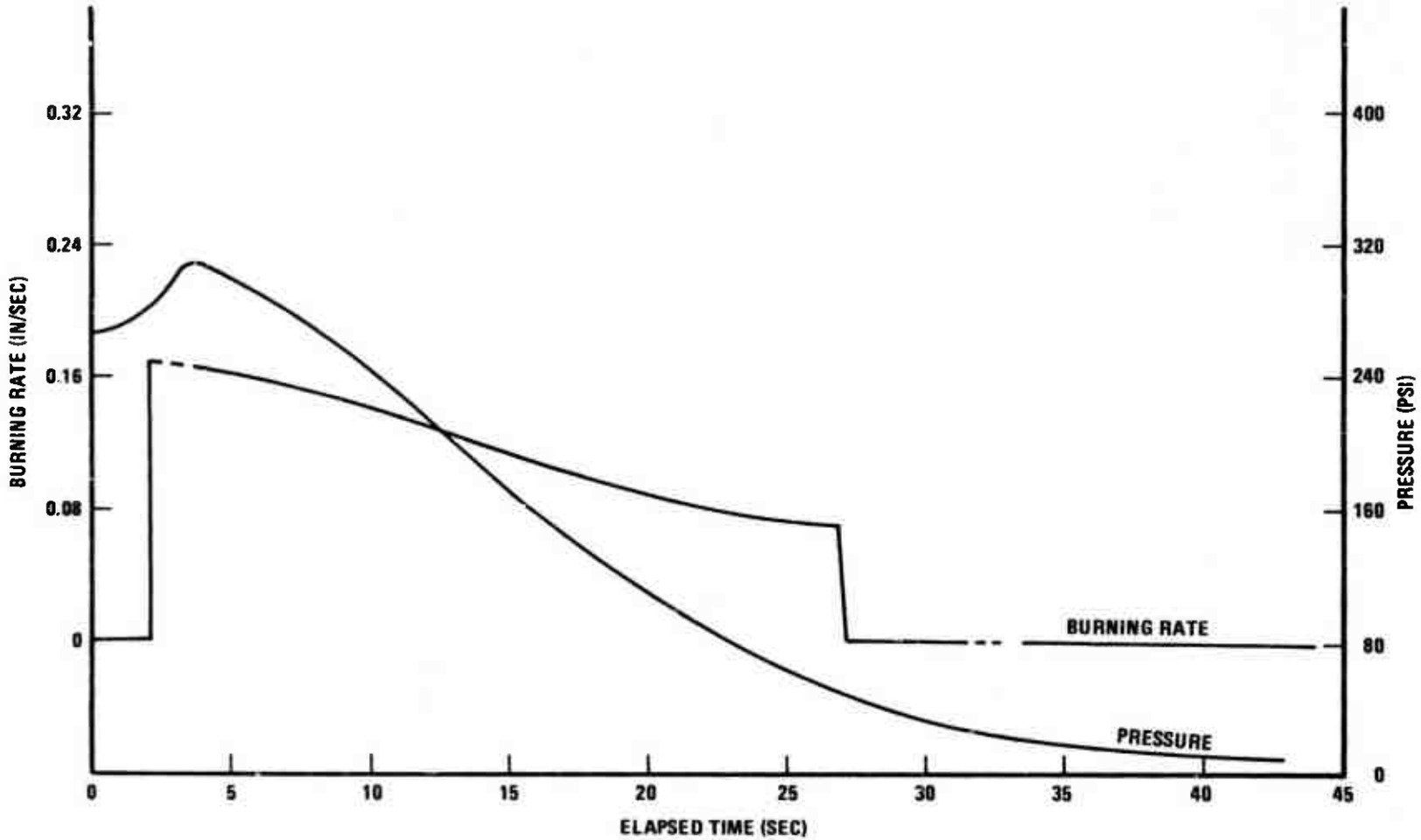

Figure 39. Burning Rates During Slow Depressurization from 300 psig.

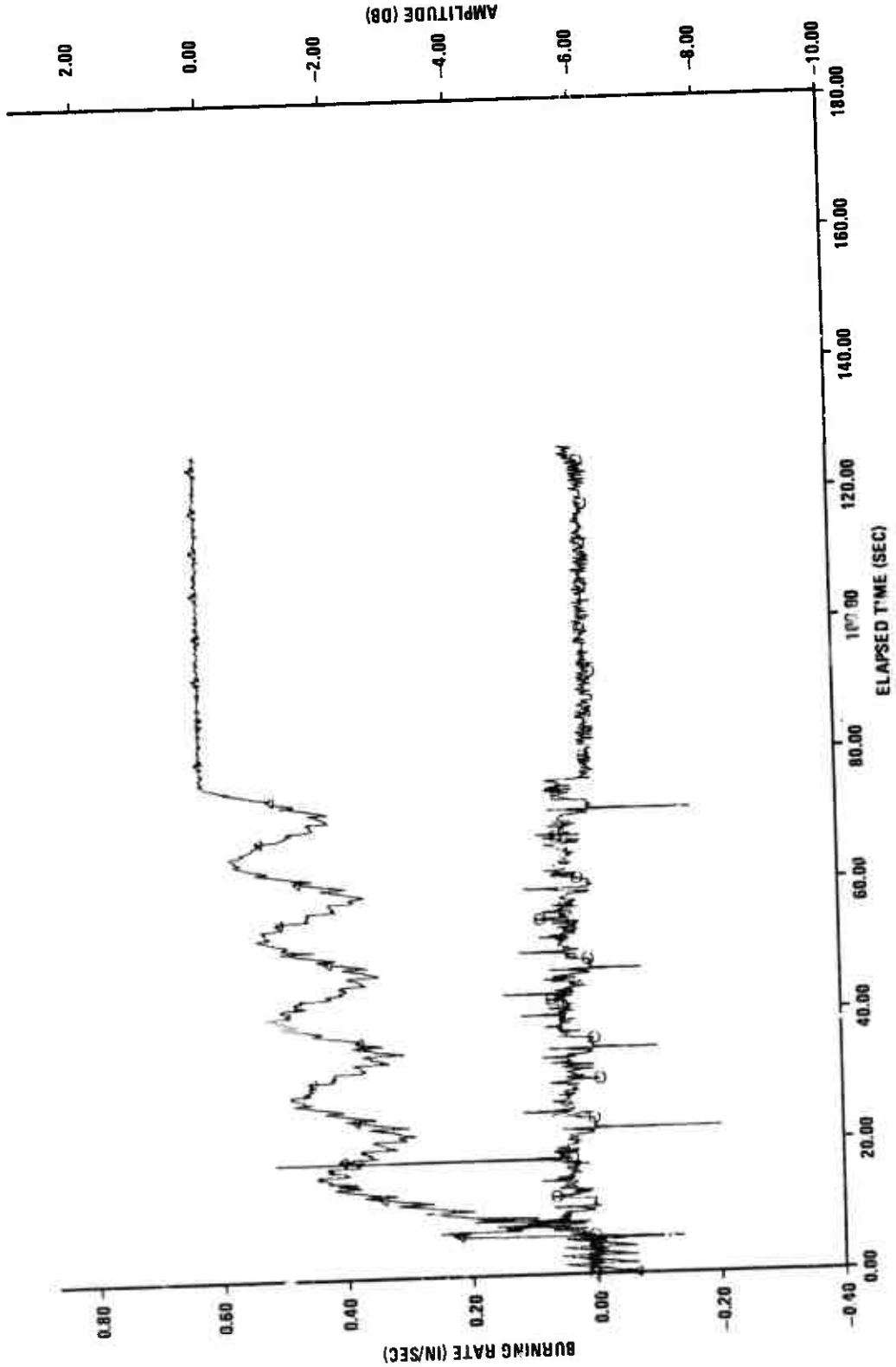

Figure 40. Burning Rate and Amplitude vs. Time at Atmospheric Pressure.

technique. The most obvious problem raised is the significant amounts of noise on the burning rate signal. The large spikes that occur in the burning rate plot are caused by the computer program's inability to account properly for the phase discontinuities and interrecord gaps. The six areas where the indicated burning rate drops to zero were due to the cut-off voltage level of the filter (the filter will not pass more than about +8.13 and -6.68 volts and, after amplification, the full scale phase voltage levels were $\pm$9.0 volts). It was thus found necessary in subsequent tests to filter the phase signal before amplifying it. The phase signal was filtered down to 200 Hz in this example (later tests were filtered down to 50 Hz). Another problem indicated in Figure 40 is the presence of fixed reflections as revealed by the sinusoidal variation of the amplitude signal (as the fixed and burning surface reflections alternately cancel and reinforce each other). The increase in mean amplitude output as the propellant burns is simply due to the fact that there is less and less propellant to absorb the burning surface reflection. As of yet, the source of these fixed reflections has not been identified, but they are not likely to be emanating from the transition waveguide section. In most cases the magnitudes of the fixed reflections were not as large as in this particular test.

The main question resolved by Figure 40 concerns reflections from the flame zone. It had been proposed that the large concentrations of ions and electrons in the flame zone would cause large reflections which could not be simply accounted for, if much energy were to pass through the solid-gas interface.

A glance at Figure 40 reveals a large increase in amplitude as

as the propellant begins to burn. This appears to indicate the presence of a reflection fromthe flame zone. However, when the propellant burns itself out there is no corresponding decrease in the amplitude. Thus, either no energy passes through the solid gas interface to be reflected by the flame zone or, if energy does pass through, the electron and ion concentration is not sufficient to reflect the signal, and it passes through the flame zone. In either case, one may discount the theory that flame zone reflections exist. However, where does that initial amplitude jump originate from? As explained before, the excess propellant outside the sample holder acts as a horn and aids the microwave energy to escape from the sample holder. When this excess is burned away, the energy can no longer propagate out of the sample holder but is reflected by the burning surface within the waveguide, causing a sudden increase of the test signal amplitude.

Rapid Decompression Tests

In order to generate burning rate data during rapid pressure transients, four tests were conducted where the burning rate was observed during rapid depressurization from 300 psi. This series of tests included two where a 1/8 inch orifice (dP/dt = 600 psi/sec) was used and two where a 1/4 inch orifice (dP/dt = 3000 psi/sec) was employed. In addition, tests were run using a 3/4 inch and 1½ inch orifice, but unfortunately, the data was rendered meaningless due to severe mechanical vibration feedback to the microwave system during decompression.

Figures 41 and 42 show traces of phase angle versus time for two runs depressurized using a 1/4 inch and 1½ inch orifice respectively (the vibrations mentioned above were of too high a frequency to cause

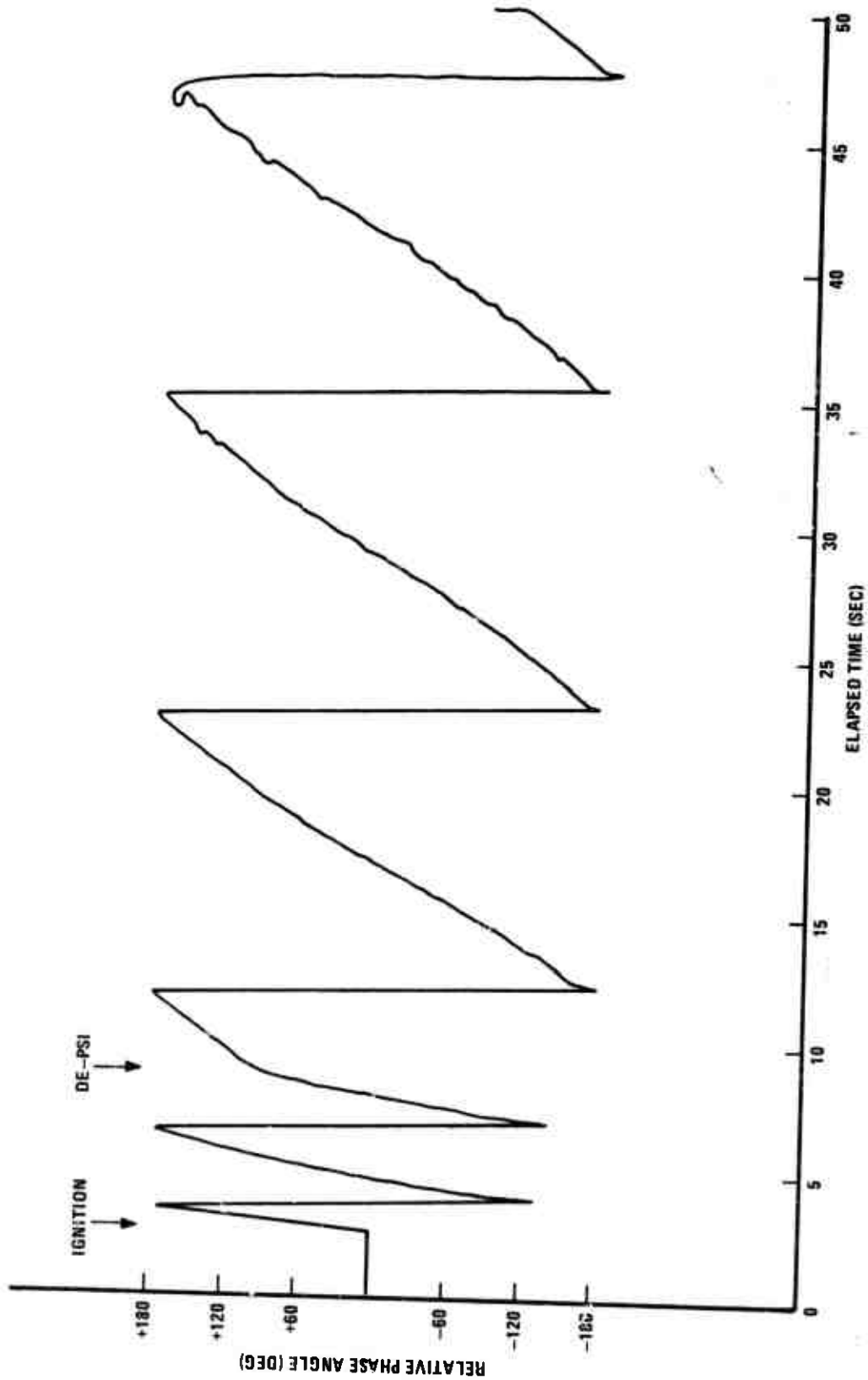

Figure 41. Phase Angle vs. Time for Rapid Decompression Using ¼ Inch Orifice.

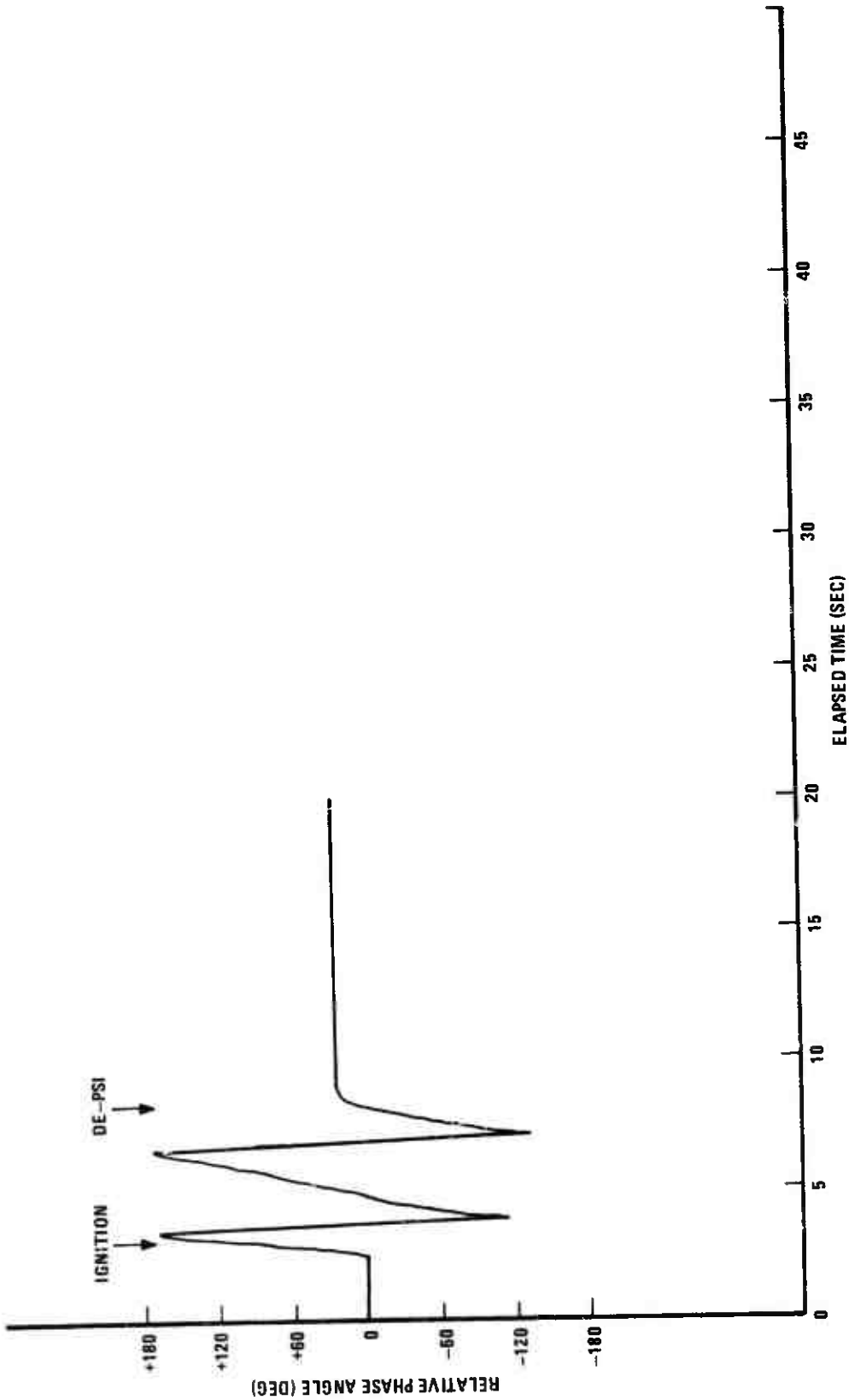

Figure 42. Phase Angle vs. Time for Rapid Decompression Using 1¾ Inch Orifice.

severe errors on the X-Y plotter which produced these traces). The arrows indicate the points in time at which ignition occurred and depressurization was induced. It was obvious from the traces that extinction was induced by the higher dP/dt depicted in Figure 42. On the other hand, Figure 41 indicates an almost instantaneous change in burning rate (but no extinction) at the time of decompression. The jagged appearance of the lines on the right hand side of Figure 41 were due to a bad electrical contact, which caused the pen to jump, in the plotter.

Figures 43 and 44 are plots of the burning rate and pressure (both normalized with respect to their values just prior to decompression) versus elapsed time after the depressurization command was given. Repetition of burning rate results was obtained within $\pm$10 percent at each dP/dt value. Also plotted on these curves are the steady state value of the burning rate obtained at the corresponding pressures. Note that the steady state burning rate is in general slightly higher than its corresponding unsteady value.

The burning rate data points during rapid decompression were arrived at by averaging over 20 actual data points on the recorded data tape. This means that the burning rates as presented were averaged over 24 milliseconds. It is hoped that with an improved phase meter, which has lower noise levels than the present Hewlett-Packard model, it will be possible to average burning rates over shorter time intervals.

Note that no data is presented during the 40 milliseconds just following the initiation of the pressure transient. In the original computer plots, high amplitude spikes appear in the burning rate trace. Several possible explanations of these spikes were considered. The first

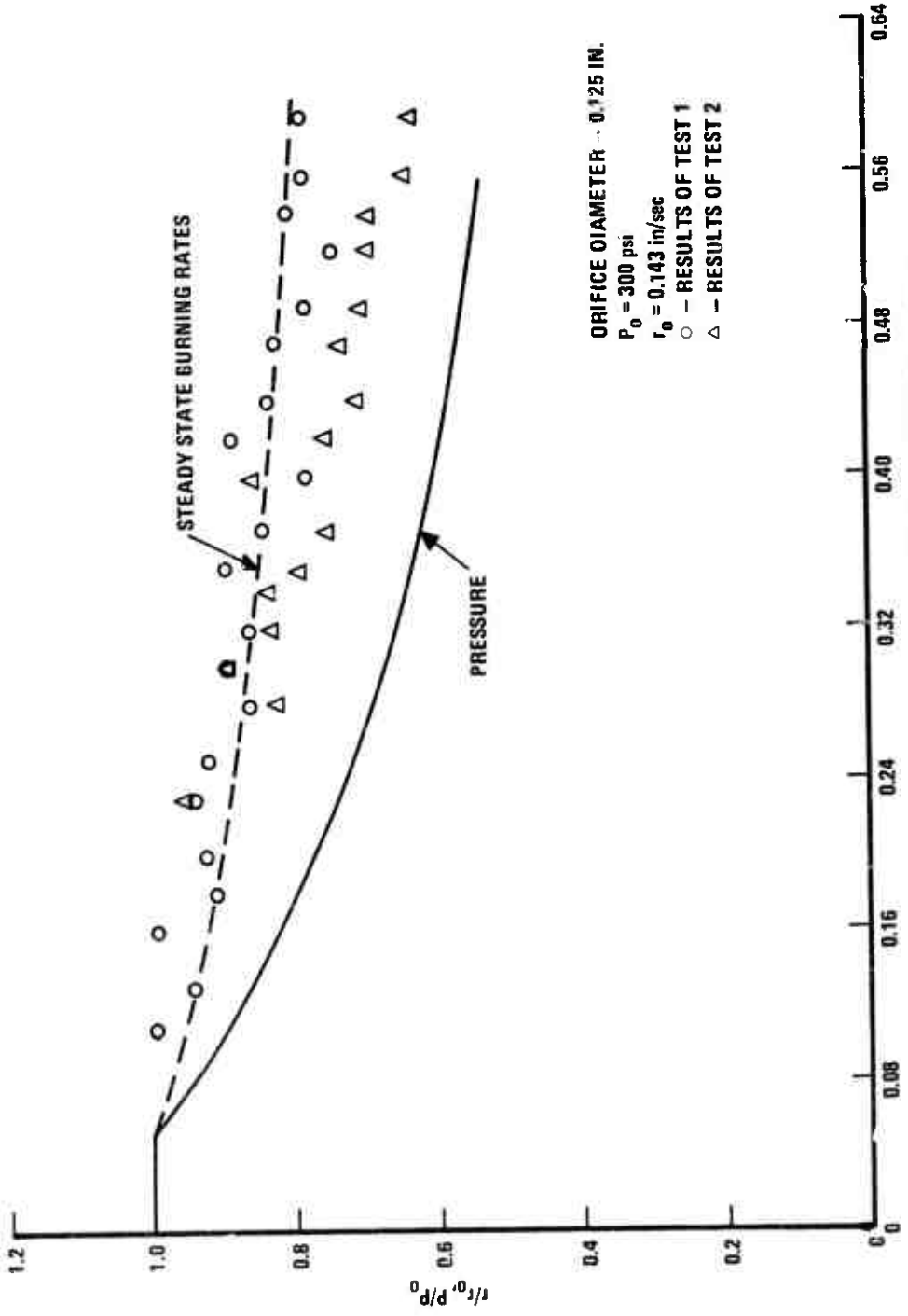

Figure 43. Burning Rate vs. Time for Rapid Decompression Using 1/8 Inch Orifice.

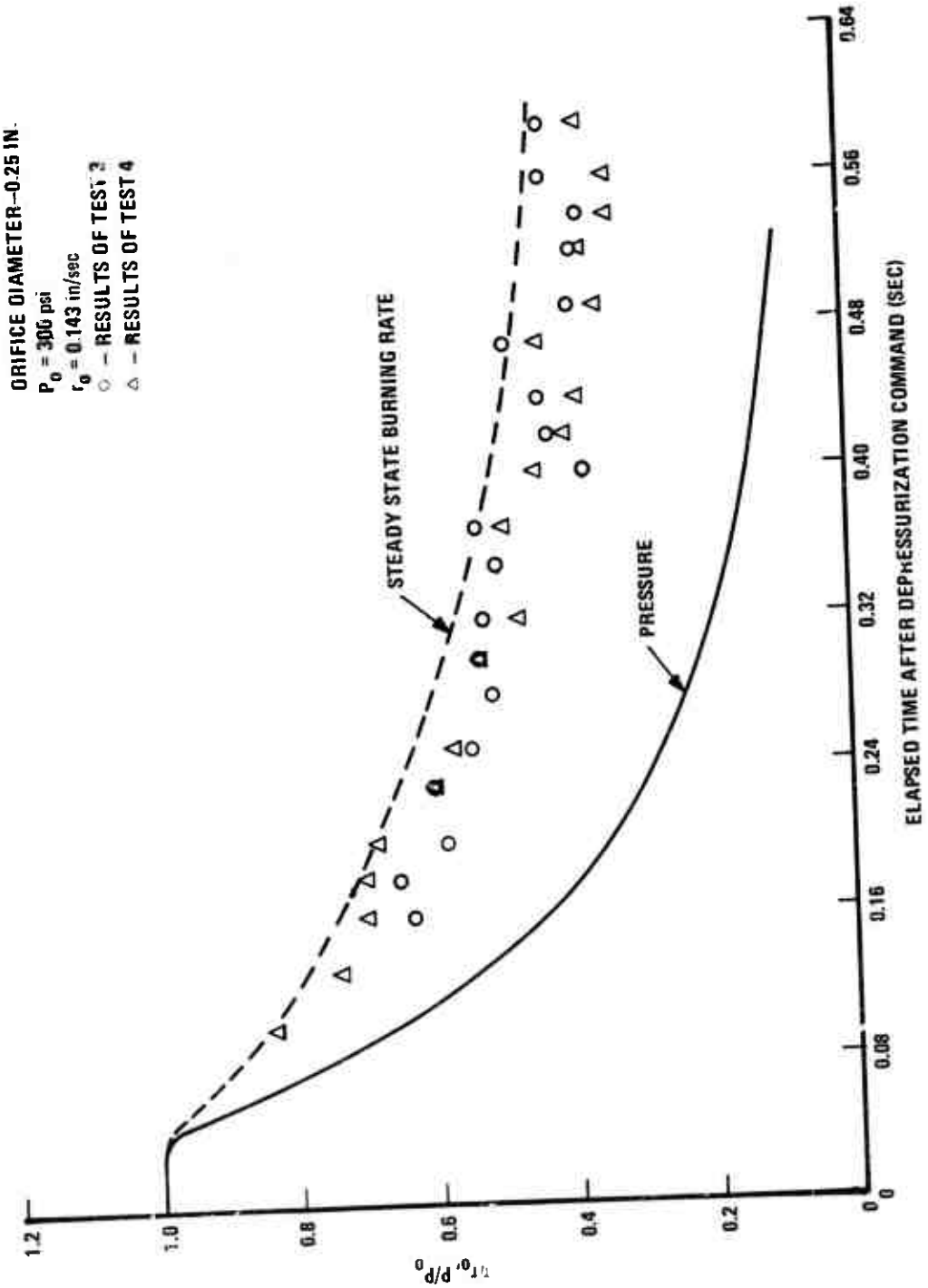

Figure 44. Burning Rate vs. Time for Rapid Decompression Using ¼ Inch Orifice.

possible answer that was proposed was an oscillation of the solid-gas interface during the rapid change in pressure. Recall that small phase changes were recorded when the bomb was pressurized prior to ignition, thus indicating a compression of the exposed propellant surface. This idea was discounted however, because, as one may note from the plots, in the time interval under consideration very little change in pressure (about 40 psi) had yet occurred. This was definitely not enough ΔP to cause such severe oscillation of the solid-gas interface. The second suggestion was that the oscillation resulted from changes in the flame stand-off distance during the rapid pressure change. Proof had already been obtained that reflections from the flame zone were negligible (refer to results of steady state tests), but in order to be certain several tests were conducted in which the apparent burning rate of a non-burning propellant strand was recorded during rapid decompression. As in the burning tests, large spikes appeared in the burning rate curve, which of course should have registered no burning rate throughout the test. Thus, once again the existence of the flame zone was proved not to be a source of error. The third possible source of the large errors was mechanical vibration feedback from the bomb to the microwave circuit. To test this theory, the phase signal was fed into a storage oscilloscope while the bomb with a propellant sample maintained at 300 psi was impacted with a rubber mallet, similar to the impulse resulting from rapid depressurization. Indeed, peaks of sufficient magnitude to cause large burning rate errors occurred. It is thus believed that mechanical vibrations is the source of these particular burning rate measurement errors and the problem can hopefully be remedied with additional braces

on the test stand and supports under the waveguide.

As mentioned before, in the plots of Figures 43 and 44, it was necessary to average burning rates over several data points due to noise on the phase signal. As with the constant pressure tests, the phase signal was filtered down to 50 Hz, but, unfortunately, sufficient noise was present below this frequency to be annoying. On the other band, to filter the signal to too low a frequency would mean sacrificing the time response of the phase sensing instrument. Some noise was also encountered on the pressure signal but it was more regular and could be averaged out. Thus, noise suppression has arisen as the major obstacle to the realization of the full potential of the system. At the time of writing of this thesis, a new phase angle meter, which will tie into the present network analyzer and give greater resolution and lower noise levels by a factor of at least ten, is on order and should add significantly to the capabilities of the system to measure burning rates accurately under unsteady conditions.

CHAPTER V

CONCLUSIONS

Though it was not possible to draw significant new conclusions concerning the behavior of the burning rate during rapid pressure transients from the data obtained so far, the subject investigation has overcome problems inherent in previous microwave systems and has answered some basic questions concerning the use of microwaves to measure solid propellant burning rates.

The following conclusions can be drawn:

1. Errors due to the roughness of the propellant burning surface will in most cases not exceed 10 percent of the true burning rate value.

2. Reflections from the flame zone (in the case of CTPB-AP propellant) are essentially non-existent and, thus, changes in flame stand-off distance or ion and electron concentration in the flame zone will have no apparent affect on the measured hurning rate.

3. The system as described in this thesis can measure burning rates with good repeatability over periods on the order of 25 milliseconds and during pressure transients on the order of 2000 psi per second.

4. The main obstacle to the attainment of the theoretical accuracy of the technique is the presence of random noise on the phase angle and pressure signals. This noise was found to be either inherent in the instrumentation or induced by mechanical vibration of the test apparatus during rapid decompression (in this case large dP/dt values).

CHAPTER VI

FUTURE WORK

Now that the basic questions have been answered concerning the ability of the microwave continuous measurements technique to measure true burning rates, efforts during the second year will he directed toward improving the technique's accuracy and obtaining burning rates during pressure oscillations.

Since the limiting accuracy is the raise generated by the phase angle measurement instrument, a new instrument, a modified Dranetz 305-PA-3002 has been ordered. When operated with the present Hewlett Packard phase measuring system, demonstrations have shown the noise level is reduced by a factor of ten. The modified version of the Dranetz instrument provides a response time of one millisecond instead of the instrument's standard ten milliseconds. This will provide higher resolution measurements by a factor of ten and allow measurements during pressure oscillations up to 100 Hertz.

After arrival of the Dranetz phase meter, additional rapid depressurization tests will be made to obtain data from various propellants with the higher resolution system.

The pressure bomb is being modified to accept a piston and crank shaft which will provide an oscillating pressure in the bomb of any required frequency from zero to one hundred Hertz.

BIBLIOGRAPHY

1. Price, E. W., "Recent Advances in Solid Propellant Combustion Instability," Twelfth International Symposium on Combustion, Paris, France, (1968).

2. Shelton, S. V., "A Technique for Measurement of Solid Propellant Burning Rates During Rapid Pressure Transients," Fourth ICRPG Combustion Conference, Stanford Research Institute, (1967).

3. Price, E. W., "Review of the Combustion Instability Characteristics of Solid Propellants," A Psper Presented at the 25th AGARD Combustion and Propulsion Panel, San Diego, California, April 22-24, (1965).

4. Dickerson, L. A., Jackson, F., and Odgers, A. L., "Erosive Burning of Polyurethsne Propellants in Rocket Engines," Eighth International Symposium on Combustion, (1960).

5. Osborn, J. R., and Bethel, H. E., "Technique for Measuring Burning Rates of Solid Propellants," Review of Scientiric Instruments, Vol. 35, No. 9, September (1964).

6. Osborn, J. R., Burick, R. J., and Ho, P. Y., "Techniques for the Continuous Measurement of Solid Propellant Burning Rates," (Final Report) JPC 421, Report Number F-66-3, Jet Propulsion Center, Purdue University, February (1966).

7. Ho, P. Y., "Feasibility Study of the Microwave and the Ultrssonic Techniques on the Continuous Measurement of Solid Propellant Burning Rates," M.S. Thesis, Purdue University, August (1965).

8. Derr, R. L., Osborn, J. R., "A Technique for Controlling the Position of a Burning Solid Propellant Sample in a Combustion Bomb," Journal of Spacecraft and Rockets, Vol. 6, October (1967) pp. 1120-4.

9. Osborn, J. R., Burick, R. J., and Pannela, R. F., "Continuous Measurement of Solid Propellant Burning Rates," Review of Scientific Instruments, Vol. 37, January (1966), pp. 86-92.

10. Seamons, R. D., "Cineradiogrsphy for Solid Rocket Motor Testing," Space/Aeronautics, June (1965), pp. 73-76.

11. Hermance, C. E., "Continuous Messurement of the Burning Rate of s Composite Solid Propellant," AIAA Journal, Vol. 5, No. 10, page 1774 (1967).

12. Yin, C. F., Hermance, C. E. "Continuous Measurement of Transient Burning Rates of a Composite Propellant Undergoing Rapid Depressurization," AIAA Paper No. 71-173, Presented at AIAA 9th Aerospace Sciences Meeting, New York, N. Y., January 25-27 (1971).

13. Hale, H. J., "The Demonstration of an Ultrasonic Technique to Measure Solid Propellant Burning Rates Under Actual Combustion Conditions," M.S. Thesis, Virginia Polytechnic Institute, June (1967).

14. "Microwaves Measure Solid Fuel Burning Rates," Electronics, November 23 (1962), pp. 50-53.

15. Cole, R. B., "High Pressure Solid Propellant Combustion Studies Using a Closed Bomb," Report S-68, Rohm and Haas Co., Redstone Arsenal Research Division, Huntsville, Alabema, August (1965).

16. Lance, A. L., Introduction to M/W Theory and Measurements; McGraw-Hill Book Company, New York, (1964) pp. 77-96.

17. Montgomery, C. G., Dicke, R. H., and Purcel, E. M., Principles of Microwave Circuits; McCraw-Hill Book Co., New York, (1948) pp. 33-35, and 365-366.

18. Varney, Michael A., "An Experimental Investigation of the Burning Mechanisms of Ammonium Perchlorate Composite Solid Propellants," Ph.D. Thesis, School of Aerospace Engineering, Ceorgia Institute of Technology, May (1970), pp. 209-210.

19. Beckstead, M. W., Culick, F. E. C., "A Comparison of Analysis and Experiment for Solid Propellant Combustion Instability," AIAA Journal, Vol. 9, No. 1, January (1971) pp. 147-154.

20. Blair, D. W., Bastress, E. K., Hermance, C. E., Hall, K. P., and Summerfield, M., "Some Research Problems in the Steady State Burning of Composite Solid Propellants," Progress in Astronautics and Rocketry, Vol. 1, (1960), pp. 183-206.

21. Crawford, B. L., Jr., Huggett, C., Daniels, F., and Wilfong, R. E., "Direct Determination of Burning Rates of Propellant Powders," Analytical Chemistry, Vol. 19, No. 9, September (1947), pp. 630-633.

22. Culick, F. E. C., "Remarks on Extinguishment and the Response Function for a Burning Solid Propellant," AIAA Journal, Vol. 7, page 1409 (1969).

23. Fletcher, Edward A., Hirahi, Tsayashi, "Cas Evolution from Solid Propellants During Pressure Decays," AIAA Journal, Vol. 4, No. 12, December (1966) pp. 2222-2224.

24. Friedman, R., "Experimental Techniques for Solid Propellant Combustion Research," AIAA Journal, Vol. 5, No. 7, July (1967) pp. 1217-23.

25. Horton, M. D., Bruno, P. S., Graesser, E. C., "Depressurization Induced Extinction of Burning Solid Propellant," AIAA Journal Vol. 6, No. 2, page 292 (1968).

26. Krier, H., Tien, J. S., Sirignano, W. A., and Summerfield, M., "Nonsteady Burning Phenomena of Solid Propellants: Theory and Experiments," AIAA Journal, Vol. 6, No. 2, February (1968), pp. 278-285.

27. Osborne, J. R., Murphy, J. M., and Kershner, S. D., "Photographic Measurement of Burning Rates in Solid Rocket Motors," Review of Scientific Instruments, Vol. 34, March (1963), pp. 305-306.

28. Penzig, F. G., "A Tracer Method for Burning Rate Measurement in Solid Propellant Motors," Air Force Missle Development Center-Technical Note, AFMDC-TN-60-8, August (1960).

29. Picard, J. P., Anderson, C. J., Del Grosso, R., and Bryant, E., "Apparatus for Determining Combustion Rate of Solid Propellants," Industrial and Engineering Chemistry, Vol. 56, No.1, January (1964).

30. Price, E. W., "Review of Experimental Research on Combustion Instability of Solid Propellants," Progress in Astronautics and Rocketry, Vol. 1, Solid Propellant Rocket Research, Academic Press, New York, (1960) pp. 561-602.

31. Price, E. W., Mathes, H. B., Crump, J. E., McGie, M. R., "Experimental Research in Combustion Instability of Solid Propellants," Combustion and Flame, Vol. 5, No. 2, (1961), pp. 1596-97.

32. Price, E. W., "Review of the Combustion Instability Characteristics of Solid Propellants, Paper Presented at the 25th AGARD Combustion and Propulsion Panel, San Diego, California, April 22-24 (1965).

33. Spenadel, L., "Burning Rate Measurement of Solid Propellants," Review of Scientific Instruments, Vol. 32, No. 7, July (1961).

34. Stewart, D. H., and Moon, E. L., "An Improved Method for the Measurement of Solid Propellant Strand Burning Rates in Closed Bombs," NAVWEPS Report 8070, NOTS TP 3076 May (1963).

35. Von Elbe, G., McHale, E. T., "Extinguishment of Solid Propellants by Rapid Depressurization," AIAA Journal, Vol. 6, No. 7, page 1417 (1968).